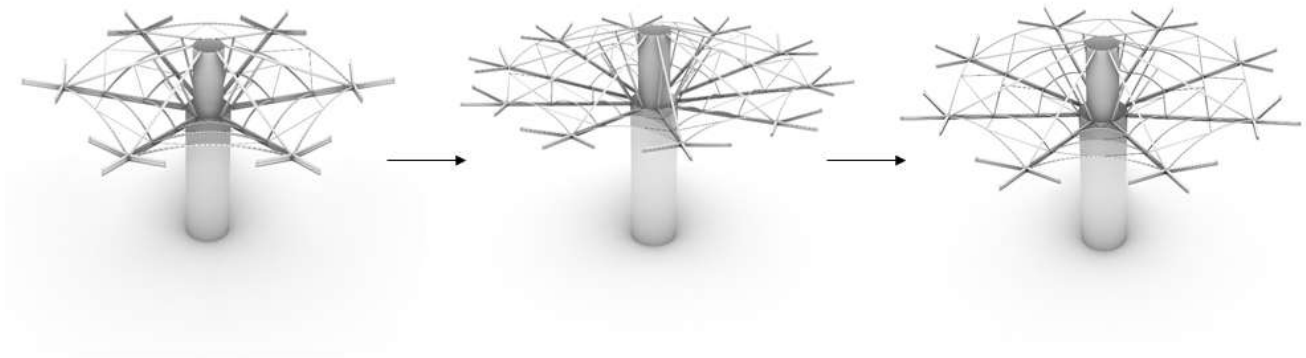


Budapest University of Technology and Economics
Faculty of Civil Engineering
Department of Structural Engineering



MSC THESIS

Geometric optimization and form-finding of steel-stretched barrel vault tensile membrane structure with self-developed module

by

András D. Nagy

Budapest
2023



M Ű E G Y E T E M 1 7 8 2



M Ű E G Y E T E M 1 7 8 2

Budapest University of Technology and Economics

Faculty of Civil Engineering

Department of Structural Engineering

**Geometric optimization and form-finding of
steel-stretched barrel vault tensile membrane
structure with self-developed module**

by

András D. Nagy

C11RK

**in partial fulfillment of the requirements for the degree of Master of
Science in Structural Engineering at Budapest University of
Technology and Economics**

Thesis committee:

Dr. Attila Joó, Department of Structural Engineering, BME, Internal Supervisor

Dr. Krisztián Hincz, Department of Structural Mechanics, BME, Supervisor

Dr. Dániel Merczel, ARC-S Innovation and Technology, External supervisor

Budapest

2023

Abstract

The research and application of tensile membrane structures in the construction industry have been receiving increased attention. This is not surprising, as tensile membrane structures offer efficient and innovative solutions for covering large areas, while they function as lightweight, durable, and impressive structures. This raises the question of whether these solutions can be very well optimized for different goals.

The main aim of the thesis was to develop a design module that enables parametric pre-design, form-finding and geometric optimization of barrel vault tensile membrane structures, in one environment. This was a complex task, we needed to include some innovative ideas to make it possible.

In the first segment, we've done a detailed overview about tarpaulin structures and different kind of steel optimization techniques. Then, a strategy was made for reaching the goals of the diploma work. Secondly, the parametric membrane form-finding was established. Two different form-finding method was introduced, examined and used for defining shapes. We've made observations about mesh resolutions, behaviours and different technical issues. Conclusions were made about how these methods can be used for every day design purpose.

We've programmed a parametric FE model, with what we could do analysis and automatic design of cross-sections. To check the model's results, a second, more complex reference model was created in Dubal RFEM. This model is able to perform nonlinear analysis on the membrane and the steel, which was mandatory to define some conditions of the design later on.

Lastly, the steel structure was geometrically optimized for the self-weight, the number of connections and the covered area. We discussed the choice of objective functions, design conditions. 2 different tools were used on two different theoretical bases. After all the simulations, we've analysed the solutions in many aspects like element number, constructability etc.

As a result of this thesis, after specifying arbitrary input parameters, an umbrella-shaped structure is automatically obtained, along with determining the shape of the membrane. Using the interpreted workflow, other structures can be solved similarly.

At the end of the research, I made the visual source code available.

Összefoglaló

A húzott membrán szerkezetek kutatása és alkalmazása az építőiparban egyre növekvő figyelmet kap. Az elmúlt évtizedben számos különböző ponyvaszerkezetű térlefedés épült Magyarországon is. Gondolhatunk itt akár a 2016-ban átadott Hidegkúti Nándor Stadion lelátó lefedésére vagy éppen a frissen megépült Nemzeti Atlétikai Központ stadionjára is. Ez nem is annyira meglepő, hiszen a húzott membrán szerkezetek hatékony és innovatív megoldást kínálnak nagy fesztávolságok eléréséhez, miközben könnyűsúlyú, időtálló és impozáns szerkezetekként működnek. Adódik a kérdés, hogy lehet-e ezen megoldásokat parametrikusan tervezni és optimálni bizonyos célok eléréhez a tervezési gyakorlatban?

Ezen diplomamunka fő célja, egy olyan tervezési modul, algoritmus fejlesztése és vizsgálata volt, melynek segítségével barrel vault ponyvaszerkezetű, esernyő kialakítású térlefedések parametrikus előtervezése válik lehetségessé. Nem volt egyszerű feladat, hisz ezt számos különböző program összekapcsolásával és saját python alapú komponensek fejlesztésével értem el, Grasshopper3D vizuális programozási környezetben. A szakdolgozat alapvetően kutató jellegű.

A folyamat során számos módon változtatható geometriát hoztam létre és a térlefedés ponyvaszerkezetének kerestem - két különböző elmélet alapján - előfeszítésből származó alakokat. A membránt kifeszítő acélszerkezeten analízist futtattam, majd létrehoztam annak keresztmetszeti méretezési modulját. Ezen parametrikus modell eredményeit egy nemlineáris pontos modellel hasonlítottam össze. Majd a szerkezeten hó és szélteher figyelembevételével geometriai optimalást végeztem genetikussal. Az optimalás során a szerkezeti tömeg volt fókuszban, azonban más a tervezés során felmerülő gyakorlati szempontok is figyelembe lettek véve.

A fejlesztés és kutatómunka eredményeként tetszőleges bemenő paraméterek megadása után, automatikusan kapunk egy megfelelő esernyő kialakítású szerkezetet, a ponyvaalak meghatározásával együtt. Az egyes feladatrészek és a teljes munka után is elemeztem eredményeimet, illetve levontam következtetéseimet egy számításon keresztül. A kutatómunka végén elérhetővé tettem a modul vizuális forráskódját is.

HALLGATÓI NYILATKOZAT A DOLGOZAT EREDETISÉGÉRŐL ÉS ÖNÁLLÓ TEVÉKENYSÉGRŐL

Alulírott **D. Nagy András** (Neptun-kód: **CIIRK**) jelen nyilatkozat aláírásával kijelentem, hogy a **Konzolos ponyvaszerkezet parametrikus tervezése alakkereséssel és optimalizálással** című szakdolgozat/diplomamunka (a továbbiakban: dolgozat) önálló munkám, a dolgozat készítése során betartottam a szerzői jogról szóló 1999. évi LXXVI. tv. szabályait, valamint az egyetem által előírt, a dolgozat készítésére vonatkozó szabályokat, különösen a hivatkozások és idézések tekintetében.

Kijelentem továbbá, hogy a dolgozat készítése során az önálló munka kitétel tekintetében a konzulenszt, illetve a feladatot kiadó oktatót nem tévesztettem meg.

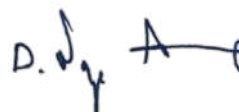
Kijelentem, hogy a dolgozatot korábban más felsőoktatási intézményben, illetve más szakon még nem nyújtottam be diplomamunkaként, vagy szakdolgozatként.

Kijelentem, hogy a diplomamunka értékelésének alapját képező elektronikusan feltöltött és papír alapon beadott törzsdokumentum mindenben megegyezik.

Jelen nyilatkozat aláírásával tudomásul veszem, hogy amennyiben bizonyítható, hogy a dolgozatot nem magam készítettem vagy a dolgozattal kapcsolatban szerzői jogsértés ténye merül fel, a Budapest Műszaki és Gazdaságtudományi Egyetem megtagadja a dolgozat befogadását és ellenem fegyelmi eljárást indíthat.

A dolgozat befogadásának megtagadása és a fegyelmi eljárás indítása nem érinti a szerzői jogsértés miatti egyéb (polgári jogi, szabálysértési jogi, büntetőjogi) jogkövetkezményeket.

Kelt, Budapest, 2023. június 3.



D. Nagy András

hallgató aláírása

Contents

1. Introduction	7
1.1 Introduction to the topic	7
1.2 Problem statement	8
2. Preliminary study	10
2.1 Tensile membranes	10
2.1.1 General characteristics	10
2.1.2 Types of tensile membranes	11
2.1.3 Supports for tensile membranes	13
2.1.4 Behaviour of tensile membranes	14
2.2 Optimization of structures	15
2.2.1 The emergence of structural optimisation techniques	15
2.2.2 Basic concepts	15
2.3 Parametric model and scripts	16
2.3.1 How Rhino Grasshopper 3D scripts work	16
2.3.2 Grasshopper application for truss optimisation	18
2.4 Form-finding of structures	21
2.5 Literature summary and strategy for solving the problem	21
2.6 The sample structure Malaysian Grand Prix Grandstand Tower roofing	22
3. Geometry of the steel structure and the membranes	25
3.1 Building the parametric geometry of the steel structure	25
3.2 Form-finding	27
3.2.1 Initial shape of the membrane	27
3.2.2 Background of the force density method	28
3.2.3 Form-finding with the force intensity method BATS	30
3.2.4 Background of Dynamic Relaxation Method	37
3.2.5 Form-finding with Dynamic Relaxation Method Kangaroo	38
3.2.6 Comparison and summary	41
4. Parametric and reference model	44
4.1 Parametric FE model	44
4.1.1 Model structure	44
4.1.2 Defining loads	46
4.2 Reference FE model	50
4.3 Load combinations to compare parametric and reference models	54
4.4 Comparison of the two models	55

5. Optimization	60
5.1 Conditions for optimal search.....	60
5.1.1 Cross-sectional check.....	60
5.1.2 Design parameters	61
5.1.3 Objective functions	61
5.1.4 Optimization conditions	62
5.1.5 Other conditions	63
5.1.6 Prestressing at different resolutions	63
5.1.7 The essence of Genetic algorithm	64
5.2 Optimization modules for running	65
5.2.1 Nelder-Mead module.....	65
5.2.2 Wallacei X module.....	66
5.3 Structural self-weight minimisation Snow load-combination	68
5.3.1 1st run - Nelder-Mead	68
5.3.2 2nd run - Wallacei X	69
5.4 Structural self-weight minimisation Wind load-combination	73
5.4.1 1st run -Nelder-Mead	73
5.4.2 2. run Wallacei X	74
5.5 Choosing a favourable and multi-beneficial solution.....	78
6. Summary and conclusion.....	80
6.1 Summary.....	80
6.2 Advantages and disadvantages	81
6.3 Future potential of the workflow	81
References	83
Appendix	86

1. Introduction

1.1 Introduction to the topic

Ever since mankind has been engaged in construction, covering the various interior and exterior spaces has been a challenge. One of the primary considerations for such coverings is to protect against various natural phenomena such as rain, sun or snow. Thanks to the new technologies of the 20th and 21st centuries, the various methods of covering spaces are now quite extensive. Throughout the history of construction, our expectations of roofing have also expanded. We want to be able to design a particular covering structure in an economical way. In addition, it must be constructed to a high standard of quality and accuracy, have a high aesthetic value or, on the contrary, 'hide' and complement the space it covers. In the design process, many things can be taken as a starting point and a solution can be arrived at both architecturally and in terms of structural work. The question is: is the resulting structure really the best solution under the given conditions? And in the case of multiple designs, which design is the most useful in which case? In such cases, the possibility of optimisation and sub-optimal design arises, which is the subject of this thesis.

The inspiration for the project comes from the Sepang International Circuit motor racing circuit in Malaysia, which has hosted various Formula 1 and MotoGP races since 1999. The Grandstand Tower (which is the main grandstand of the circuit) has a structure and tarpaulin covering that is reminiscent of a hibiscus flower, the national emblem of the country. Since the roof structures were renovated in 2019, the question arises: what is the optimal geometry and static performance of such an umbrella-shaped tarpaulin cover? How can we find the most realistic shape for the stretched structural elements? In other words, can we create the best model objectively, taking all aspects into account? The thesis answers these questions, among others, by linking several design areas.

My thesis is largely based on the knowledge and experience gained during my project work in the specialisation of structural engineering. There, I carried out the geometric and section optimization of a 20x20 m two-layered sine wave space grid. I was curious to find out whether serious and accurate results could be achieved for more complex structures with more complicated behaviour and multiple materials, despite the many factors and parameters involved.

1.2 Problem statement

The research work is focused on the development of a modelling algorithm for umbrella coverage very similar to the Malaysian structure (only different in sections). The task parts described in this thesis are implemented by coordinating different target software and self-developed modules, combining Grasshopper3D and Python programming.

The thesis was preceded by a lengthy preliminary work, as its full feasibility was not clear. I investigated the majority of the most common software available on the market for the analysis of tensioned cable and tarpaulin structures and the preparation of sectional drawings. Several of them were capable of form finding and nonlinear analysis for predefined edges (e.g. ixCube, MPanel), but typically only for the tarpaulin itself and not for the steel structure that stretches it. There has also been software (e.g.: Dlubal RFEM or Oasys GSA) that can perform nonlinear analysis of the sheet, form finding and FEM analysis of classical structures at the same time. However, they lack some components of parametric modelling or automation. A common problem of this kind is the lack of membrane shape-finding for a continuously changing steel structure or even the rapid access to results in a Grasshopper3D environment. This may not be necessary for a design task, but since we are performing an optimization task, the finite-time execution of calculations, the ability to quickly change input data, the ability to link to an optimization engine and the potential for other workflows were all important factors.

After the preliminary work, I concluded that, apart from the exact nonlinear analysis of the membrane itself, all other tasks can be performed in the calculation. Thus, the main steps of the overall optimization process are as follows:

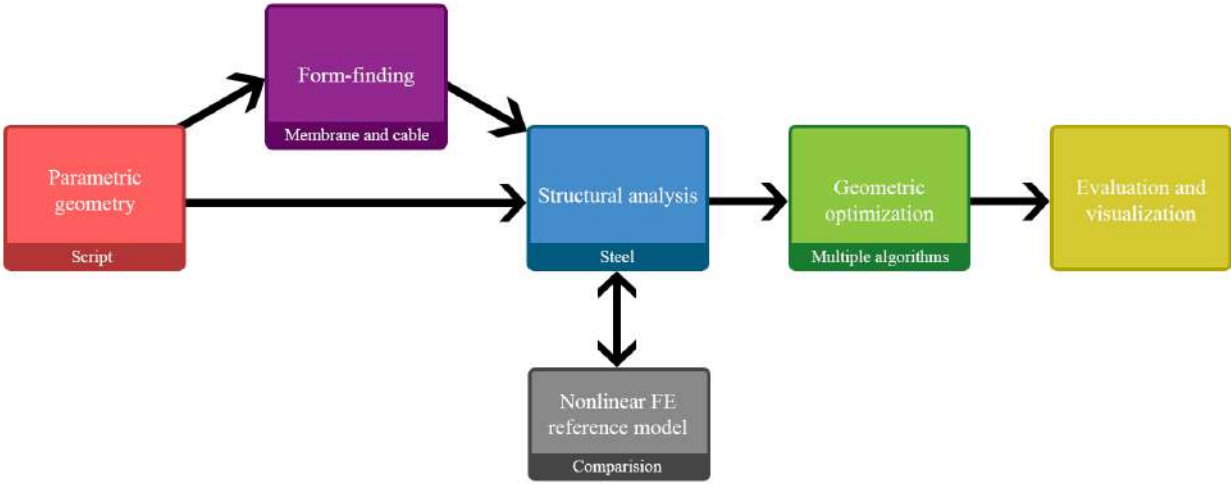


Figure 1: Steps for optimising hibiscus coverage

First, we build a geometric parametric model. The prestressed shapes of the membrane structure between the main beams are found using 2 different form-finding methods. Using prestressed loads and weather loads generated by an approximate method, a finite element

analysis of the steel structure is performed in accordance with the geometry of the original structure. This model will be compared with a nonlinear finite element model created in another program, including tarpaulin, cable and steel structure. Then, the parametric VEM model is optimised with respect to the steel structure geometry by using two modules based on different genetic algorithms with different structures, based on different objective functions. Of course, by using approximations, certain constraints are imposed and the conclusions are also drawn at the end of each process.

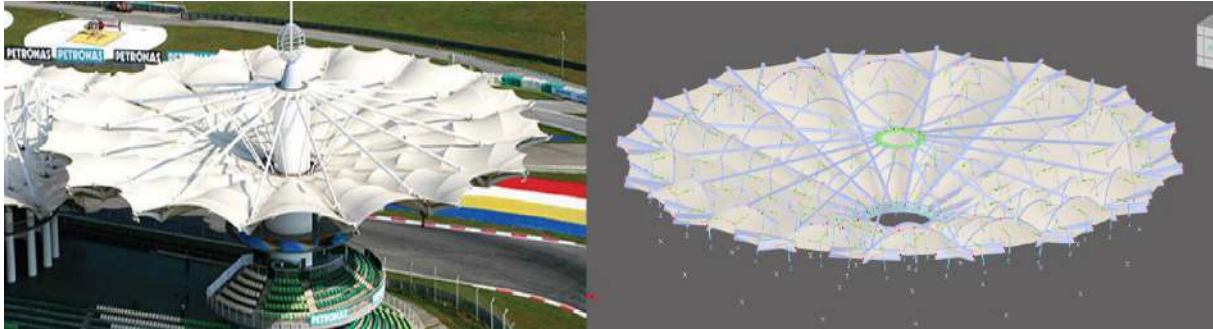


Figure 2: RFEM model of Hibiscus and its VEM in Dlubal

2. Preliminary study

In the next section, we go through all the perimeter areas needed to solve the problem.

2.1 Tensile membranes

2.1.1 General characteristics

Tensile membrane structures are a specific element of architectural and engineering installations. The structural material is extremely thin and flexible, able to withstand only tension and some shear. This significantly limits the possibilities for installation. These membranes are related to truss structures and can be used to build similar structures. Tarpaulin structures are built up from a fabric from which a surface structure can be formed, and are therefore related to single-layer rope nets. The design principles of the two are similar, the main difference being that the surface and the line element allow for different connectivity and network construction, and the load carrying capacity of the tarpaulin materials is much more limited than that of high tensile steel wire. [8]

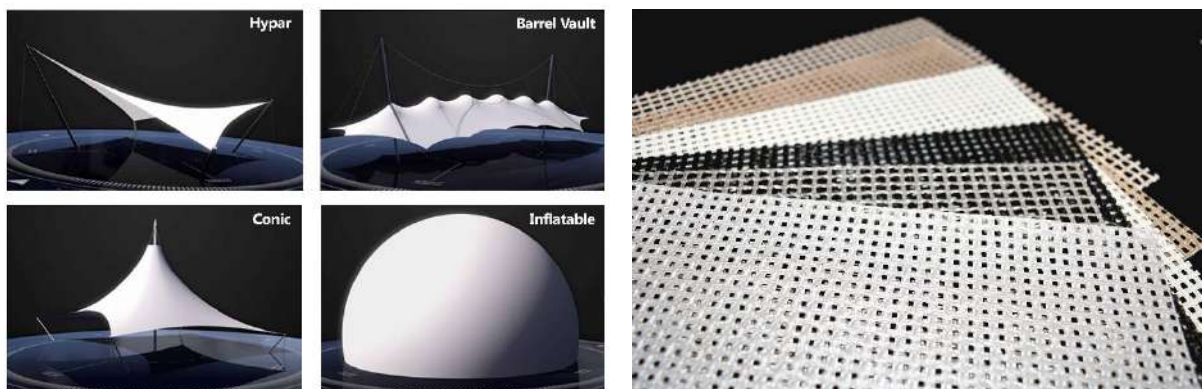


Figure 3: Main types of membrane structures [14] and PTFE fibreglass membranes [15]

Historically, the materials used for tarpaulin structures were of animal or vegetable origin: animal skins, fabrics. Modern tarpaulin construction has been made possible by the development of the plastics industry, which has been able to produce high-quality, durable materials that can be used to build long-lasting, resistant space coverages. The materials used for tarpaulin structures are commonly referred to as technical textiles. The fabric itself is made by simple warp or Panama weaving. In warp weaving, the weft direction is interlaced between the stretched warp direction threads. In Panama weaving, the weft threads are interlaced only between every other warp thread. [8]

The fabric behaves differently in the two fibre directions. Such materials are called orthotropic materials. The shear stiffness of the fabric is negligible until the fibres are locked together. The coating on the fabric provides only some shear stiffness, which is about fifty-fifths of the tensile stiffness associated with the fibre directions. For this reason, the stiffness of the tarpaulin fabric is greatly reduced in the directions between the two fibre main directions. Due to the curvature

of the fibres of the fabric and the non-linear behaviour of the elementary fibres, the behaviour of the web is highly non-linear, so the relationship between stresses and elongations cannot be described by a linear function (see Hook's law). The fibres in the warp direction remain straight during manufacture, so this direction is both stiffer and stronger. The stress-strain function starts very flat in the direction of the projection, then as the fibres straighten out the function becomes steeper. The load capacity is also smaller in this direction. The behaviour of the pre-tensioned materials produced by Ferrari is slightly more favourable: the fibres are tensioned before coating, and the pre-tensioning also causes the warp direction to bend slightly, so that the behaviour of the two directions is similar. The fabric is coated, which has several functions: it makes the surface continuous, protects the fibres, provides some shear stiffness and allows the material to be welded. Tarpaulin fabric is made from a combination of several materials. The fibres can be polyethylene, polyester and glass fibre, but polyethylene is no longer used. The coating is made of PVC or Teflon. [8]

2.1.2 Types of tensile membranes



Figure 4: Skysong membrane roofing - tensioned structure at ASU University of Arizona [15]

Tarpaulin structures must always be designed in a tensioned condition. This is necessary to ensure that the structure is stable and does not float in the wind. Since tensioning provides the support, the main load on the structure will also be tensioning. Tensioning can be created in several ways, and different types of structures are defined based on these [8]:

- stretched tents
- hosepipe tarpaulin structures
- airtight tents
- TensAirity structures
- cushion structures
- tanks

In the design of stretched tents, the tensioning required for the form is provided by the edges of the structure. The two principal curvatures must be in opposite directions so that the tension forces can be balanced without external force. Thus, any tensioned tent must have a hyperbolic surface. [8]

In *hosepipe structures*, air pressure is created inside the tarpaulin. Hose structures also require active engineering during construction and operation. However, it uses less air than an airtight tent, therefore air leakage is significantly less. For this reason, it is often sufficient to operate

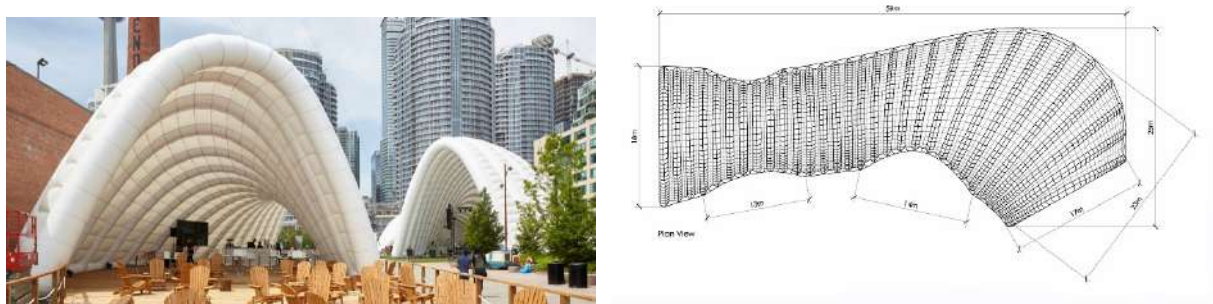


Figure 5: Hosepipe pavilion in Toronto [16]

the machinery at low capacity, often intermittently after the installation. With this type of building, many different forms can be achieved. Even something completely different from the sphere or the cylinder. However, attention must be paid to the fact that more complex geometries can lead to very uneven stress distributions, which are not beneficial for long-term operation. [8]

Hose structures are similar in behaviour to conventional structures, as they can be made in bent, pressed and tensioned elements. Tensile stresses in a beam are absorbed by the sheet material and compressive stresses are absorbed by the internal air pressure. The other changes caused by air pressure cannot be analysed so easily, but it can be stated in principle that air pressure hoses can be used in a similar way to conventional structural elements. [8]

The *airtight tents* are also powered by the tensile force effect of air pressure. Here the air pressure is between the tarpaulin and the ground. The amount of overpressure required for operation is determined from the potential loads on the structure. For the external forces, they take the meteorological loads into account (wind and snow). The external force of an extreme snow load of 2kN/m^2 can be compensated by approximately $1A \approx 105\text{Pa} = 100\text{kN/m}^2$, i.e.: $0,02A$. This may be interesting because it is still an acceptably low value in terms of the building pressure's physiological effect. Since $0.03A$ is the maximum air pressure value that does not cause symptoms in the occupants, it is perceived that we need a relatively small overpressure. It results that the machinery required for operation does not need too much power and their energy requirements are acceptable. Airtight tents can also be made up of several layers, which are used for thermal and insulation reasons. [8]

TensAirity structures are related to hosepipes. However, in this case, ropes and rigid poles are used in addition to provide stability to the support structure. They act as a traditional beam element: pressure is taken by the air pressure or the side rods under pressure, tension is typically taken by the cable or the fabric. The above-mentioned air pressure hoses connect the pressurised rod and the tensioned cables, and take the shear. Since we are talking about flexible elements, the chance of loss of stability is reduced, but the risk of buckling is not eliminated! [8]



Figure 6: Tensairity carpark covering in Montreux, Switzerland [17]

2.1.3 Supports for tensile membranes

The principle of supporting tarpaulin structures is the same as for rope structures or other shell structures. However, the design of the edges is specific. Three main types of support are distinguished in the literature: cable support, rigid flanges and masts. [8]

Cable edges and rope splices are the most typical and most appropriate type of edges for tent structures. The stress that is applied and acting on the surfaces determines the shape of the rope curve as a load. The shape of the rope must be matched to the shape determined by the principal load. Since the shape of the tensile membrane, the magnitude and distribution of the stresses are unknown at the time of the shape determination, the shape of the edge cannot be determined explicitly. Therefore, we specify or assume some stress acting in the surface and in the cables so this can give a clear edge shape. For instance, with a soap-bubble-like stress distribution and cable strength. If we specify different stresses, the plan projection of the edge will have an elliptical shape. Its axes can be rotated by the horizontal projection of the shear force. The shear curve is scalable, for each stress distribution infinite number of shear curves can be assigned, which can be transformed into each other by affine transformation. Parameters must always be specified for the rope, such as the tangent of the initial, the horizontal component of the rope force, etc. [8]

Rigid perimeters are typically considered for architectural integration rather than structural specificity. There are no constraints on the shape of rigid flanges, but there is a condition that a

continuous surface can be included between the flanges under the stress distribution. The geometry of the edges can be either straight, planar curves, or space curves. [8]

Masts are also a typical support for tarpaulin structures. This type allows the internal points to be raised to give the surfaces greater curvature. The load capacity can be increased significantly by allowing large differences in height or curvature. However, since the masts are point supports, the introduction of concentrated force would cause singularities which would also destroy the structure of the material. For this reason, ring spacing or rope spacing is used at the interfaces, sometimes with local reinforcements in the material. [8]

2.1.4 Behaviour of tensile membranes

An elementary piece of membrane can have two types of force. The internal forces in the element can either balance themselves or balance the external forces. Accordingly, the two principal curvatures of the elementary membrane can be opposite or equal, giving a negative or positive multiplication curve. [1]

The shape of a tensile membrane structure can only be a hyperbolic surface, so it must have opposite curvature in two directions. Importantly, all points of the tarpaulin must be under biaxial tension in all design conditions, even without external load. Thus, no load can be used to create compression. It also follows that such structures must not have free edges and must be structurally indeterminate. They have no bending stiffness. Their shear stiffness is also negligible compared to their tensile stiffness, so they must be counted as cable nets. They have large deflections, small horizontal support displacements. The open sided stretched tents tend to have problems with floating when it comes to wind loads. The inner parts, which are close to the plane, float slowly and are not dangerous. However, fast floating of free edges is dangerous, which is why tight edge ropes should be used. The support acts on the structure and essentially determines its shape, its curvature and, through this, its stiffness. Designing a

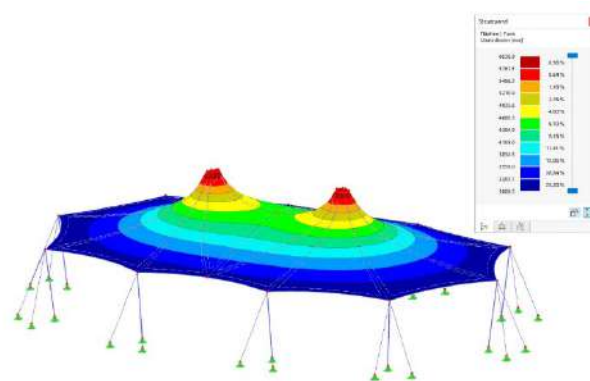


Figure 7: Analysing the tensile membrane in FEM software [18]

tensioned structure is therefore not only a matter of designing the net or the membrane itself, but of designing the supports and defining the boundary conditions. [13]

As explained above, there are two main ULS requirements for the design principles of tensile membrane structures. One is the strength requirement, whereby the amount of tension and pull from the load must not exceed the tensile strength of the material, otherwise the fabric will break. The other is the anti-wrinkle requirement. The difference between the tension and the pressure from the load must be positive so that there is no pressure at any point.

2.2 Optimization of structures

2.2.1 The emergence of structural optimisation techniques

Civil engineering structures incur high costs generally. Increasing costs of materials, energy, manufacturing and operation have made it necessary, while advances in numerical methods have enabled the widespread adoption of optimization methods in engineering practice. In the early stages of the optimal sizing, the aim was to reduce the mass and volume of the structure, later on the problems were approached from the cost point of view. [9]

The need for optimisation is complex and covers many areas. It has appeared in many fields, including structural design, vehicle component design, architecture and various aspects of industrial design.

2.2.2 Basic concepts

Design variables are variables that can be modified by the optimization procedure. *Design parameters*, on the other hand, cannot be modified by the optimisation procedure and are not covered by the optimisation. *Design responses* are output variables that can be used to describe objective functions and constraints. The procedures seek the minimum or maximum of the objective functions. Optimization boundary conditions are constraints that impose a geometric or operational constraint on the simulation. "When formulating the optimization problem, it is necessary to decide which values are considered unknowns. In general, geometric dimensions can be variables when designing structures. For example, when sizing a support, in most cases the dimensions of the cross-section are the unknowns. In some cases, material properties may also be variables. [9]

In physical terms, four main types of design variables are distinguished [20]:

- **mechanical or physical properties of materials,**
- **topology of structures,**
- **shape of structures,**

- **cross section dimensions**

When optimising the mechanical or physical properties of a material, a typical task is to search for the optimum from the conventional materials that can be used. This case, we work with discrete design variables. This kind of task significantly increases the computational demand and complexity. In the case of modern composite materials (e.g.: glass fibre reinforcement), a number of new characteristics can be used as design variables: the volume fraction of reinforcing fibres, the fibre direction, the elastic modulus or, in the case of layered composites, the thickness, number, location and shape of the layers. [20]

The main objective of *topological optimization* is to tell where the structure or structural element exists in a given interval. Topology optimisation procedures therefore search for the optimal design over a predefined range, usually from a viewpoint of high priority. The resulting shape usually cannot be considered as a final solution. It may be found by further optimisation on the proposed topology, using several aspects or other types of optimization under different conditions, e.g.: size. The topological design variables describe the topology (spatial filling), the form of a structure. The topology of a structure can be automatically optimised by allowing elements to become zero size, thus eliminating inefficient elements. [20]

Determining the shape and location of a structure leads to the field of geometric optimisation, for instance when changing the coordinates of the connection point of a rod or the length of a rod element. Such design variables typically fall into the continuous category [20].

Size optimisation typically works with simpler, more tractable design variables than shape optimisation, but has many practical applications as well. Examples include the cross-sectional area of a bar element or the moment of inertia of a flexible element, plate thickness. [20]

2.3 Parametric model and scripts

2.3.1 How Rhino Grasshopper 3D scripts work

Grasshopper is a visual programming language and environment that can run inside the Rhinoceros 3D software. The great advantage of visual programming languages is that, rather than the precise knowledge of how to code in a given language, the focus is on the visual components and their relationships. This makes the work of designers easier. [10]

The program basically works by connecting the defined components to each other in a graph-like way. We can create a chain whose component outputs are connected to and depend on the inputs of the components that are in front of them. This solution is primarily used to build algorithms that can be used for design and structural engineering. The outputs are often numerical values or even 3D objects, which is what we need in many cases. With Grasshopper,

we can quickly change the shapes, layouts, curvatures, widths or heights of square grids or other even more complex geometries like freeforms, which will output a set of information that we can apply in other numerical software. This can be a finite element program like AxisVM or Consteel. Importantly, the run results are returned back to Grasshopper with a well-written algorithm, which can be immediately used or analysed by the script. This data can then be used to run another workflow (for example in product design) [10].

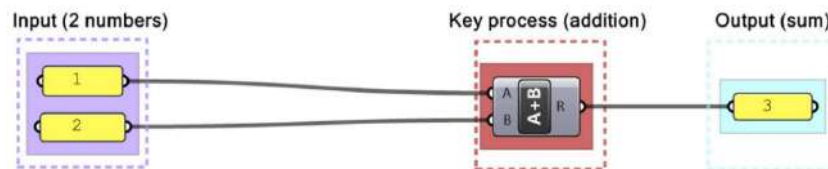


Figure 8: Grasshopper 3D: simple addition [10]

In Grasshopper, the solution runs from left to right. On the left we have the inputs and parameters, while on the right we have the outputs. In between there are one or more key processes/components, possibly additional inputs and outputs. In the simple example above, you can see that a simple addition algorithm contains two numbers (as inputs), a sum (as output) and a key process that converts the numbers into a result. [10]

Another example that creates a circle on XY plane by specifying a circle centre and a radius:

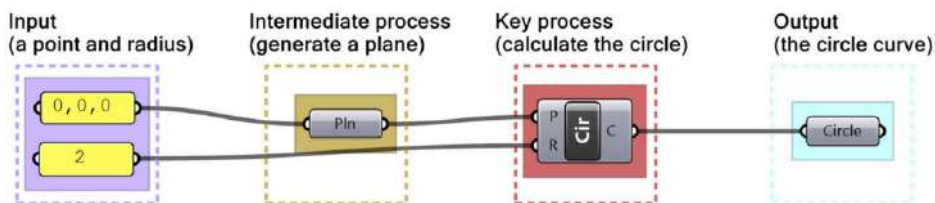


Figure 9: Grasshopper 3D: creating a circle [10]

It is therefore possible to create curves, planes or geometric objects in space, from simple definitions and references of points. These objects can be associated with domains of interpretation, mathematical transformations and much more. We can add information to them, generate data sets from them, and modify, replace or combine the information content of these data sets. The environment has many components, plugins that can perform structural analysis, animation or simulation, without any loss of data. Most components are predefined, but it is also possible to write components or even modify existing ones in many programming languages (Python, C#, etc.). We can run script of components over and over again, forming a loop, thus automatically repeating a given operation large number of times, performing simulations. Finally, it can even be passed as data to additional third-party applications if necessary.

2.3.2 Grasshopper application for truss optimisation

This section presents a way to geometrically optimize two types of trusses using a Grasshopper plugin. In both examples, the performance indicator is the volume of structural material required for a given load condition. The dimensions of the structural elements are defined so that the allowable stresses are not exceeded and deflection is avoided in all cases using the Euler deflection formula. The internal forces are calculated using Karamba3D software, which works well with scripts in the Rhino Grasshopper environment. [11]

Example 1: truss beam

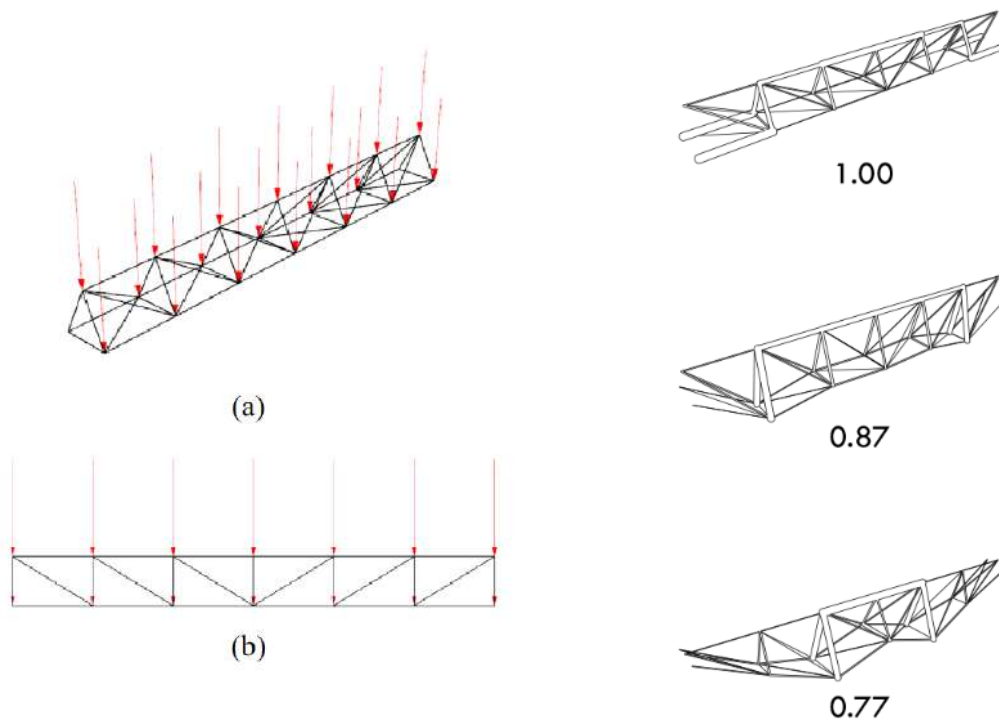


Figure 10: Initial geometry [11]

Figure 11: Different results with material to volume ratios [11]

The spatial truss beam shown in *Figure 10* is defined with a parametric model containing 8 design variables. These control the vertical and horizontal positions of the nodes, limited to a defined range. The structure is symmetric, 10 m span and supported by 3 hinges at each end. A vertical load is defined for all unsupported nodes. A plugin called Stormcloud was used to optimize the structure. A geometric optimization was performed where the goal was to minimize material usage. Quite surprising solutions were found by the algorithm, highlighting the qualities of the method. It can be seen that the written algorithm varied the number of nodes, their coordinates and the thickness of the connecting elements. In the course of the work, a loop was written that runs until it finds a better solution within a certain error bound.

Example 2: Space grid

The second structure is a three-dimensional grid covering an area of 60 m x 60 m. The inspiration for this study was the so-called "Earth Canopy" structure designed by Feilden Clegg and Atelier One. It is a double layer timber grid shell with a freeform lower layer and a flat upper layer on which solar panels are placed. Nine design variables define the vertical coordinates of the 12 nodes of the lower shell, and symmetry is what is prescribed over the entire lower surface. [11]

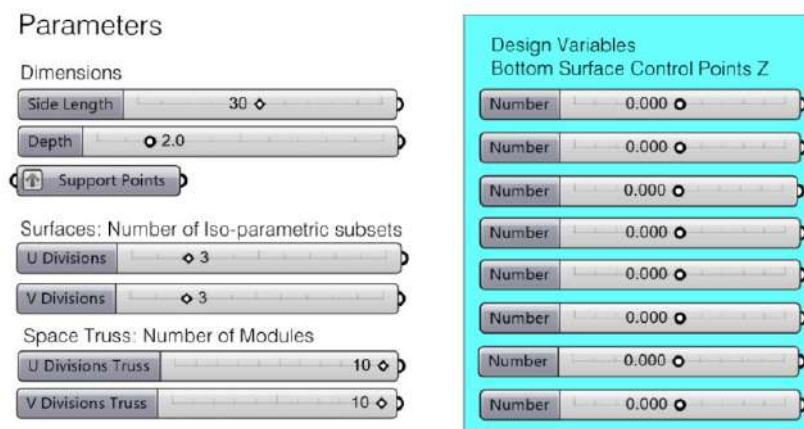


Figure 12: Grid generation parameters [11]

The structure is optimized to balance the gravitational loads, which are defined as concentrated loads on each node. The controlled points can only move vertically, the areas between each node are equal [11]

First, surfaces were generated to form the lower and upper layers of the roof. Here the parameters were the side lengths and the distance between the two planes. However, the lower shell was curved in concept, so the vertical coordinates of its points were changed by the next step. The created surfaces were the inputs to the component that generated the space grid itself. The variables were grid resolutions interpreted in vertical and horizontal planes. After the obtained grid geometry, the locations of the supports were determined, with their coordinates as parameters. [11]

Although the parametrization of the problem is limited and does not return the absolute optimal solution, the example illustrates that with this method there are also several different forms with better utilization than the original model. For a given complexity of structure, 3D visualization and selection mechanism are essential for effective design. *Figure 15* shows different solutions with material volume ratio compared to the original geometry. [11]

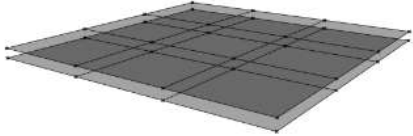
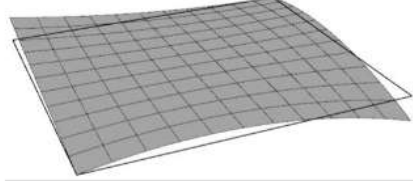
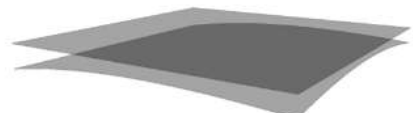


<i>Geometry</i>	<i>Step</i>	<i>Parameters</i>
	rectangular surfaces generation	side length depth
	Bottom surface manipulation through vertical translation of control points	$x_i \in \mathbb{R} \mid -3 \leq x_i \leq 3$ with $i=1,2,\dots,18$
	surfaces used as input for the space truss component	
	lines describing space truss output by component	u divisions truss v divisions truss
	4 supports points are connected with bars to the four closest truss nodes	support points positions

Figure 13: Grid optimization process

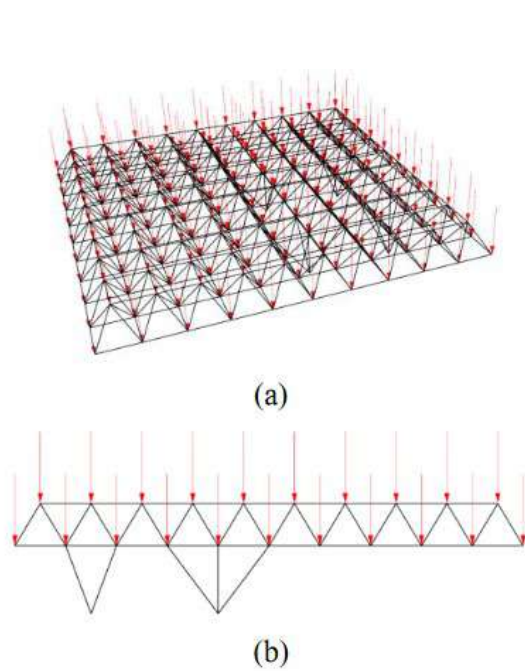


Figure 14: Initial geometry and loads [11]

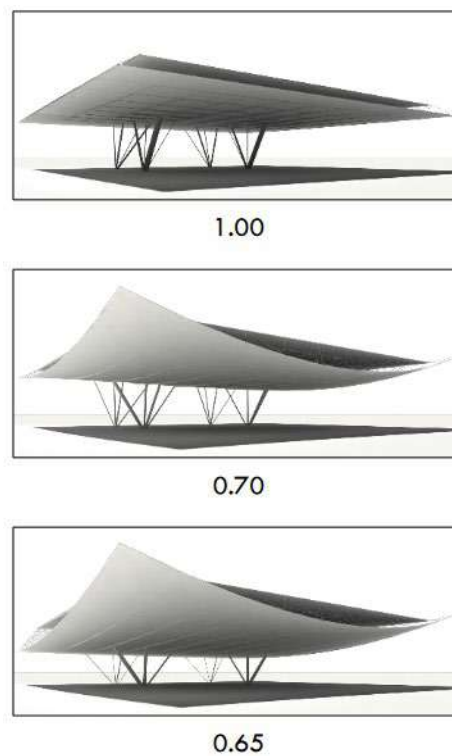


Figure 15: Results with different material volume ratios [11]

2.4 Form-finding of structures

One of the first steps in the design of membranes is to find the exact form. Form finding is the process where the goal is to find a structural shape that matches the initial equilibrium of a given structure. For tensioned membranes, this process is based on the principle of 'shape follows force', where the geometry depends on the relationship between topology and forces. [12]

In the past, form-finding was associated with experiments on physical models. But the problem with physical form-finding was that it was extremely time-consuming. Newer, more technologically advanced physical shape searches appeared in a series from the 1970s onwards, known as various numerical methods. [12]

In 1975, Argyris developed a method based on the finite element method. Barnes then introduced the DRM (Dynamic Relaxation Method). The principle of DRM was essentially based on strings and particles. The force applied on the structure acts on the particles so they are in motion until the equilibrium forces are equalized. It is also important to mention the Stiffness Matrix Method, which can be derived from the application of structural analysis, as it uses elastic and geometric stiffness matrices. The method is characterised by the use of 'redundant' material properties, which are problematic in several aspects, for instance, they are a burden on the runtime. Also in the 1970s, Schek was the first to introduce the FDM (Force Density Method), which has been the most widely used method ever since. With FDM, we can solve the equilibrium equations for tensile membrane structures that can be modelled as a discrete cable network with nodes and lines. Within cable networks, the connected elements are in equilibrium when the external and internal forces acting on them are in equilibrium. The Force Density Method is a material independent method. It often gives results that do not appear to be a final shape, in which case further iteration is typically required. [12]

2.5 Literature summary and strategy for solving the problem

During the preliminary study, we looked at areas that were in some way related to the task. First, we looked briefly at the types of coverage. Since the task is about tensile membrane structures, we went into a little more depth on this topic. We looked at their main types, ways of construction, main descriptions of their structural behaviour. Then came the topic of optimisation. We were introduced to the basic concepts, the different types of structure optimization, then we looked at the operation, advantages and applications of the Grasshopper 3D visual programming environment. Application examples included a discussion of the geometric optimization of a truss beam and a spatial grid roof from a study. Lastly, we moved

on to the development of form-finding, its main types and the specifics of the modules to be applied.

The problem-solving strategy consists of five main points. In order to solve the problem presented in section 1.2, the sample structure in section 2.6 needs to be examined. This will be our starting point. Then we will build and use the parametric geometry in Chapter 3. We generate and compare two ways of the membrane form-finding algorithm. In Chapter 4, we build the parametric finite element model and compare it with a complex reference model. In Chapter 5, we implement the other main objective of the task, the geometric optimization of the steel structure. The solutions will be analysed, compared and conclusions will be drawn.

2.6 The sample structure | Malaysian Grand Prix Grandstand Tower roofing

As I mentioned in the introduction, the source of the idea for this project is a field covering at the Sepang International Circuit motor racing circuit in Malaysia. The grandstands next to the track have several designs. In addition to tarpaulin field covers, there are also trapezoidal plate covers with a double-layered grid structure. The sample structure is provided by the tensile membrane covers, including the hibiscus-shaped roof structure of the Grandstand tower.



Figure 16: The iconic grandstand of the Malaysian Grand Prix: the Grandstand tower [27]

The structure is basically a tensile membrane braced by steel beams supported on reinforced concrete column. Given that very few plans of the structure are available, the dimensions are estimated proportionally. The main column of the tower is a cylindrical reinforced concrete core, roughly 6 m in diameter and 2 layers of reinforced concrete up to 15 m high. A spiral staircase runs upwards between the two layers. On the top of the thicker layer of the column there is a steel ring from which the main beams are used to stiffen the tarpaulin structure radial direction. Another steel ring is also placed on top of the inner layer. The roof structure consists of 16 beams, point-symmetrically, distributed radially. The beams are 21.4 m long I-sections

of variable height. The I-sections have also been extended at the outer ends in a branch-like triple spacing. However, the beams are not cantilevers, they are also supported at the point of extension by suspension rods connected to the upper steel ring of the column. Between each beam there are braces of equal curvature in concentric distribution.



Figure 17: The space covering from above [27]

The structure and all the stands were built in 1995. In 2016, the tarpaulin of the tower was replaced, which meant the replacement of around 4,800 square metres of fabric. The tarpaulin type is Verseidag PVDF TXA, a PVC-based membrane material, which has the strength of maintaining its colour well while having above average light transmission capability. [27]

In *Figure 19* we can see the fabrications of 5 different types of awning elements for the roof's membrane. Only the first design was used to cover the tower (with slight differences) to achieve a circular geometry. The edge points of the circular section are connected to the branch-like extension's points of the main beams. At the free edges, 16 mm diameter flange cables were used to keep the edges of the material taut. [27]



Figure 18: Beams and their bracing [28]

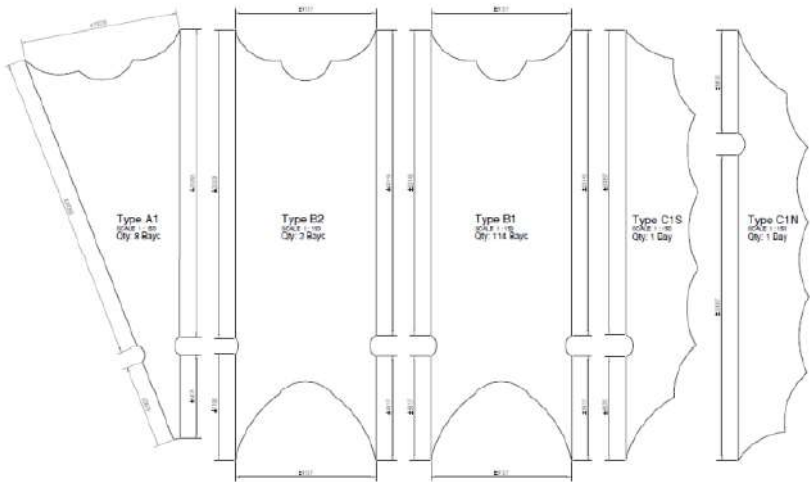


Figure 19: The segment types of the membrane [27]

As the structure is located in a fairly flat environment, it is often exposed to high winds. Therefore, the deflections of the membrane are high, while the steel framing's movement is quite limited. The designers are proud that its durability is proven and this option has been taken as the final solution instead of a solid option for its 30-percent weight. [27]

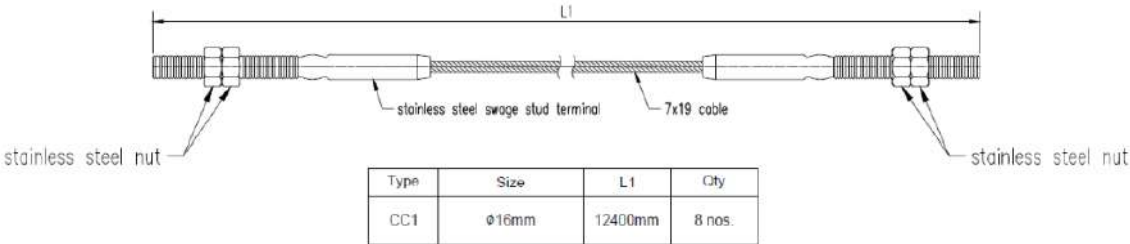


Figure 20: A type of perimeter cable which was used [27]

3. Geometry of the steel structure and the membranes

The geometric model was created using components based on the Grasshopper3D programming language. There are several reasons why this was chosen. Firstly, it is becoming a popular and commonly used environment in various design and research fields in the market over the last decade. It is oriented towards solving design problems, so you don't have to start the programming completely from zero. Due to its broader scope, its literature is also expanding exponentially, new fields are being added. It is also fortunate that more and more tools for numerical modelling are becoming available.

It is also possible to work with a code written in Python or C#, as Grasshopper3D has a dedicated component that translates one language to the other, providing a link between the two. I have used this several times because of the complexity of the task.

3.1 Building the parametric geometry of the steel structure

Essentially, the geometric model is a scaled-down replica of the original Malaysian hibiscus structure. It consists of points, lines and surfaces. To create these, I used various numerical and iterative components that form a data set. The individual data (coordinates of points, vectors, curves, etc.) are organized into data trees, which not only allow me to define the objects to be created faster, but also to manipulate the existing ones easily. The entire structure can therefore be instantly brought up or modified within the Grasshopper environment without any external data.

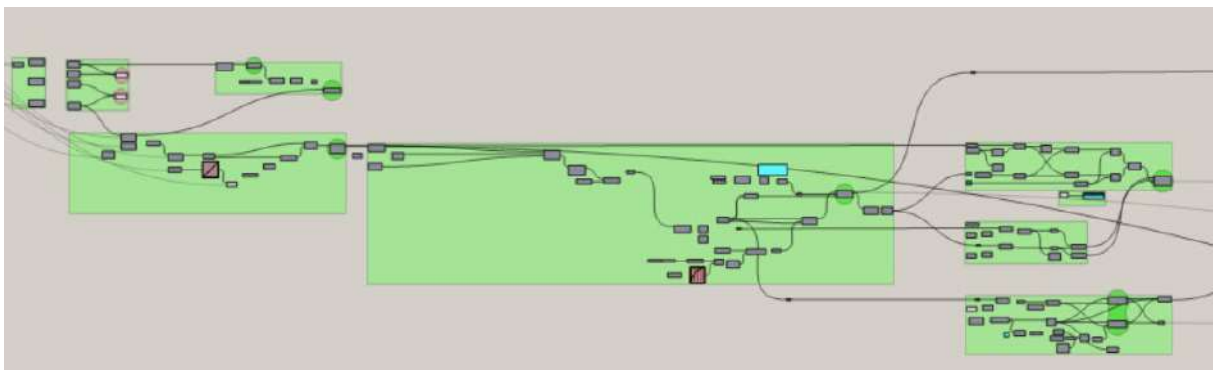


Figure 21: Geometry script

Inside the structure, there are predominantly linear elements, with which we start the modelling. The steel framing stands on a double-layer reinforced concrete column. It is created by starting the 16 main beams from the top edge of the external cylinder. The length of the main beams can be calculated from the radius of the entire roof. We place extensions at the outer ends of the beams which can be rotated 180 degrees around axes set up vertically from the end points.

The fifth points of the beams are connected in the annular direction by stiffeners. These form 4 rings, each of these stiffeners being defined as an arc of constant curvature (circular arc). Since the arches will play an important role in the stiffening and stretching the membranes, their geometry must be variable. The curvature of each arc increases as the radial direction approaches the origin. As in the original structure, V braces will be placed in the outermost ring, as well as inserted radially between every fourth main beam up to the column. The main beams are simply supported, not cantilevers, so they are suspended by rods at their endpoints. The other ends of the bars are connected to the top edge of the inner concrete core. These suspension rods are also supported by inclined rods (hereafter support rods), which in the case of the Sepang Hibiscus roofing are probably intended to increase the resistance of the suspension rod to deflection in the case of high wind uplift. These rods are tensioned between the inner supports of the main beams and the third decimal point of the suspension rods.

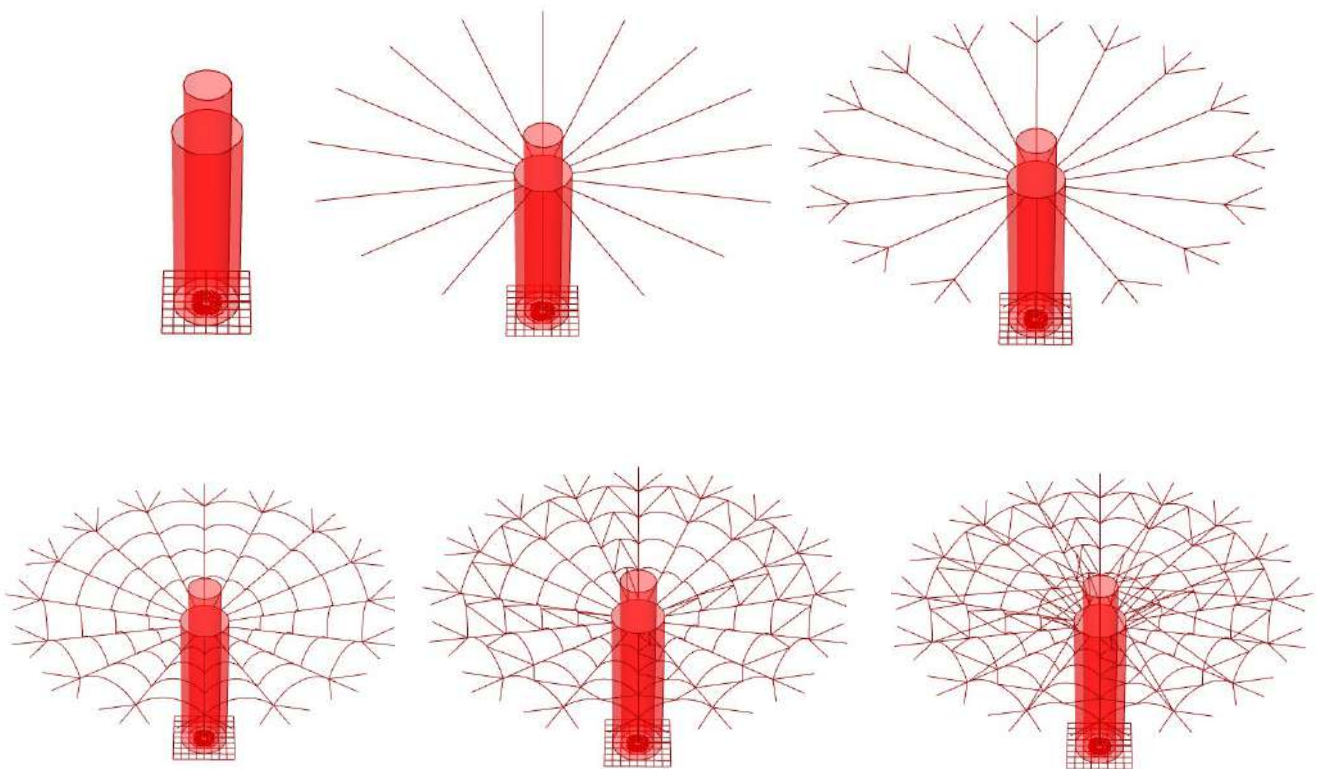


Figure 22: Defining the umbrella-like steel structure

During the definition, it was not yet clear exactly which geometric values would be the parameters to be searched for and which values were already known or predefined during the further computational processes. Thus, the written script is basically constructed in such a way that it can influence the shape of the canopy structure and initial surfaces, their individual extents, in a very large number of ways. Examples include the curvature of the main beams, the pitch angle of the roof or the height of the upper supports and thus the internal cylinder column.

3.2 Form-finding

The geometry of the structure continues with the production of the surface elements. The shape of a membrane is complex and intricate, very dependent on the method of definition, boundary conditions, initial geometry and many other factors. There are many different methods to define these forms, whether it is a membrane or a rope structure.

3.2.1 Initial shape of the membrane

In order to use any form-finding algorithm, we need an initial geometry, so we first need to define it. A hibiscus structure is a so-called barrel vault or bumblebee type of membrane structure consisting of cuttings. Thus, between the main beams, membrane elements are defined to be connected indirectly. It is therefore necessary to generate surfaces whose shape will be interposed between the main beams, the ring of the inner column and the outer cables at the ends of the splices. The length and shape of the cables also require a form-finding method so we need to add line elements to the initial shape.

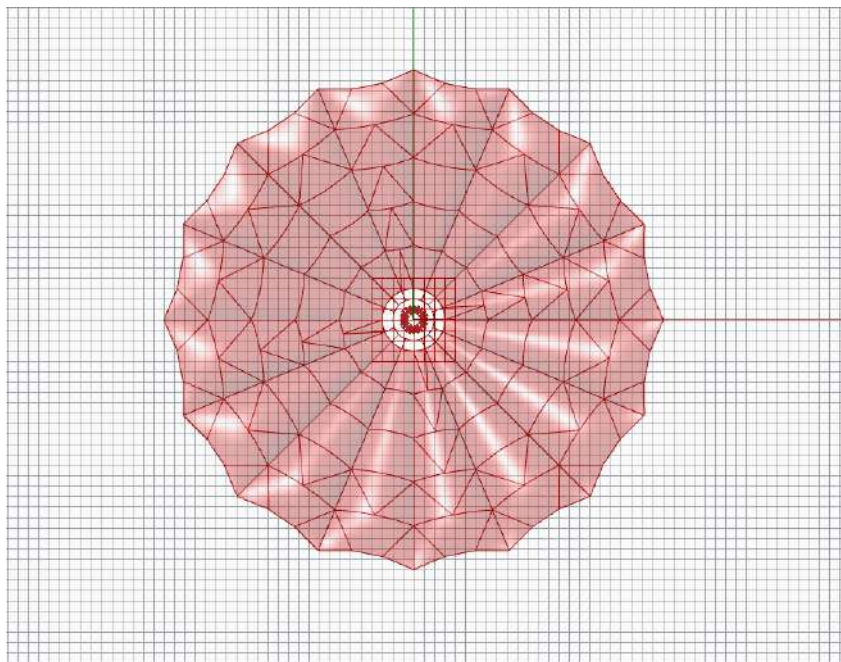


Figure 23: Initial geometry of the membrane

A surface is then created for each beam span, the curvatures of which are determined by the bi-directional interpolation between axes of the cables, main beams and the arch stiffeners. (*Figure 23*)

In the model, two main form-finding methods will be used: the force-intensity method and the dynamic relaxation method. The first one allows us to directly use force-like quantities as both input and output data, which can later be used for the analysis of the steel structure. With the second algorithm, we will generate a shape based on a different principle and calculation, then

compare them and make conclusions. Before applying, let's look at the principle of these methods.

3.2.2 Background of the force density method

The plugin used is called BATS (Basic Analysis of Taut Structures), which is a form-finding and analysis plugin for tensioned structures based on the natural force density method. Its developers are Dr. Ruy Pauletti and M arcio Sartorelli from the University of Sao Paulo.

The Force Density Method (FDM) is a shape search method that estimates a continuous surface shape from a mesh of linear elements. The Natural Force Density Method (or NFD) is a further development that preserves the linearity of the original method, but can go beyond its limits, for example in terms of its operation on non-regular meshes. [21]

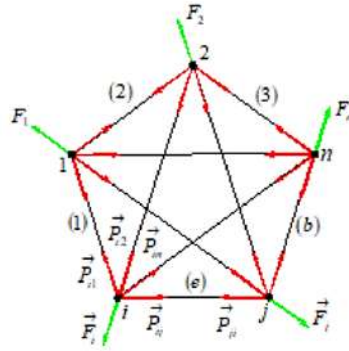


Figure 24: Internal and external forces in the cable network [21]

Force Density Method

The force intensity method is based on the equilibrium of points in a cable network. The resultant of the internal forces acting on *node i* can be written as follows [21]:

$$\vec{P}_i = \sum_{j=1}^n \vec{P}_{ij} = \sum_{j=1}^n N_{ij} \vec{v}_{ij} \quad (3.1)$$

Where N_{ij} is the force that can be interacted between *nodes i* and *j*, while \vec{v}_{ij} is a unit vector pointing from *i* to *j*. By defining a force density value n_{ij} (3.2) for each element in (3.2), the system of linear equations can be written in terms of $3n$ equations and easily solved using the boundary conditions (3.3) [21]:

$$n_{ij} = \frac{N_{ij}}{\|\vec{x}_j - \vec{x}_i\|} \quad (3.2)$$

$$\sum_{j=1}^n n_{ij} (\vec{x}_j - \vec{x}_i) = \vec{F}_i \quad (3.3)$$

Equation (3.3) can be rewritten into a different form by introducing several other definitions and interpreting certain vectors as elements:

$$K_d X = F \quad (3.4)$$

where K_d is the force-intensity stiffness matrix of a system. (See source [21] for more details)

Natural force density method

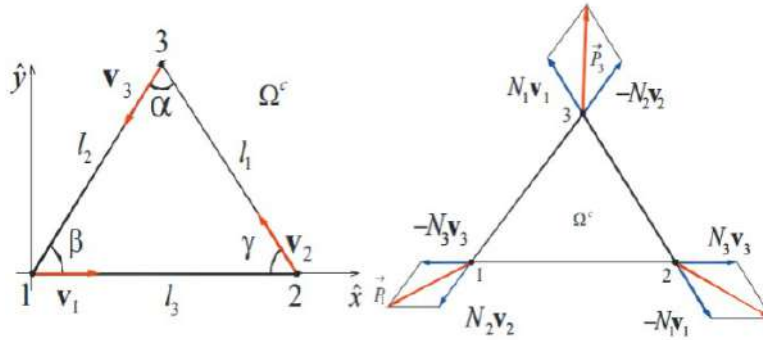


Figure 25: A membrane finite element's unit vectors and internal forces [21]

Natural force densities are derived from forces defined at the boundaries of membrane finite elements. To define the internal forces, it is useful to define the vectors of the natural forces N_i perpendicular to the opposite sides. The relationship between the internal forces and the N_i vectors can be written down from *Figure 25* [21]:

$$p = \begin{bmatrix} p_1 \\ p_2 \\ p_3 \end{bmatrix} = \begin{bmatrix} N_2 v_2 - N_3 v_3 \\ N_3 v_3 - N_1 v_1 \\ N_1 v_1 - N_2 v_2 \end{bmatrix} \quad (3.5)$$

After some algebra, each N value can be rewritten to the following definition:

$$N = VL^{-1}T^{-T}\bar{\sigma} \quad (3.6)$$

Where $V = t^*A$ is the volume of the element, L is a diagonal "length" matrix and T is a transformation matrix. Applying the natural force density $n_i = N_i / l_i$, the equation can be written:

$$n = \begin{bmatrix} \frac{N_1}{l_1} & \frac{N_2}{l_2} & \frac{N_3}{l_3} \end{bmatrix}^T = VL^{-2}T^{-T}\bar{\sigma} \quad (3.7)$$

This determines the natural force density vector. We can also write a natural force-density stiffness matrix by n_i , whose sign is k_{nd} . The stiffness of a system of n linear and m triangular elements will be the sum of K_d and K_{nd} :

$$K = K_d + K_{nd} = \sum_{b=1}^n A^b T^b k_d^b A^b + \sum_{c=1}^m A^c T^c k_{nd}^c A^c \quad (3.8)$$

Although this linear procedure provides a functional and usable model for the examination of momentless forms, the use of natural force intensity alone is not suitable for achieving a uniform stress state surface. However, the process can be recursively used by applying equation (3.6) by assigning a constant stress field $\bar{\sigma}_0$ ($\bar{\sigma} = \bar{\sigma}_0$) and determining an iterative K stiffness. Of course, each step is applied to the new reference form. In the source [22] it is shown that the results obtained by this method indeed converge to a surface of minimum size. The Cauchy stress origins of the solution are equal to the second Piola-Kirchhoff stress origins, which is an

analogous solution of a mathematically described minimum surface analogy, the soap bubble analogy. The natural force-density method is therefore able to determine minimum surface shapes in a linear approach, quickly and in relatively few steps. [21]

3.2.3 Form-finding with the force intensity method | BATS

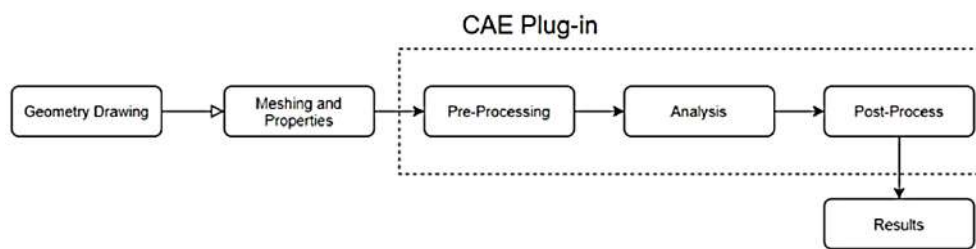


Figure 26: How the BATS plugin works in CAD [21]

The general working operation of BATS and other similar plug-ins in CAD-type programs is illustrated in *Figure 26*. The geometry written in grasshopper3D must have line and surface elements. These are discretised, and the size of their resolution affects the shape of the result as well as the computation time.

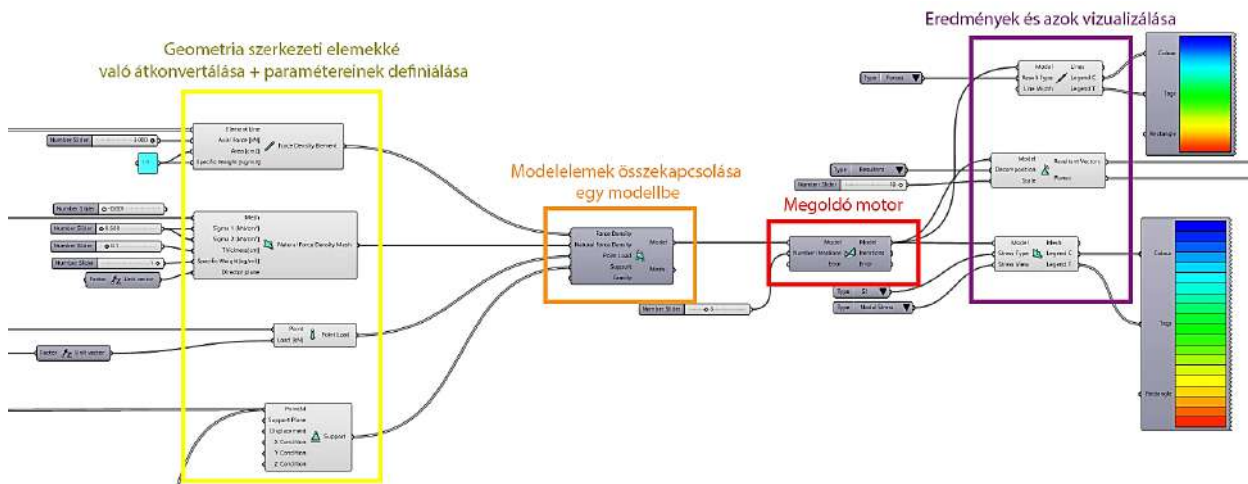


Figure 27: Form-finding script for the hibiscus tarpaulin by BATS

The data are subsequently processed. Depending on the software configuration of the finite element packages, there may be pre- and post-processing before and after analysis, then the results are returned to the CAD environment. These can be referred to later on or used for other processes. We can also check on the results with a quick hand calculation due the visible inner forces or the resultants of the supports.

In our model, we define the elements which are necessary for the calculation from the geometric data. The cable elements running along the outer boundaries of the roof are modelled as Force Density (FD) elements, and the meshes of each membrane partition are modelled as Natural Force Density (NFD) elements. The supports on the branches, arch braces and at the end of the main beam spans are defined as point supports. In all three directions they are considered to be fixed.

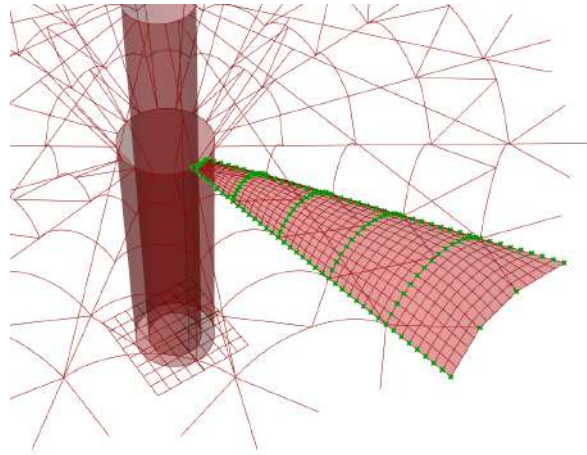


Figure 28: Defining the membrane supports

For the calculation, we include commonly used quantities on the market for thickness, cross-section, specific gravity and other data. We assume a membrane thickness of 1mm and a cable cross-section area of 1.17 cm². For now, we basically want to calculate a pre-stressed shape, so we do not define any external load on the structural elements. The elements are combined into a structural model as shown in *Figure 27* and the calculation is performed on this model using the solver engine. We set up the iteration and after the run the results for the supports, cables and membranes are retrieved separately.

The question arises, what mesh resolution and therefore what number of cable elements should we use? The runtime is very short, practically within milliseconds, thanks to the linear approach of BATS described above. Therefore, it would be a legitimate idea to increase the mesh resolution as much as possible, approaching the theoretical surface of the real mesh structure as closely as possible. However, the reaction vectors from the form-finding will be further used in another finite element program to analyse the steel structure. However, for the main beams, boundary elements and rods - as it is recognised later - won't be necessary to use an excessively large number of elements.

The original barrel-vault structure is stretched by a cable, which gives it its final shape. The amount of pre-tensioning force in the cable can be measured in many ways. We approach it from the point of the cable's inward deflection. A well-known formula, used for centuries, is the catenary formula, of which there are several variants. In this case we can use the version describing the reactions of a two-strand cable with constant load intensity and a prescribed deflection:

$$S_{\max.v} = \frac{p \cdot L}{2}, \quad S_{\max.h} = \frac{p \cdot L^2}{8f} \quad (3.9)$$

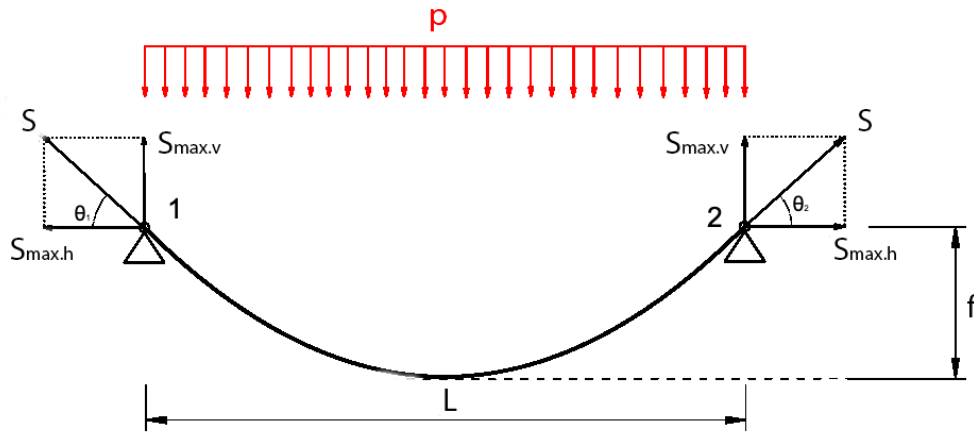


Figure 29: Rope structure's reactions under equally distributed load

where p is the load intensity, L is the distance between the two supports, and f is the deflection of the structure.

The membrane is also under tension after the rope structure is stretched. It is assumed to be around 1 kN/m (in both directions), which is common value in the industry. This can be equated to p , as the distributed load transferred from the membrane to the rope. The magnitude of the inward deflection can be inferred from the dimensions of the original structure, which is taken to be 1 metre . By averaging the distances of the cable supports, the magnitude of the reaction force can be calculated, which is equal to the magnitude of the prestressing for this amount of inward deflection and prestressing:

$$S_{\max,h} = \frac{p \cdot L^2}{8f} = \frac{1 \text{ kN/m} \cdot (3,20 \text{ m})^2}{8 \cdot 1 \text{ m}} = 1.28 \text{ kN} \quad (3.10)$$

$$S_{\max,v} = \frac{p \cdot L}{2} = \frac{1 \text{ kN/m} \cdot 3.20 \text{ m}}{2} = 1.6 \text{ kN} \quad (3.11)$$

$$S_{\max} = \sqrt{S_{\max,h}^2 + S_{\max,v}^2} = \sqrt{1.28^2 + 1.6^2} = 2.05 \text{ kN} \quad (3.12)$$

Giving the cable a 2.05 kN preload, we run the form-finding analysis. The run starts with a 9×25 mesh. In this case, 5-5 edges will be placed between each arc support radially, while the cables will also be equally composed of 3-3 cable elements. 10 iterations of the simulation are performed.

The principal stresses, cable stresses, form and support reactions are visualized on the selected membrane circular sector in *Figure 30, 31 and 32*.

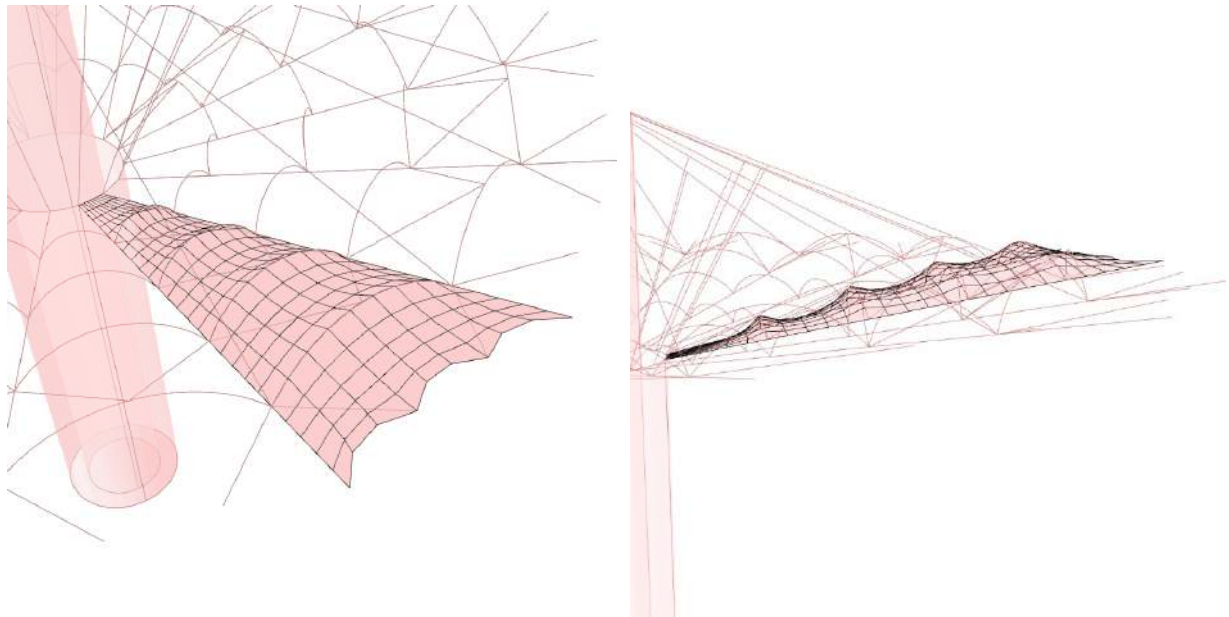


Figure 30: 9x25 membrane form after 10 iterations

After the calculation, we get the shape of the first 9x25 mesh. In the two opposite directions, we can see opposite curvature, which is a good sign, since this is the way of stabilisation of barrel vault type membrane structures. The membrane appears to be pulling the cables inwards, towards the origin of the structure, which was originally perfectly straight. The magnitude of the pull-in is 0.89 metres, at such a low resolution.

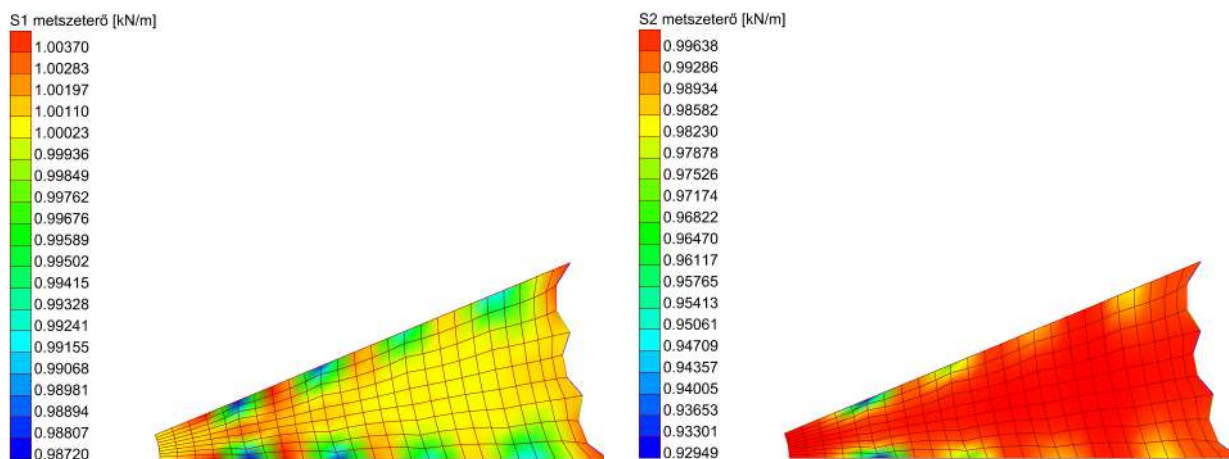


Figure 31: S1 radial and S2 perpendicular membrane forces

S1 is the radial direction, S2 the ring direction. It can be clearly seen that in both directions, the membrane forces are retrieved and the nodal point values are close to 1 kN/m everywhere. The value and distribution of the forces are influenced by the geometry of the edges and of course by the distorted shape of the mesh. In the ring direction, the distribution can be described as constant except for the nodes where the supports work in two different directions (the connection points of the arch support to the main beams). In the radial direction there are smaller differences between the mean values and local minima, which are also concentrated at the nodes

just mentioned. In a few places the membrane force increases above 1 kN/m, due to the tension of the cable.

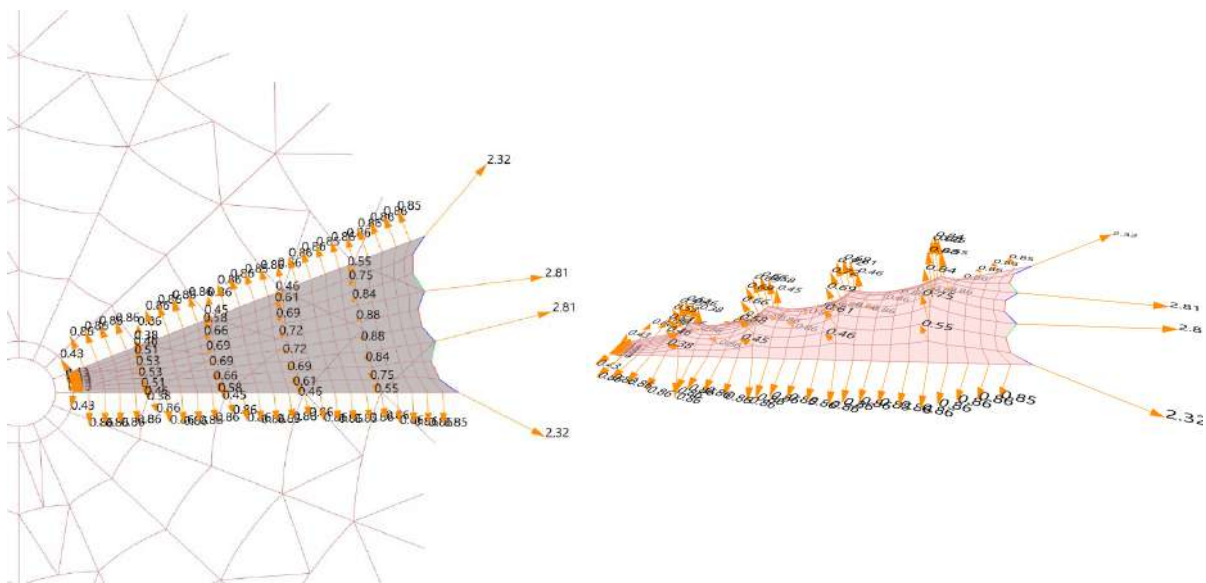


Figure 32: Reaction forces of the tensioned membrane

Figure 32 shows the reaction forces. In the radial direction, there are 4 intermediate supports on the main beams in the partitions between each arch support. In addition, half of the reactions at the connection points of the arches are loaded on one partition. This gives $4 \cdot 0,86 + \frac{1}{2} \cdot 0,86 \cdot 2 = 4,3$ kN as support forces. One partition is 4,28 m long, so $4,3$ kN / $4,28$ m = $1,005$ kN/m distributed load works in S2 direction on the main beams. This is nearly equal to the magnitude of the applied membrane prestressing, so the result is good. There are small magnitude vectors on the arch supports perpendicular to the plane of the initial shape, since the components parallel to the plane are practically balanced. At the supports of the ropes, the tension value is 2.05, 2.32 and 2.81 kN. The last two are obtained because the load transferred from the net is increased.

Load-case	Mesh resolution	Average mesh length [m]	Intermediate point deflection [m]				
			partition 1	partition 2	partition 3	partition 4	partition 5
pretension	9 x 15	1,00	0,3710	0,6166	0,4852	0,4698	0,4006
	9 x 20	0,94	0,4110	0,6968	0,5510	0,5337	0,3900
	9 x 25	0,83	0,3999	0,6807	0,5360	0,5171	0,3663
	9 x 30	0,71	0,3596	0,6817	0,5369	0,5044	0,3676
	15 x 20	0,68	0,4161	0,7017	0,5545	0,5367	0,4357
	15 x 25	0,60	0,4042	0,6847	0,5386	0,5171	0,3978
	15 x 40	0,52	0,4194	0,7165	0,5649	0,5389	0,3756
	15 x 50	0,43	0,4199	0,7185	0,5663	0,5384	0,3746
30 x 50	0,30	0,4216	0,7176	0,5661	0,5366	0,3748	

Table 1: Results for meshes with different resolutions

Let's examine the deflection and behaviour of the membrane with different mesh resolutions:

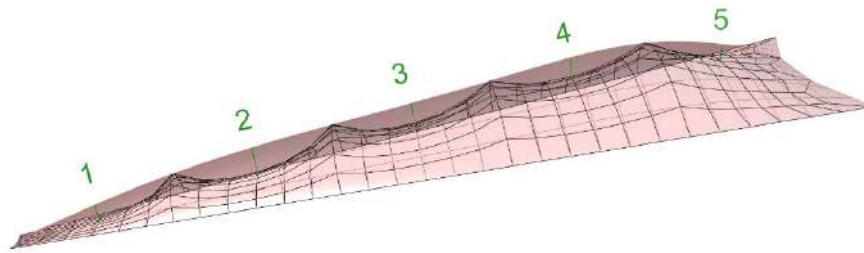


Figure 33: Deflections the centres of partitions

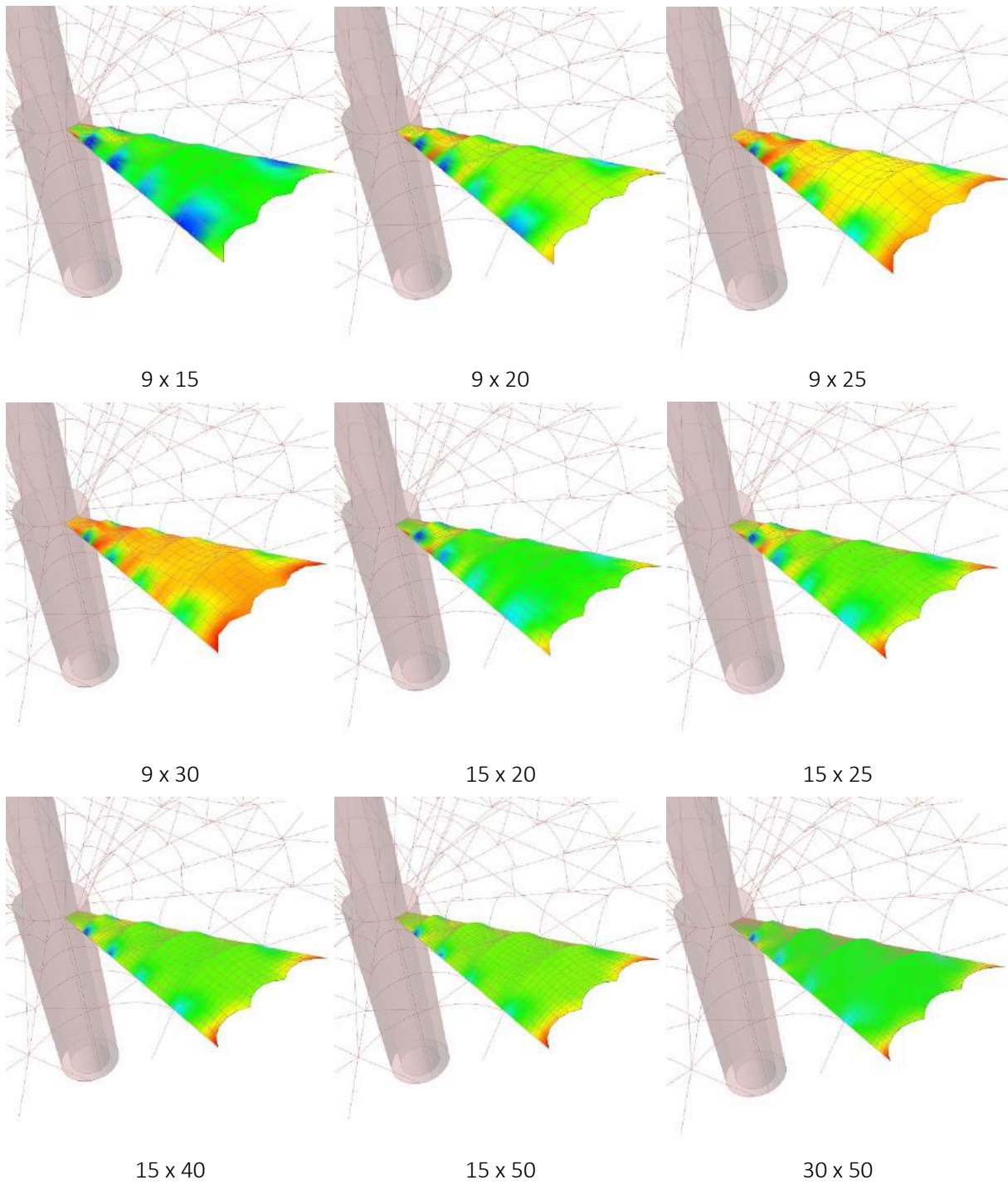


Figure 34: Found forms for the resolutions in BATS

The membrane is divided into 5 partitions using the arch supports. By examining the displacements of the intermediate points of these partitions, we find that, regardless of the resolution number, the shape characteristics obtained by the force-density method are very similar. A larger mesh is nevertheless recommended, as the more accurate form will be accompanied by a more accurate shape of the cable structure. The internal forces obtained during the run are almost identical each time, as the integral of the support forces is identical along each support line.

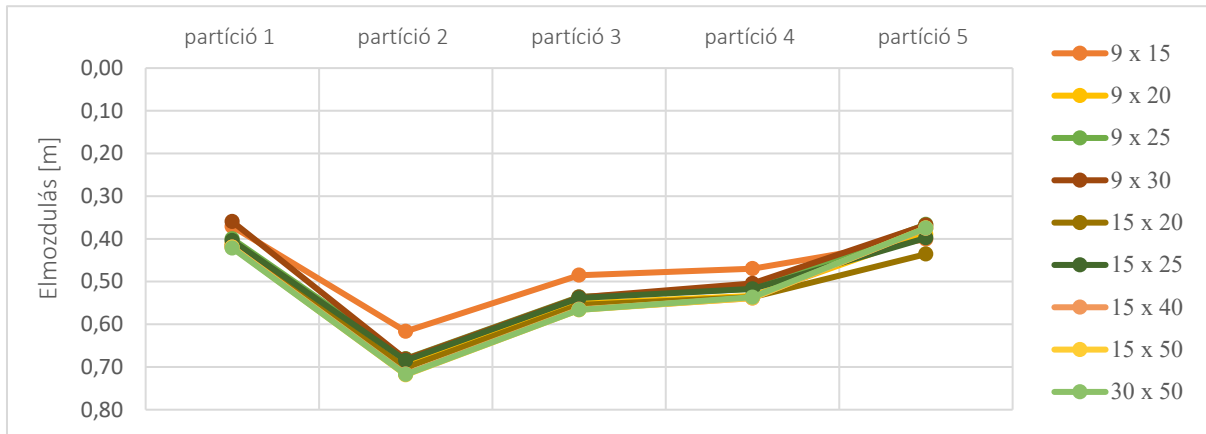


Figure 35: Deflection characteristics of intermediate points

The computation time is always measured in milliseconds. Even when changing the arch stiffeners, main beams or any other geometric elements, we always got a quick result thanks to the fully parametric script and environment. This feature will be exploited more in future processes.

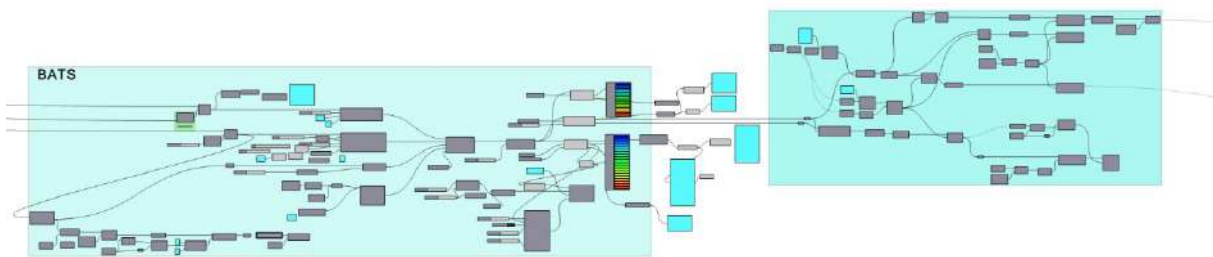


Figure 36: Visual script for force-density form-finding (*available in appendix*)

3.2.4 Background of Dynamic Relaxation Method

The dynamic relaxation method is a numerical method of shape determination that is well suited for solving the nonlinear systems of equations that arise in such cases. It is suitable for the analysis of large displacements and elongations if the structure used is sufficiently discretized. It is also capable of calculating large structures with relatively small computational requirements. [23]

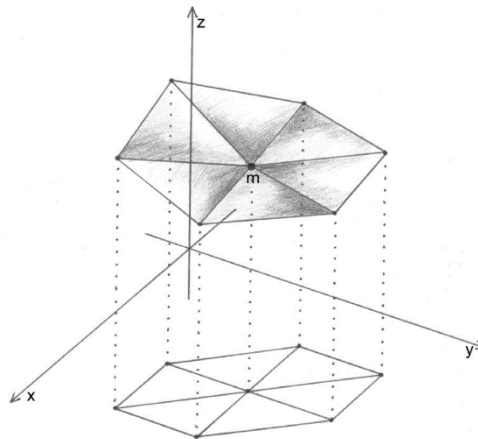


Figure 37: Step of coordinate calculation for a node [23]

Fictitious masses are placed on the structure under test and are set in motion by unbalanced forces acting on them. The method was pioneered by Day and Barnes, but since then a number of researchers have approached the technique from different perspectives. Gáspár and Hincz present a method where the plan projections of triangular meshed membrane's nodes have a fixed position in the search for an equilibrium shape. The program defines the fictitious masses at the vertices of each triangular element and reduces the prescribed internal forces in these nodes. The internal stress can be given in two ways: 1. constant for the real membrane forces (the soap-box analogy), 2. constant for the internal forces reduced to the horizontal plane. [20]

According to Newton's second law, unbalanced forces set fictitious masses in motion, resulting in an oscillatory motion. The kinetic energy of a mass point in an oscillatory motion is at its maximum when it passes through the equilibrium point, since no force is acting on it. Each point on the surface being analysed reaches this equilibrium point at a different moment. At certain times, by calculating the total structural kinetic energy, local maxima are found. By applying kinematic damping, the velocity of the structure's points is reduced to zero and convergence towards the equilibrium state of the whole structure is obtained. This requires the use of the appropriate time step and mass quantity. In these calculations, linear equations of one unknown are solved. The shape of the resulting equilibrium surface is highly dependent on the boundary conditions and the required stress distribution.

Solutions published by other researchers have also been published, such as the method of Gosling and Lewis, where the stiffness matrix of the structure is used instead of calculating fictitious masses. [20]

Dynamic relaxation has long been a popular method for calculating large displacements. Its computational complexity is relatively small and usually convergent. It avoids the solution of ill-conditioned systems of equations that are typical for membrane structures. [23]

3.2.5 Form-finding with Dynamic Relaxation Method | Kangaroo

The second program we use for form-finding is Kangaroo. The Kangaroo form-finding software works on the principle of minimizing total energy. The so-called targets in the software contain energy definitions that are zero under certain geometric conditions. Kangaroo's solver iteratively moves the freely movable points of a system so that the sum of the energy interpreted at the system's points is minimized. As an example, the target *length* behaves as a spring interpreted by Hooke's law, whose energy is zero when it is free and relaxed, but changes when it is under tension. [24]

If the objectives do not conflict (let's say starting from an arbitrary quadrilateral with angles of 90 degrees and equal lengths), then the solver acts as a solver of geometric constraints by extracting all the energy. In many cases, however, it is not possible to satisfy all objectives simultaneously (for example, in the case of bending a hanging cable, where the length and load objectives are "conflicting"). In this case, the solver finds the shape for which the total potential energy is the smallest possible. If the inputs and stiffnesses are set correctly, this can be a numerically accurate model of the elastic deformation. [24]

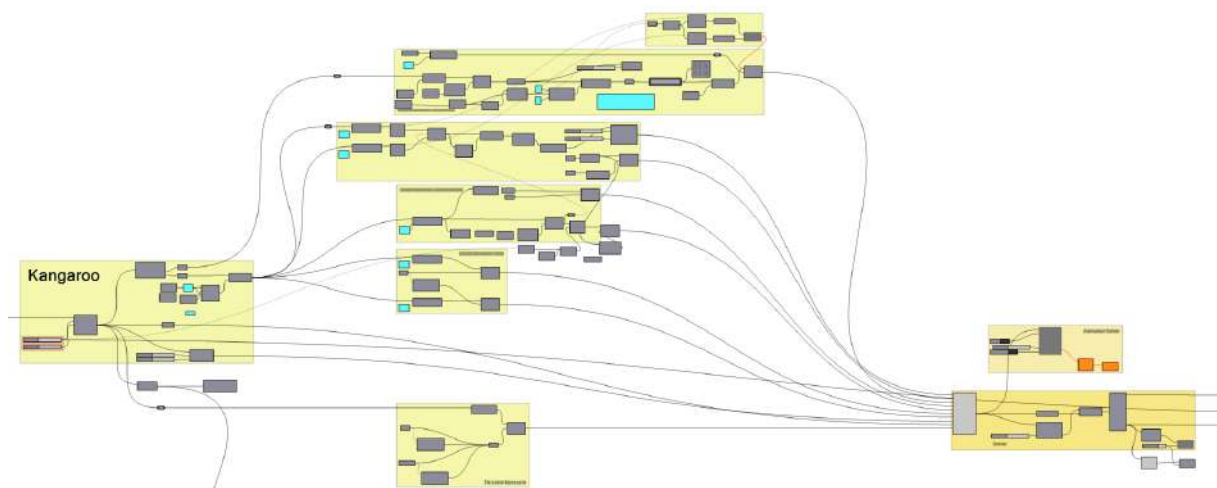


Figure 38: Full membrane visual script for Kangaroo form-finder (*the module is in the appendix*)

First, we define the supports here. Sliding supports are used on the main beam and arch supports, these can slide freely along a defined curve. However, they have a fixed stiffness in the direction perpendicular to the axis of the curve. The four outer corner points of the initial

shape are connected to the points of the fixed supports with infinite stiffness. Here, practically all factors influencing behaviour are given as a target in the simulation. These include the stiffness of the supports, the pre-tensioning and length factors of the membrane, or even the cable. For the membrane and cables, a prestressing of 1 kN/m and 2,05 kN is applied, as in the previous test.

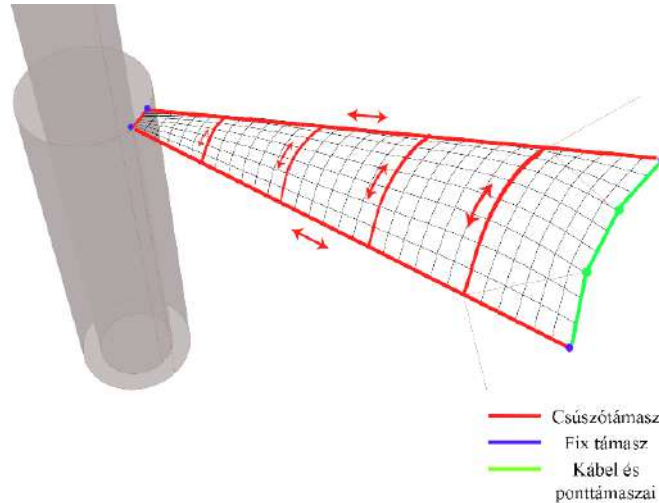


Figure 39: Applied supports

For each *target component*, a *length multiplier* between 0 and 1 is also specified, which represents the target length relative to the original length of the line and mesh elements. A multiplier of 0 is assumed for the length targets in all calculations. The computation is first performed with 10 iterations, and it is still a priority to use resolutions that are equally distributed in the radial and ring directions.

The following results were obtained:

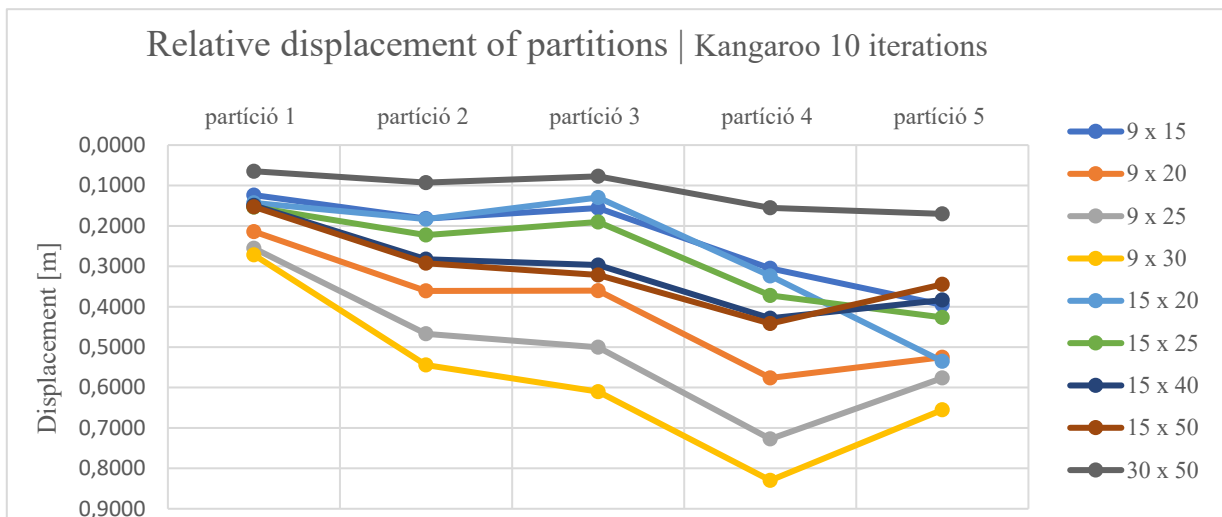


Figure 40: Characteristics of mid-point deflections under dynamic relaxation for 10 iterations

The characteristics of each resolution are similar, but there is a significant variation in the displacement values. The main reason for this is that different resolutions converge to the final shape at different iteration quantities. Since this is difficult to estimate in advance, the calculation is repeated from 1 to 100 looking at all iterations, and above 100 in steps of 10 up to 500. However, it is worth adding that this requires more attention than the previous method!

The smallest resolution is also around 80 iterations and the largest ones give a converged shape with nearly 300 iterations.

Mesh resolution	Average mesh length [m]	Number of nodes	Displacement of intermediate point [m]					Iteration	Run time [ms]
			partition 1	partition 2	partition 3	partition 4	partition 5		
9 x 15	1,01	135	0,0970	0,1408	0,1195	0,2368	0,2836	78	189
9 x 20	0,94	180	0,1401	0,2348	0,2324	0,3751	0,3468	100	290
9 x 25	0,84	225	0,1676	0,3071	0,3281	0,4771	0,3924	110	415
9 x 30	0,71	270	0,2091	0,4049	0,4513	0,6194	0,4776	120	515
15 x 20	0,69	300	0,0940	0,1203	0,0851	0,2130	0,3626	100	591
15 x 25	0,59	375	0,1657	0,3535	0,3602	0,4680	0,3858	130	935
15 x 40	0,52	600	0,1693	0,3758	0,3930	0,5470	0,4713	220	2052
15 x 50	0,42	750	0,2117	0,4104	0,4576	0,6275	0,4817	250	3890
30 x 50	0,30	1500	0,1903	0,3903	0,4261	0,5793	0,4688	290	11760

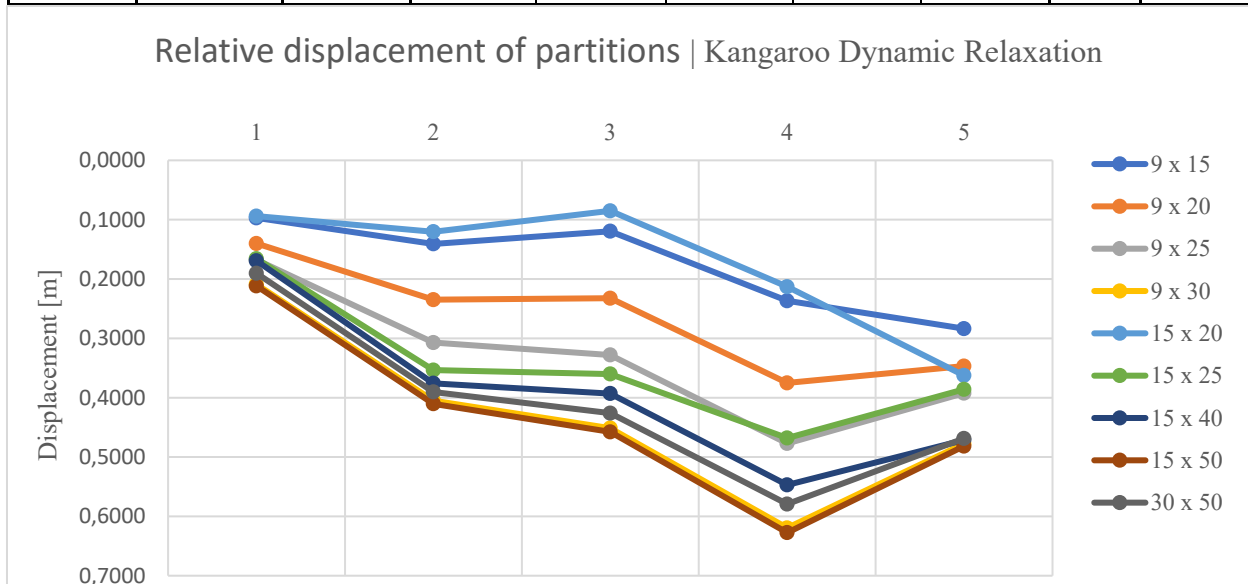


Table 2 and Figure 41: Displacements of converged shapes using the Kangaroo DR method

The standard deviation of the converged results is large. From *Figure 41*, we can see that for higher mesh resolutions, the converged values of each deflection are getting closer to each other. From *Figure 42*, it is very noticeable that the plug-in carries the tension into the membrane via the discretized cables, so that for higher resolutions, a higher specific tension

occurs (e.g.: in the radial direction). Therefore, the resolution is practically a design parameter here.

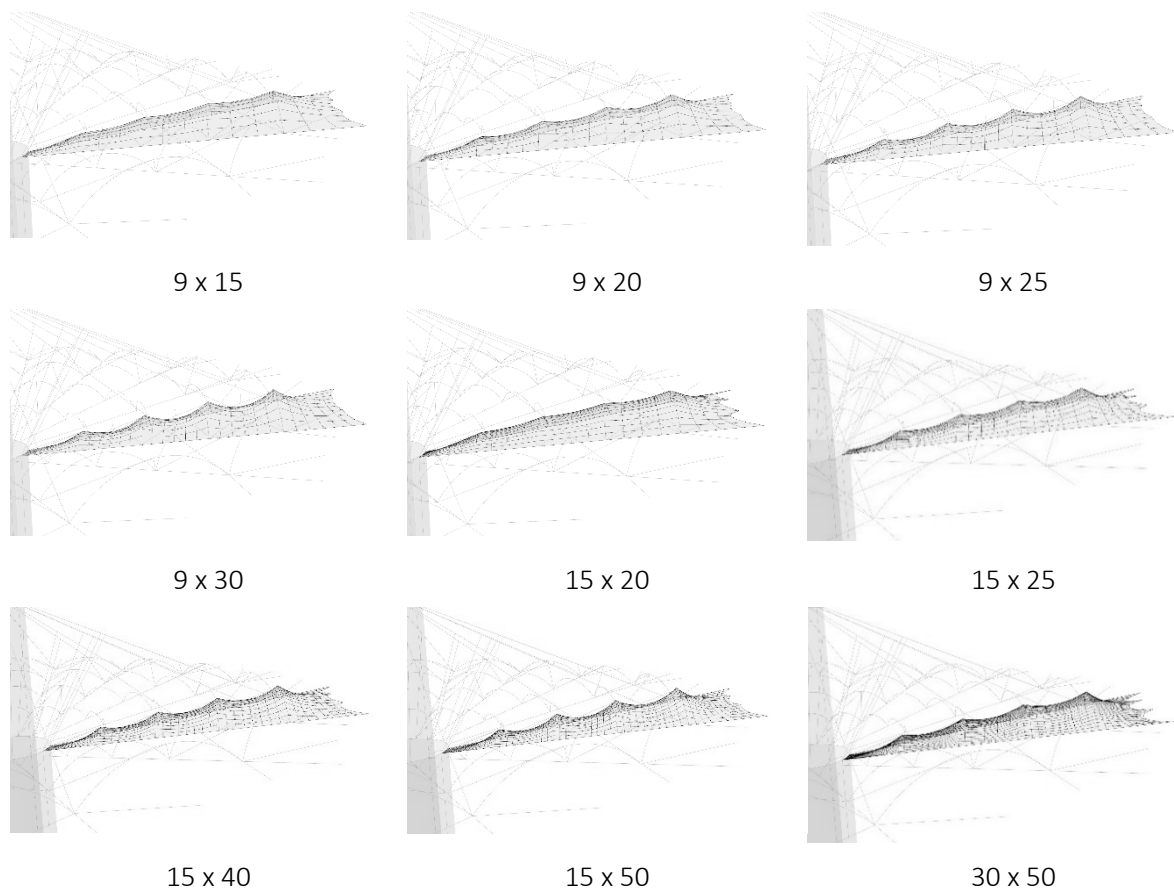


Figure 42: Shape of each resolution in Kangaroo

As we have seen in Table 2, the higher iteration and accuracy of Kangaroo also implies a non-negligible increase in runtime. It took the iterating solver almost 12 seconds to solve the 30x50 form.

3.2.6 Comparison and summary

In the previous sections, we have described the background of two form finding methods, and then performed simulations to determine the prestressed shape of a membrane sector. In form-finding, we can determine what effect we want to get the form of. We wanted to do this in the usual way for prestressing in tensile membrane design. We applied a deflection value to the edge cables at the edges of the sections, induced by the distributed stress in the membrane, for which we assumed a frequent membrane force value with a uniform stress distribution.

Using force-density based BATS, we could obtain consistent values for the displacements of the intermediate points of the intermediate intersection plane. A major advantage of the method was that the internal stresses/forces and the reaction forces on the supports could be traced and easily verified.

Kangaroo is a more complex plugin based on a version of the dynamic relaxation method. It has several modelling options and behaviour simulation components. But what it has the advantage in also has the disadvantage, as it requires the inclusion of several input parameters for simulation, such as the length coefficient, which is mandatory to include as a geometric objective, but its value is not completely clear. Also, the output of the calculation is in fact only geometry and coordinates.

Mesh resolution	Difference in offset between two methods [m]				
	p1	p2	p3	p4	p5
9 x 15	0,2740	0,4758	0,3657	0,2330	0,1170
9 x 20	0,2709	0,4620	0,3186	0,1586	0,0432
9 x 25	0,2323	0,3736	0,2079	0,0400	-0,0261
9 x 30	0,1505	0,2768	0,0856	-0,1150	-0,1100
15 x 20	0,3221	0,5814	0,4694	0,3237	0,0731
15 x 25	0,2385	0,3312	0,1784	0,0491	0,0120
15 x 40	0,2501	0,3407	0,1719	-0,0081	-0,0957
15 x 50	0,2082	0,3081	0,1087	-0,0891	-0,1071
30 x 50	0,2313	0,3273	0,1400	-0,0427	-0,0940

Table 3: Differences between the shapes of the two methods

From the results we can see that BATS has nearly equal deflections of the tarpaulin regardless of the mesh, while Kangaroo's deflections depend significantly on the size of the resolutions. In many cases there are differences of several decimetres between the two solutions. It is true that we are talking about a large space coverage, with 4.3 metres between each arch support, while the length of the branches is close to 24 metres. There is also a large, practically hundredfold difference in the calculation time, which in the case of more precise forms is many seconds. This is not significant for a one-off test, but will be needed later. In case of optimisation, for example, when hundreds of shapes are tested at the same time.

Mesh resolution	Running time	
	Kangaroo [ms]	BATS [ms]
9 x 15	189	3
9 x 20	290	5
9 x 25	415	7
9 x 30	515	9
15 x 20	591	9
15 x 25	935	11
15 x 40	2052	21
15 x 50	3890	25
30 x 50	11760	41

Table 4: Running time differences

The results obtained during the study were generated using a visual script I programmed all along, automatically loaded into Excel spreadsheets, which were then separated by a custom component written in Python. This also allows us to find fast but realistic forms for other edges, using varying main beams or arch number.



Force-density



Dynamic Relaxation

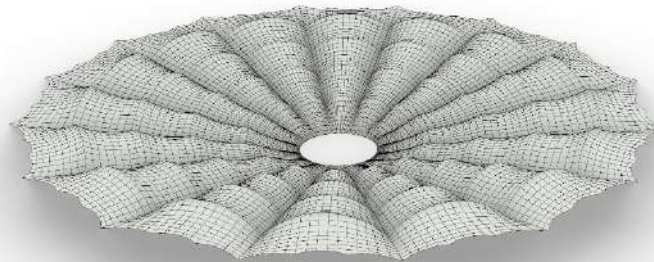


Figure 43: Full pre-stressed membrane structure

4. Parametric and reference model

Finite element analysis of the structure can be performed in a wide range of programs. The only requirement is that the Grasshopper plugin that establishes the connection provides a two-way and automatic flow of information between the environment and the software. This is because the geometry, load definition, meshing, material definitions and other parameters need to be set up the calculation from the script. At the end of the run, however, we require the data to be returned. In addition, reliable computation capability and communication speed, as well as a stable operation, are very important.

After trying AxisVM, Consteel, Dlubal, Oasys GSA and Karamba3D finite element softwares, I decided to do the parametric based computation with Karamba3D and the validation with one of the most popular FE software in Europe, Dlubal RFEM. A big advantage of Karamba3D is that it runs within the GH environment, therefore the computational speed for this kind of application is significantly fast. Its high-speed data processing allows data to be extracted in multiple constructs and formats. The reference model used for the complex nonlinear computation is built using Dlubal. It is used to verify the parametric model and to define the optimization conditions.

4.1 Parametric FE model

4.1.1 Model structure

The umbrella structure is supported by 21.4 m long main beams, which are arranged radially in the plan. There are 16 of them, I-sections of variable height in the original structure. In our model, we use continuous I-sections and straight-axis beams for simplification. The same simplification is used to define the extensions. In the original structure, the main beams are simply supported, at one end they are connected to a steel ring fixed to the reinforced concrete columns, while the other support (which is not at the very end of the beam) is connected to the

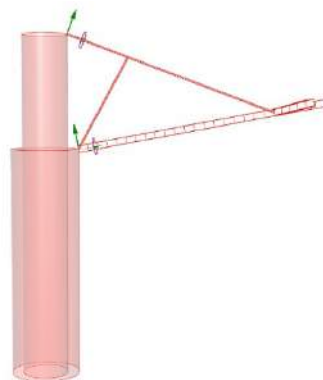


Figure 44: Main support structure

hanger rods. The hanger rods also have supports, which will be referred to hereafter as support rods.

In the analysis, we consider only the steel structure, so instead of finite element modelling of the reinforced concrete column (and the steel rings at the ends), we define point supports at the connection between the two different structures. The supports are restrained in their translation displacement and rotation about their axis.

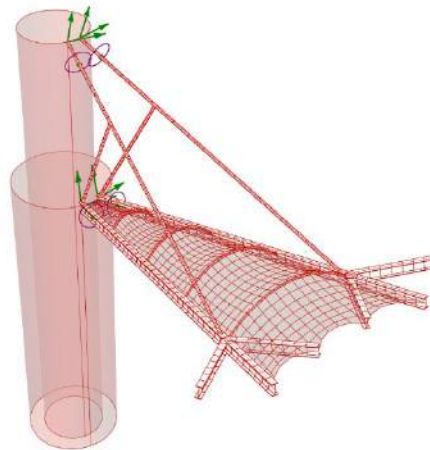


Figure 45: Part of the steel structure with membrane

The finite element resolution of the main beams and arch braces will depend on the resolution of the mesh of the membrane, because we want to transfer the loads from the prestressing at the points between the finite elements. For a 40x15 resolution we have seen in the form-finding chapter that the cable entanglement is nicely formed and the form achieves a decent accuracy while the computation time and capacity requirements can remain low. For this reason, the main beams are broken down into a total of 40 finite elements, 8-8 per partition. The arch stiffeners connecting them are made up of 2x15 equal to 30 elements. This is necessary because the V braces are connected to the centre of the arch braces in several places, so an intermediate node is needed.

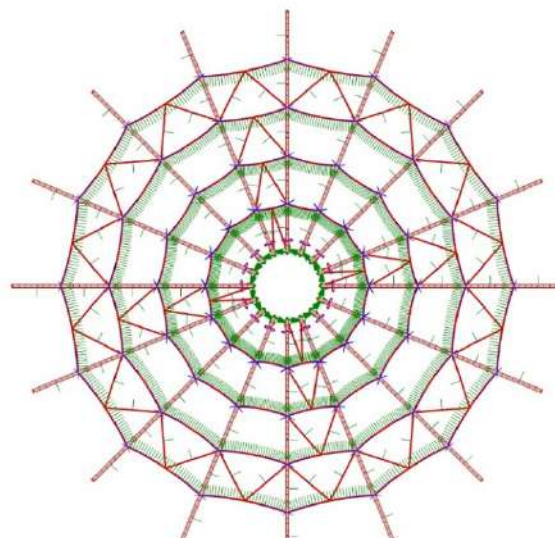


Figure 46: Bracing system

Practically all elements of the whole steel structure are defined as line elements. Due to the large span, the structural material is always S355. The initial cross-sections are taken as follows: main beams and extensions HEA600, arch supports, suspension rods, V braces CHS168.3x10. The main beams, their extensions and arch supports are actual beam elements, the V braces and suspension rods are taken as truss bars.

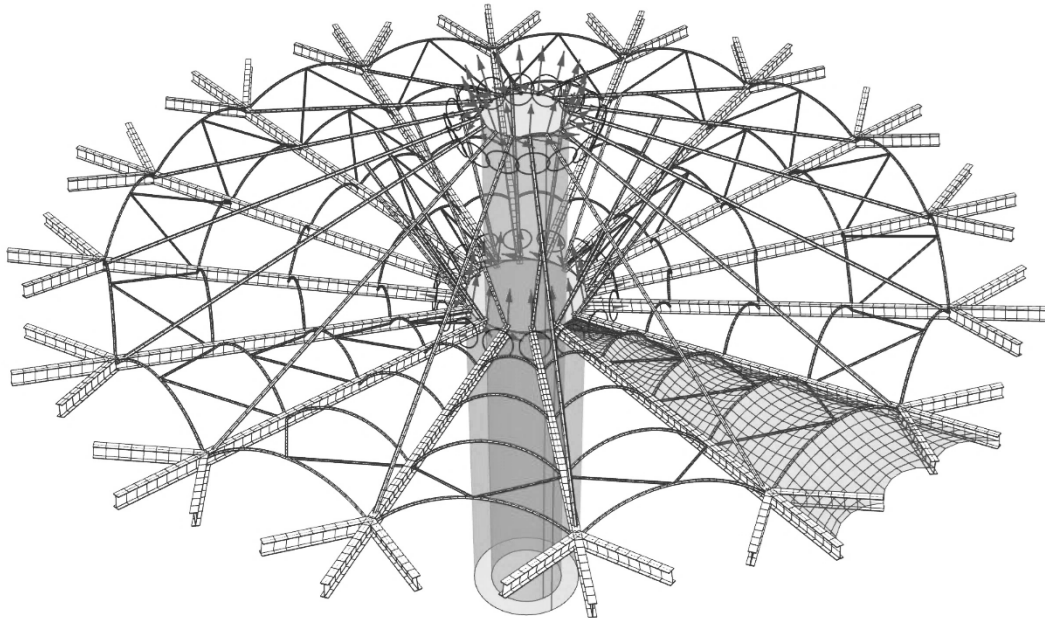


Figure 47: The whole FE model with the prestressed membrane geometry

4.1.2 Defining loads

During the form finding, we were able to run a calculation with fixed node supports. BATS and Kangaroo are plugins which are only capable of form-finding, we cannot use them to perform direct nonlinear analysis. This also means that the membrane and boundary structures - which otherwise work together and directly relate back to each other - must be included in the calculation as hierarchically related:

- The assumption is made that the loads on the membrane are hierarchically transferred to the solid structure, which carries them to the supports. We therefore use substitute loads

Attention must be paid to the fact that we do not know for sure if the preload meets different design criteria and if the membrane will not fail under external loads! Furthermore, the magnitude of the membrane forces, and therefore the stresses, must be positive, meaning that there must be tension everywhere in the membrane and cables. We also require 'realistic' displacements, i.e.: that the membrane moves by a finite displacement under external loads.

Each component is parametric, so later on, it will be able to predict the magnitude of the substitute loads for any size of membrane partition, fully automatically.

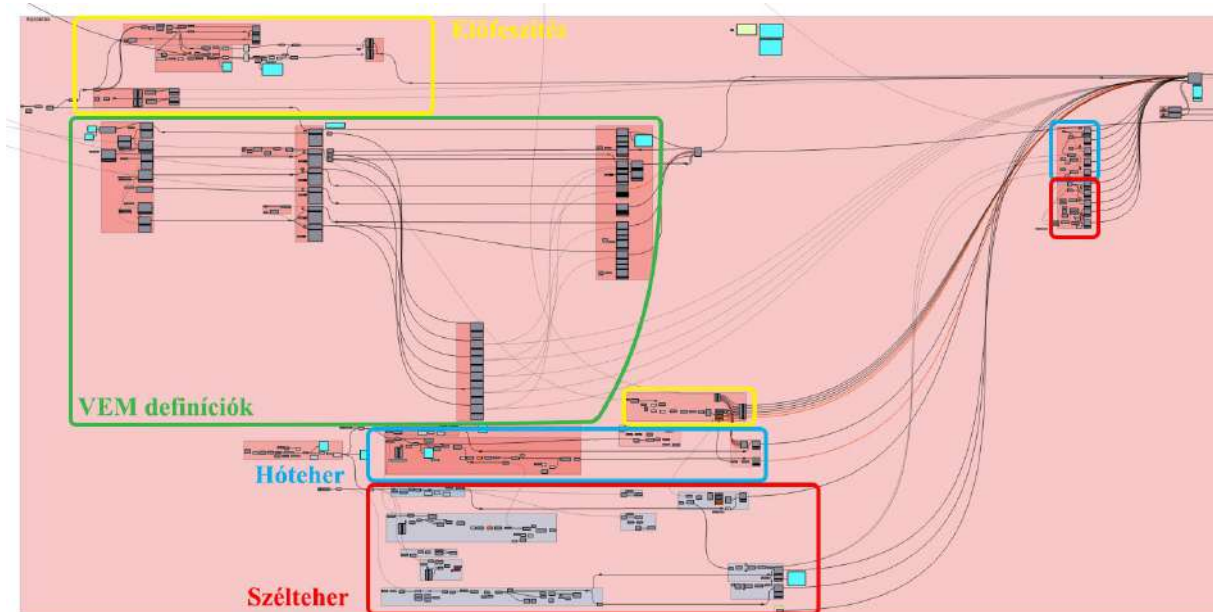


Figure 51: Automatic script for defining substitutonal loads (*available in appendix*)

4.2 Reference FE model

Before interpreting the computational results of the parametric model, the reference nonlinear finite element model is also introduced. The aim is to compare the results of the two analyses.

The model was built in Dlubal RFEM version 6.02. The steel structure geometry is fully identical to previous one defined in Grasshopper. The same initial sections and finite element resolution are used. For the material model we use the characteristics of products actually on the market, imported directly from the Dlubal library.

Name	Type of material	Material details	Elastic Modulus E [N/mm ²]	Shear Modulus G [N/mm ²]	Poisson's Ratio ν [-]	specific weight γ [kN/m ³]	Density ρ [kg/m ³]
S355N EN 10025-3:2004-11	Steel	Isotropic Linear Elastic	210000	80769,2	0,300	78,50	7850
Glass-PTFE Typ II	Fabric	Orthotropic Linear Elastic (Surfaces)	1220			10,50	1050
Cable PE (Pfeifer) Z-14.7-411	Metal	Isotropic Linear Elastic	130000	50000	0,300	80,00	8000

Table 5: Reference model materials

After the modelling the steel framing, we define the membrane partitions. There are multiple mesh types for modelling a membrane, like triangle, rectangle, NURBS or pipe. Because of the unusual geometry at the outer partitions, using quadrangle elements is a must for having a correct behaviour. To reach the full potential, the form-finding is performed on a significantly high-resolution quadrangle element mesh, using 66500 2D elements.

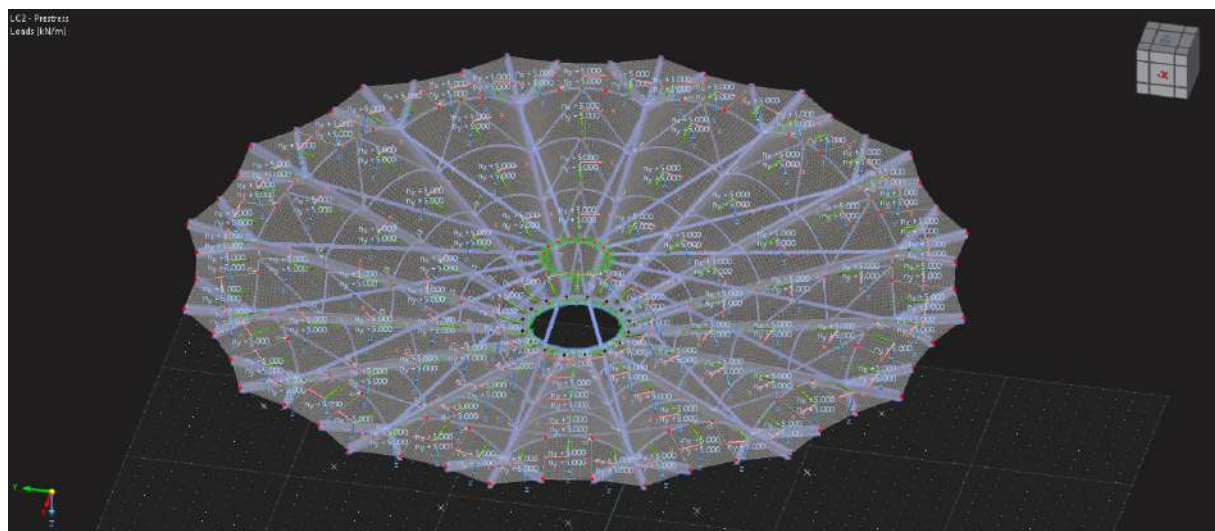


Figure 52: Reference model

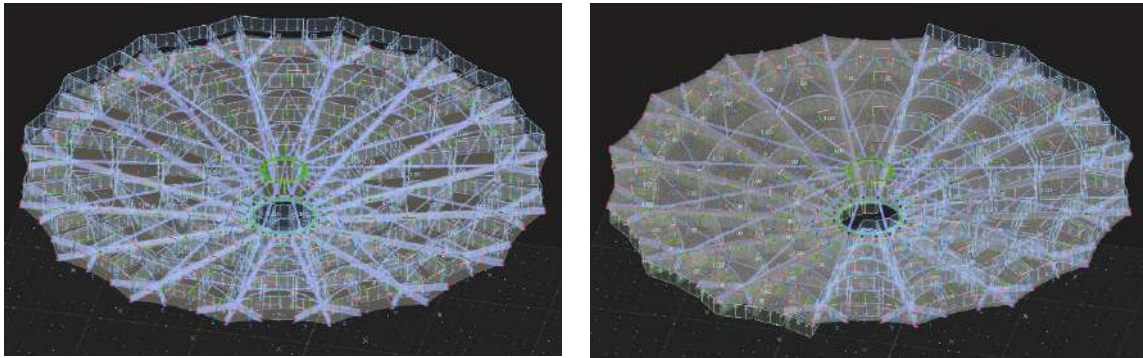


Figure 53: Snow and wind loads – reference model

Here, loads are defined as surface loads: projective loads in the case of snow, and local loads in the case of wind. Local load type is being used for the initial membrane form. The reason being that the wind which loads on a continuously moving form, could not converge once in a time step test even for a bigger iteration quantity.

The program offers several non-linear solvers for the calculation. For example, Picard method, which can be used alone or in combination. The computation is now performed using the Newton-Raphson iteration procedure, the form-finding is performed in 15 iterations and the nonlinear analysis in 100 iterations. The analysis of 1 combination took about 35 seconds in total.

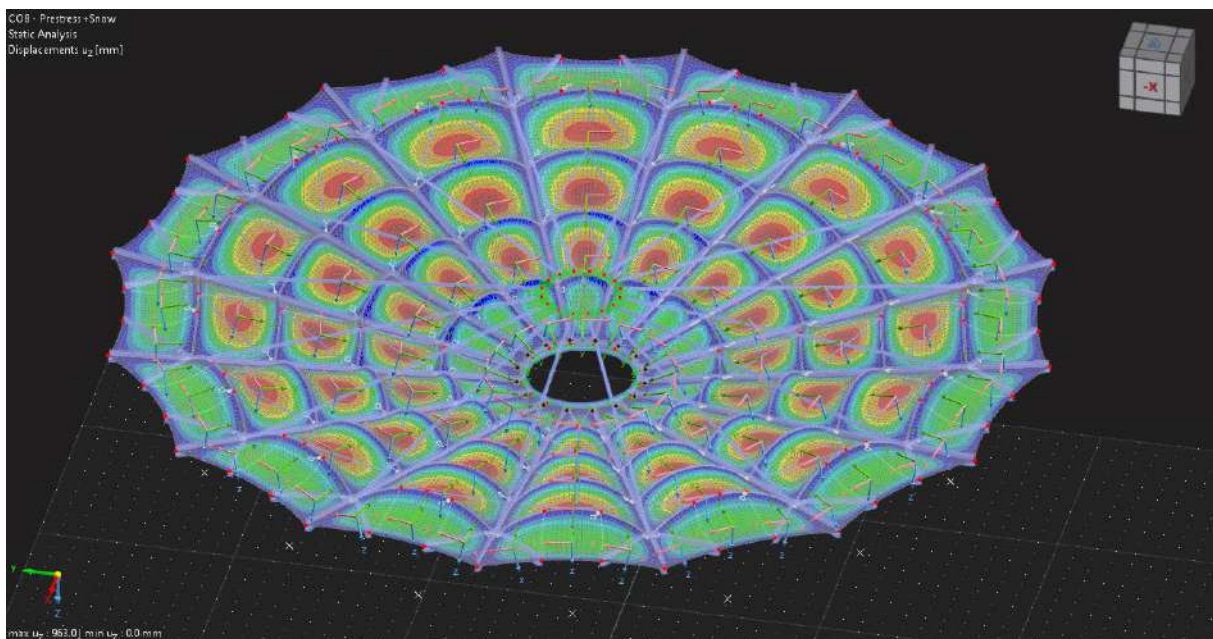


Figure 54: u_z local relative displacement of surface elements | *snow and prestressing effect*

In case of prestressing, the maximum relative deflection was 680 mm, for load combination 2 it was 963 mm. The critical value of the radial forces was 4.957 kN/m, while for the case combined with snow it was 5.69 kN/m (causing an increase of 15%). The difference in deflections and shear forces appear to be somewhat small, but it is worth noting that this is for relatively small partitions of 4.3 m.

Figure 56 shows that the radial membrane forces in the intermediate parts of the partitions have increased minimally or to a greater extent, while they have typically decreased compared to 5kN/m in the ring direction shown in Figure 55. Since the snow load acts down in the z direction, the forces and stresses in the upward hanging curves should be increased and decreased in the opposite direction. This is also the basis for simplifying the inclusion of approximate loads.

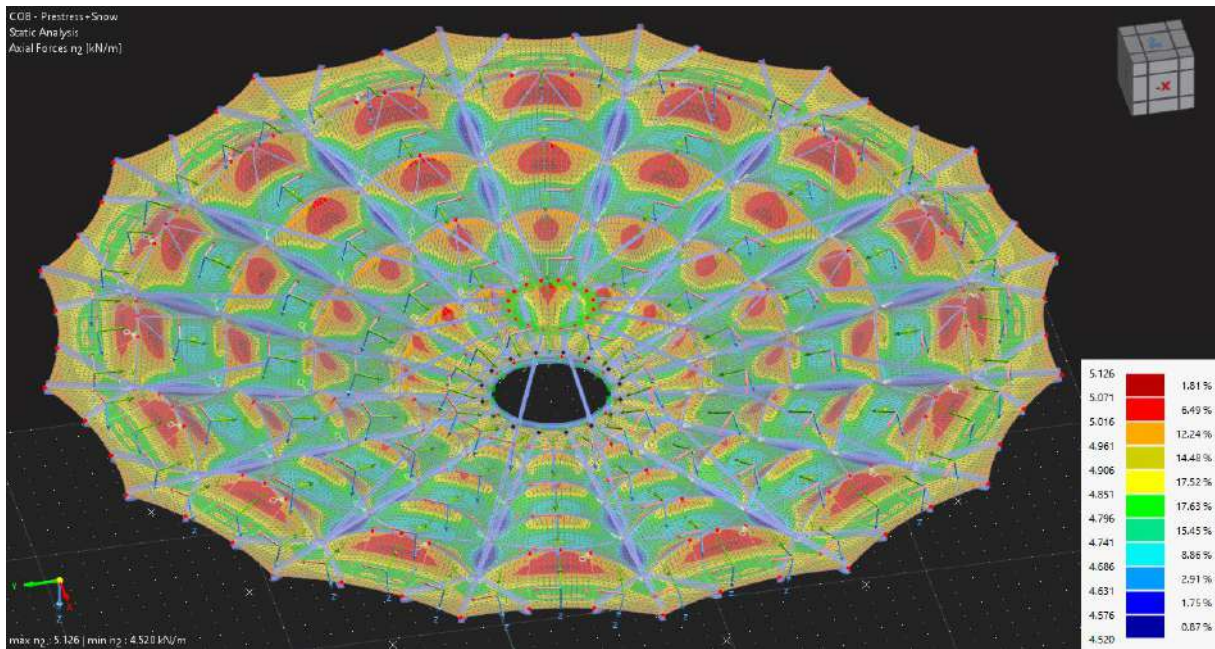


Figure 55: n_2 membrane forces in ring direction [kN/m] | snow and prestress loads

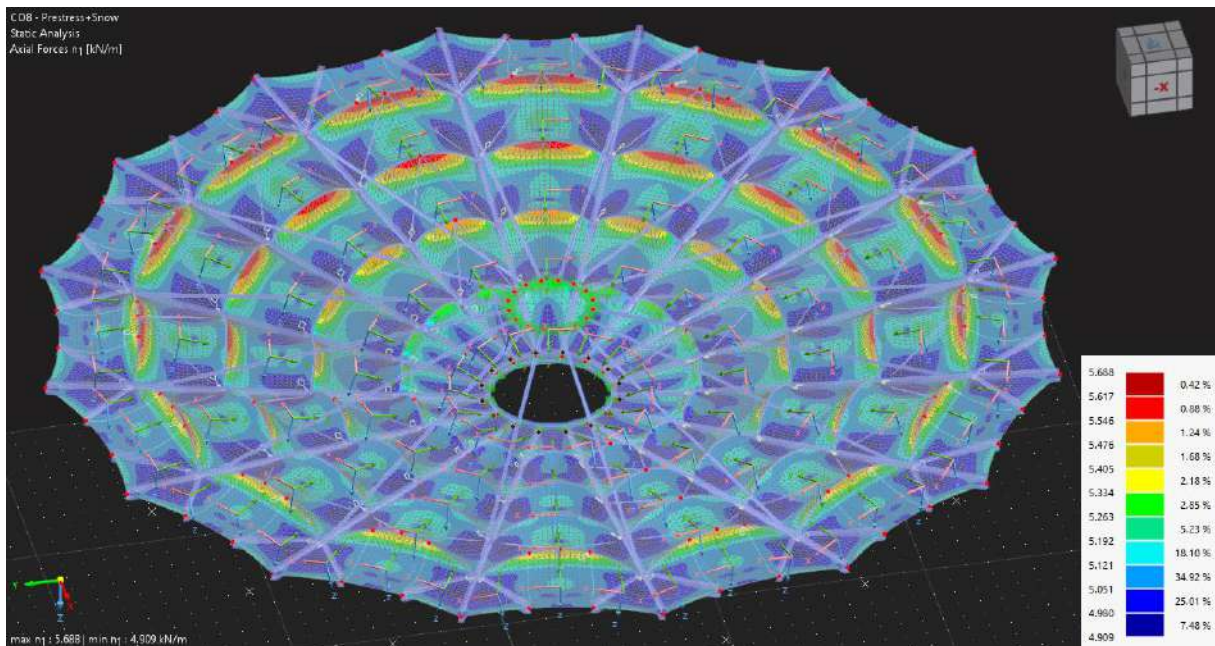


Figure 56: n_1 membrane forces in radial direction [kN/m] | snow and prestress loads

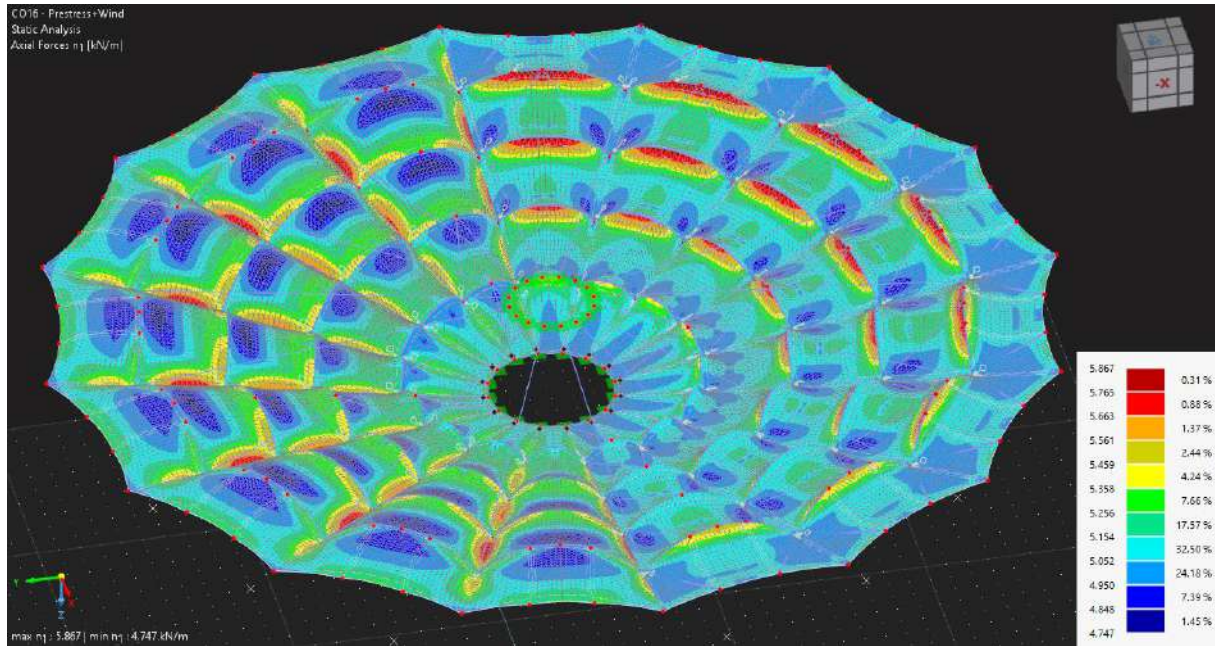


Figure 57: n_1 membrane forces in radial direction [kN/m] | *wind and prestress loads*

If we look at the displacement due to the wind effect in *Figure 58*, we see that relative displacements on the wind-pushed (left) side move the structure in the other direction, sometimes even causing negative relative displacements. *Figure 57* clearly shows that the behaviour of the wind-pushed membrane partitions is also reversed.

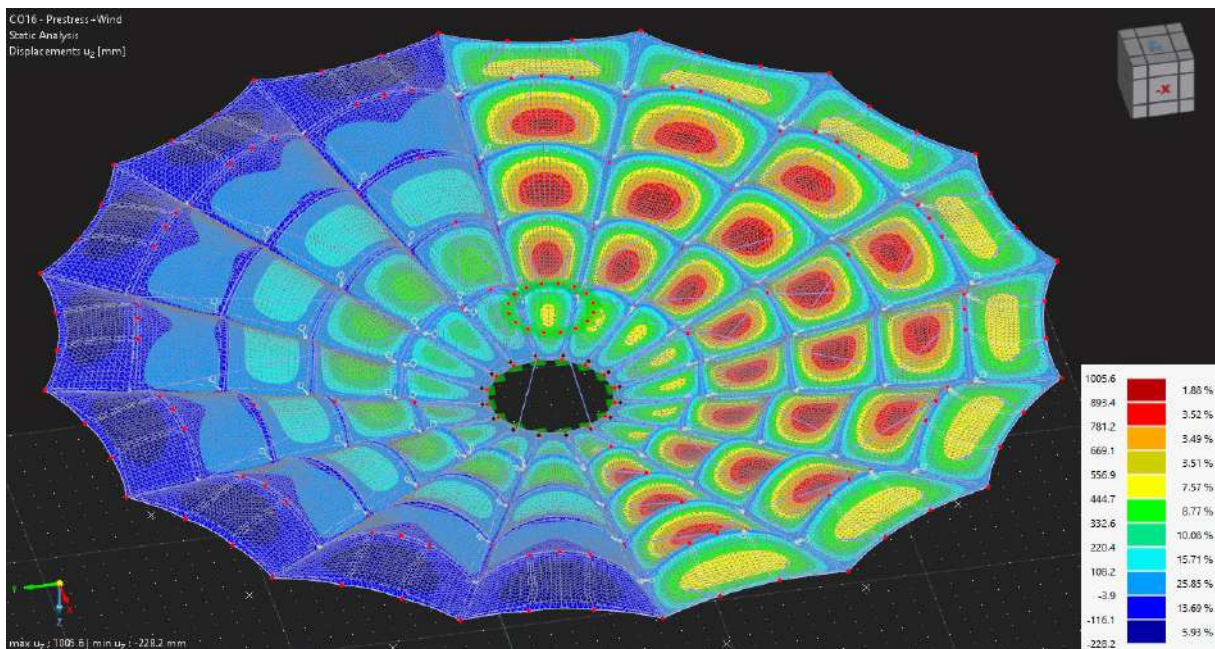


Figure 58: u_z local relative displacement of surface elements [mm] | *wind and prestress loads*

In the calculation, we observed a traceable structural behaviour everywhere. The simulation generally meets the conditions we have set up. That is:

- **Positive internal forces and tension everywhere** in the membrane structure
- The **deflections/movements** should be **reasonable**
- The internal forces induced by each combination are significantly lower than the radial or annular tensile strengths | Strength capacity check:

Membrane strength: $f_{y,k.23} = 100 \frac{\text{kn}}{\text{m}}; f_{x,k.23} = 84 \frac{\text{kN}}{\text{m}};$

$$\max(n_{1,\text{max.snow}}; n_{1,\text{max.wind}}) < f_{y,k.23}; \max(n_{2,\text{max.snow}}; n_{2,\text{max.wind}}) < f_{x,k.23}$$

4.3 Load combinations to compare parametric and reference models

Let's compare the performance of our parametric model with the newly introduced nonlinear model, which includes all structural elements and considers large deformations. The comparisons will be made from the viewpoint of the stresses. Three load combinations will be used in the analysis. The structural behaviour is slightly different. For the purpose of simplicity, a multiplier of 1.0 is used for each load factor.

Number	Load-combination
1	Self-weight + Prestress
2	Prestress + Snow
3	Prestress + Wind

Table 6: Applied load combinations

4.4 Comparison of the two models

The internal forces and behaviour of the calculated steel structure is compared with the results of the parametric model.

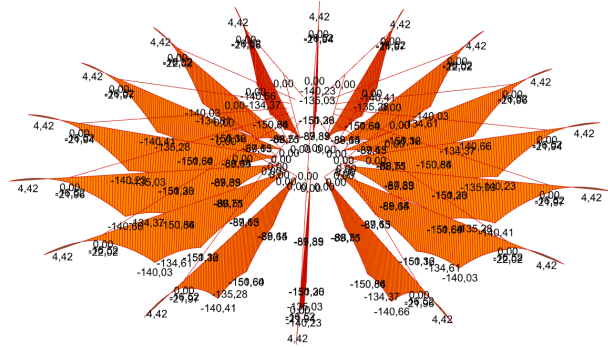
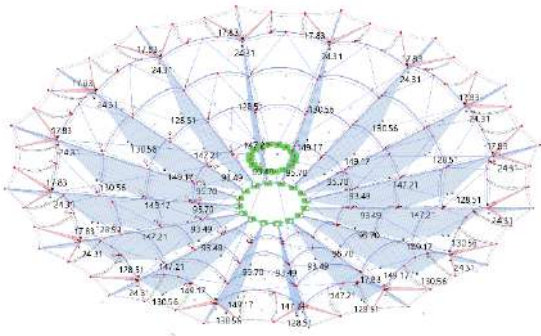


Figure 59: Reference and parametric model - M_y diagram | snow load

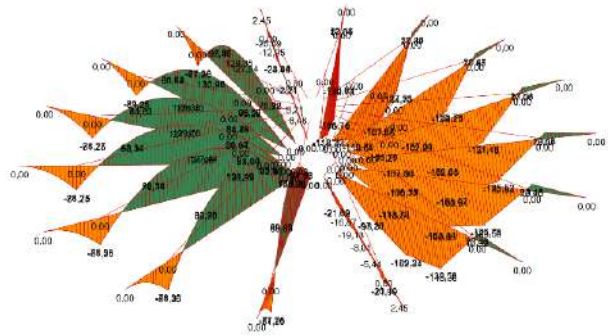
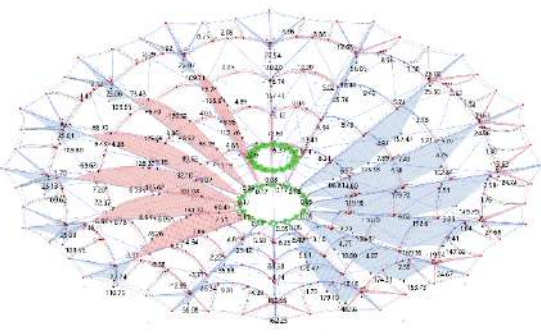


Figure 60: Reference and parametric model - M_y diagram | wind load

The bending moment diagram is very similar for snow load and wind load in the two models. In addition to the characteristics, the local peak values are also within 5% difference, which is very good for such complex membrane and steel structure having large deformations. The moment diagrams are higher degree due to the variable distributed load.

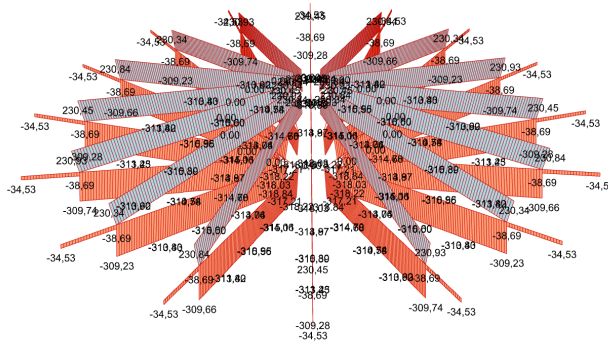
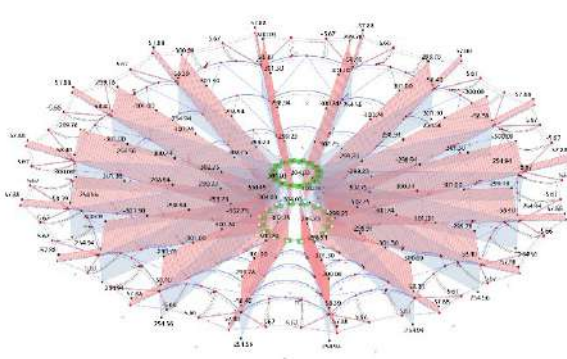


Figure 61: Reference and parametric model - N_x diagram | snow load

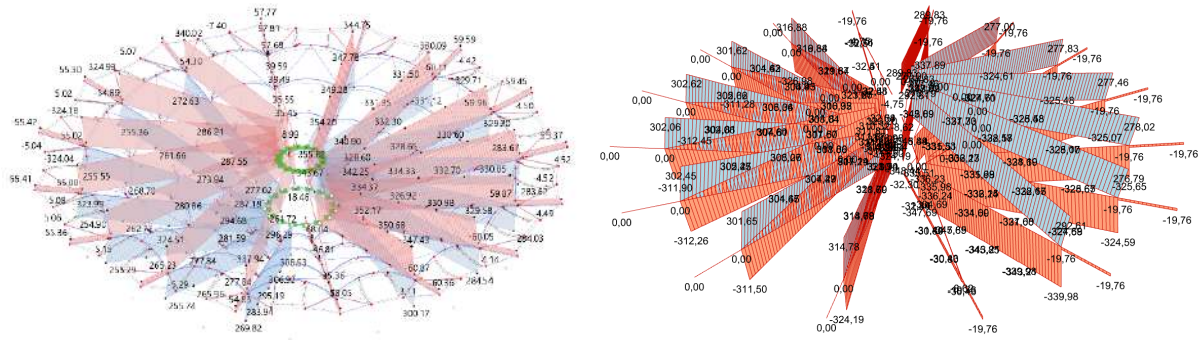


Figure 62: Reference and parametric model – N_x diagram | wind load

The normal force diagrams give exactly the same characteristics. In all cases there is a maximum difference of 5-10% between the values. Typically, in favour of the parametric model and thus in favour of safety. At the end of the main beams in the reference model, however, there is 20-23 kN increase in compressive force. The reason for this is dual. The first is that the analysis includes the cable in addition to the membrane, which in turn takes up an additional tension of 50 kN around the entire roof in addition to the tension. This effect is also loaded on the main beams. The other reason is due to the modelling uncertainty of the equivalent loads around the cable supports.

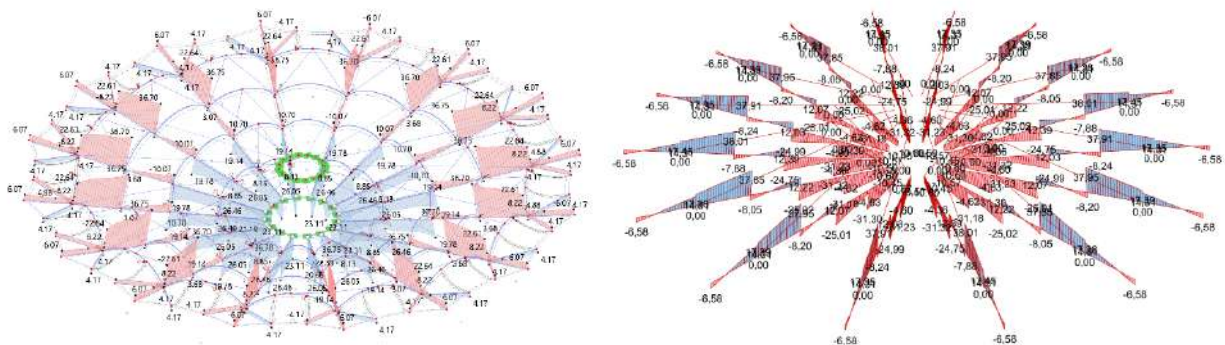


Figure 63: Reference and parametric model - V_z diagram | snow load

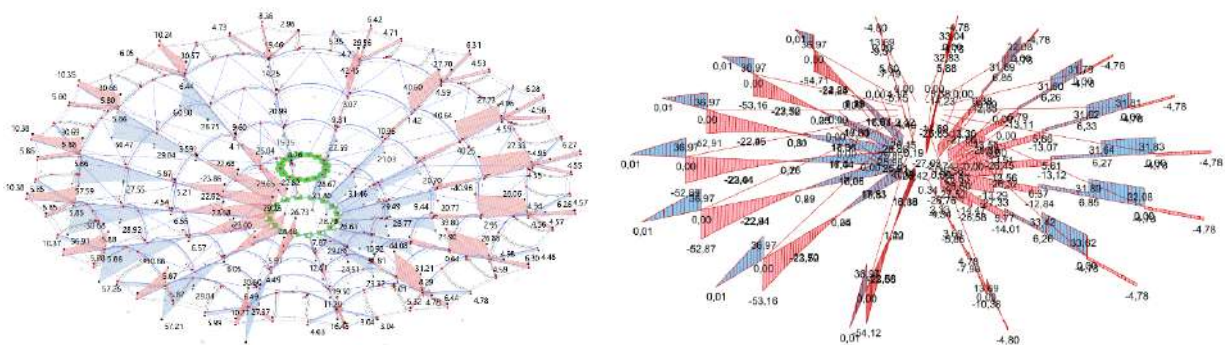


Figure 64: Reference and parametric model – V_z diagram | wind load

Among the diagrams, we can notice visible differences in shape for the shear force diagrams. The difference of several orders of the two functions is due to the fact that in the parametric model the downward loads are all applied to the arch stiffeners, from where they are

concentrated and transmitted to the main beam. The forces and moments measured at the main points of all types of structural elements and their comparison are shown in the following tables:

1. Load combination (preload and self-weight)							
Element	Inner forces	Location	Ref Model		Parametric Model		Diff. [%]
Main beam	Nx [kN]	maximal	-217,85		-227,17		4,28
	My [kNm]	In middle	88,86		95,08		7,00
	Vz [kN]	max and min	22,36	-19,38	23,1	-21,28	3,31
Suspension rod	Nx [kN]	Whole elem.	165,5		166,57		0,65
Arch stiffener	Nx [kN]	Outer ring	-26,36		-28,73		8,99
	My [kNm]	Inner ring	2,12		2,27		7,08
	Vz [kN]	Outer ring	5,77	-5,77	6,016	-6,016	4,26
Extension	Nx [kN]	minimal	-6,75		-7,79		15,41
	My [kNm]	max and min	-6,67		-5,81		12,89
	Vz [kN]	max and min	6,68	-6,68	5,97	-5,97	10,63
V stiffener	Nx [kN]	Inner ring	-1,18		-1,27		7,63

Table 7: LC1 – internal forces and comparison

In the simplest combination, the difference is in the prestressing loads, since the self-weight of the structure is the same in both calculations. The values can be considered close, larger differences only in the bracing in the partition bounded by the external cable.

2. Load combination (preload and snow)							
Element	Inner forces	Location	Ref Model		Parametric Model		Diff. [%]
Main beam	Nx [kN]	maximal	-304,03		-318,84		4,87
	My [kNm]	In middle	149,17		151,64		1,66
	Vz [kN]	Max, min	36,75	-20,66	37,06	-32,22	0,84
Suspension rod	Nx [kN]	Whole elem.	254,94		230,84		9,45
Arch stiffener	Nx [kN]	Outer ring	-39,28		-42,48		8,15
	My [kNm]	Inner ring	3,71		3,41		8,09
	Vz [kN]	Outer ring	10,21	-10,21	10,96	-10,96	7,35
Extension	Nx [kN]	minimal	-58,41		-49		16,11
	My [kNm]	max and min	24,31	-17,83	20,13	-13,92	17,19
	Vz [kN]	max and min	6,07	4,14	5,11	2,93	15,82
V stiffener	Nx [kN]	Inner ring	3,57		3,23		9,52

Table 8: LC2 – internal forces and comparison

Also, the results of the outer (5th) partition are less accurate for snow and wind load. During the optimization, a good solution could be to set up a cross-section group for the main beams, aiming to avoid the selection of an inappropriate cross-section.

3. Load combination (preload and wind) Pushed side							
Element	Inner forces	Location	Ref Model		Parametric Model		Diff. [%]
Main beam	Nx [kN]	maximal	308,53		323,9		4,98
	My [kNm]	In middle	-125,69		-133,61		6,30
	Vz [kN]	max and min	56,91	-29,65	54,12	27,08	4,90
Suspension rod	Nx [kN]	Whole elem.	-337,94		-312,26		7,60
Arch stiffener	Nx [kN]	Outer ring	-19,11		-20,97		9,73
	My [kNm]	Inner ring	-7,51		-7,66		2,00
	Vz [kN]	Outer ring	15,21	-15,21	14,32	-14,32	5,85
Extension	Nx [kN]	minimal	-25,01		0		-
	My [kNm]	max and min	25,6		0		-
	Vz [kN]	max and min	5,86	-30,69	0	0	-

Table 9: LC3 – internal forces and comparison | wind push

3. Load combination (preload and wind) Suction side							
Element	Inner forces	Location	Ref Model		Parametric Model		Diff. [%]
Main beam	Nx [kN]	maximal	-355,62		-337,29		5,15
	My [kNm]	In middle	179,1		169,35		5,44
	Vz [kN]	Max, min	40,16	-29,56	36,53	-27,79	9,04
Suspension rod	Nx [kN]	maximal	300,17		292,34		2,61
Arch stiffener	Nx [kN]	Outer ring	-43,22		-39,92		7,64
	My [kNm]	Inner ring	8,49		9,16		7,89
	Vz [kN]	Inner ring	17,62	-17,62	15,96	-15,96	9,42
Extension	Nx [kN]	minimal	-4,58		-12,84		180,35
	My [kNm]	min	-19,61		-11,35		42,12
	Vz [kN]	max	4,78		4,33		9,41
V stiffener	Nx [kN]	Inner ring	33,01		39,42		19,42

Table 10: LC3 – internal forces and comparison | wind suction

On the wind loaded side, we have only placed distributed replacement wind loads on the main beam, so there will be no stresses on the extensions. The differences on the main beams increase in proportion when weather loads are applied. This is because there is more uncertainty in

modelling these. Their magnitude is highly dependent on the deflection of the shape, which is also subject to large displacements even for small changes in tension.

Given the many assumptions and approximations used in the modelling, we set a maximum difference of 10% between the individual internal forces and moments. The accuracy of the approximate calculation was exceeded almost everywhere, with good results. The approximate values of the loads induce very similar behaviour of the structure at intermediate partitions 1, 2, 3, and 4. The good substitute load values are largely due to the relatively good form-finding, as the components were able to produce loads calculated for that form. For the 5th outer partition, it is more difficult to induce the cables and tarpaulin to work together by real simplification, and therefore the difference is slightly larger.

We can start the optimization task with the parametric model.

5. Optimization

5.1 Conditions for optimal search

5.1.1 Cross-sectional check

The cross-sectional checking of the parametric model is performed using the 'Utilization of Elements' module of Karamba3D. The module performs the calculation according to Eurocode EN 1993-1-1. In addition to the usual stress checks in the approximate calculations, several local stability calculations are computed. The extent of the structure is large and slender, for several elements the failure in simple or lateral torsional buckling may be the relevant factor.

The following checks are carried out:

- **Normal force, shear, bending and torsional moment** strength analyses
- **Buckling and Lateral torsional buckling** check for beams
- **N-M-V** interaction
- **N-M-Buckling** interaction for both directions
- **N-M-LTB** interaction for both direction

The interaction factors (e.g.: k_{yy} , k_{yz} , etc.) for normal force, bending, buckling or LTB interactions are calculated according to Annex B of EN 1993-1-1. The values of C_{my} , C_{mz} and C_{mLT} are limited to a minimum of 0.9. The lengths of each buckling are given for each element one by one. These will change proportionally during the optimization with the change in the actual length of the elements.

In practice, the scaling is done by iterating through a cross-sectional data set, where a component tries each option for each retrieved element and stops at the cross-section with the highest, already satisfactory utilization. Only cross sections rank 3 or lower are allowed to be in simulation. Then the iteration process is used to perform the cross-section optimization in practice.

Since we want each element to have a constant cross-section, we sort the element types into groups and prescribe the optimizer to take a cross-section for each group. Initial experience has shown that it is recommended to change the cross-sections carefully and in little steps, because when it's working in pairs with the geometric optimizer, the stiffness relations change. This means the rearrangement of stresses, therefore causes local structural failure that would not have occurred with a different cross-sectional configuration of the same geometry!

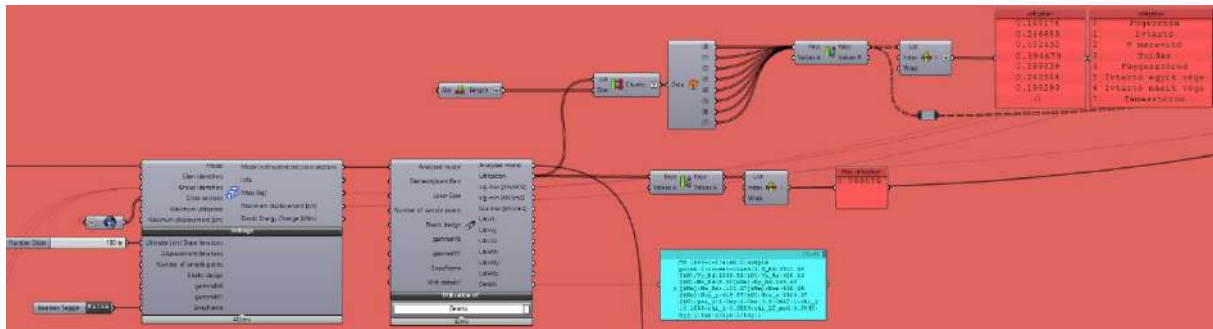
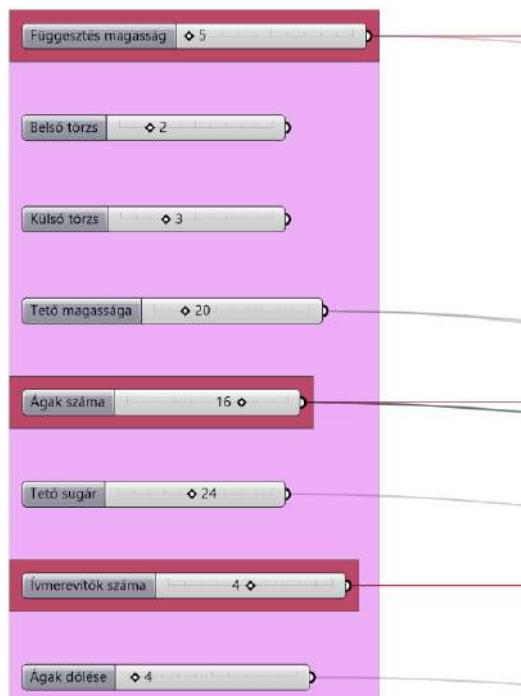


Figure 65: Cross-sectional optimizers and utilizations

5.1.2 Design parameters

There are many parameters/variables that can be selected in the analysis. The height of the roof and columns, the area of the base circle to be covered, the height of the arch stiffeners, the diameter of the column and the beam's angle of inclination are considered as prescribed. We want to know that under these conditions, what number of main beams, how many arch stiffeners, how much suspension rods and the supports will be geometrically optimal. In other words, what resolution and what support height will be optimal to achieve the different objectives. Each parameter (purple) is interpreted on the set of natural numbers.



Parameters	Interval
Height of upper supports [m]	5 - 18
Number of branches [pcs]	6 - 20
Number of arch stiffeners rings [pcs]	2 - 6

Figure 66: Design parameters and their intervals

5.1.3 Objective functions

1. One of our targets, and perhaps the most important one, is the **self-weight** optimum. In the tests, we neglect the self-weight of the membrane and cables and minimise the self-weight of the whole steel structure:

- Restriction of *deflection* may also be a condition that can be imposed. The analysis is not essentially run according to Serviceability Limit State, but we can require the structure to have realistic displacements.

$$\forall \mathbf{u}_{z,e} \leq \frac{L}{200}$$

5.1.5 Other conditions

- For arch stiffeners, the supporting effect of the membrane is taken into account, therefore buckling and LTB failures are not considered (the latter would not be significant for a circular section anyway). Besides approximating reality, it is important because otherwise unrealistically large sections would be used for all smaller resolutions (big spans).
- The utilisation of the V braces is excluded from the check, as the pressed ones always buckles. Karamba3D 2.2.0 cannot yet process only stretched elements, which is why this step is necessary.

5.1.6 Prestressing at different resolutions

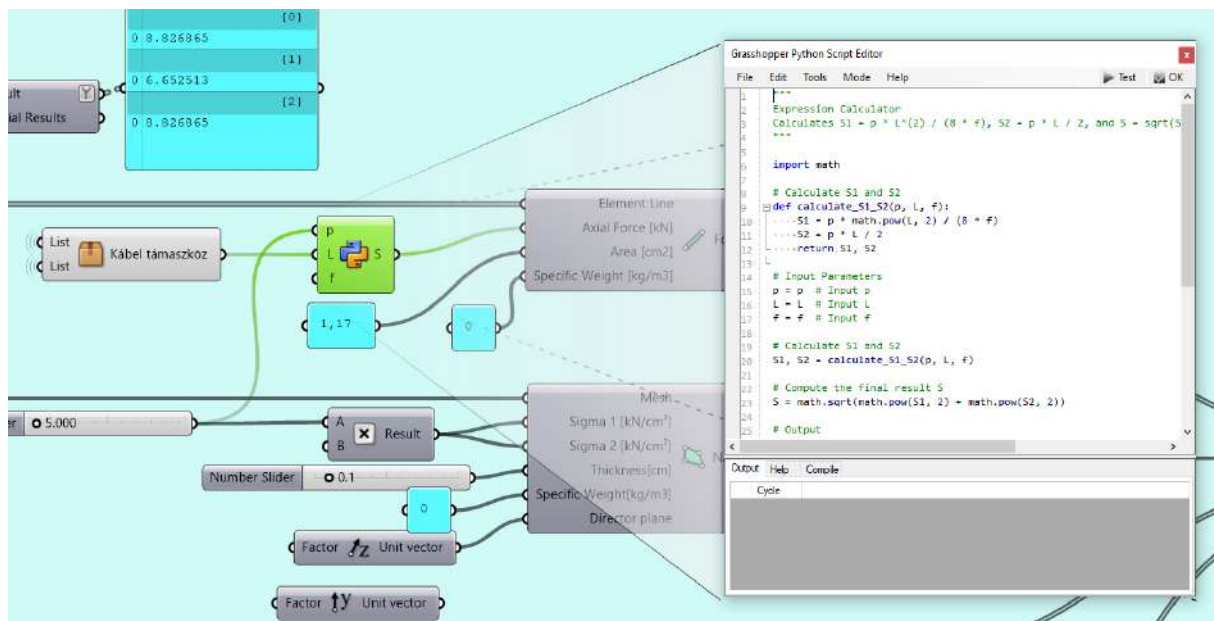


Figure 68: Component of the cable forces for each resolution

Given that there can be significant size differences between bracing resolutions, the same membrane tension can have significantly different cable pretensions. By writing the cable curve as a component, Python automatically calculates for each shape a corresponding pretension to be performed for 1 meter of inward deflection.

Based on the parameters, a nonlinear analysis was performed for the lowest bracing resolution of 6 main beams and 2 arch stiffening rings. Here also the displacement of the structure under meteorological loads was investigated. The relative displacement value at mid-partition was 0.97 m at 6.228 m in radial direction. Of course, along with this, there was significant membrane force degradation in the n2 direction, while there was a similar increase in the n1 direction. Trying several other resolutions, experience showed that 5 kN/m might be adequate for each membrane. The cable tension is also better to be set to 1 meter deflection in each case instead of directly applying different cable tensions.

5.1.7 The essence of Genetic algorithm

Genetic algorithms are very useful tools to solve optimization problems with constraints. There are several methods to handle the constraints, the most commonly used are the penalty function methods. In these methods, the objective function is augmented with a penalty term, which is associated with the violation of the condition. [20]

If we look at all the possible steel bracing solutions in terms of design parameters, we are looking at a total of $14 \times 15 \times 5 = 1050$ geometric designs. However, the genetic algorithm does not try all the solutions, but follows a certain logic to find the optimum.

The three input design parameters are defined as *genes* in GA jargon. From these *genes*, *chromosomes* are constructed. The *chromosomes* are used to create a *population*. We evaluate each chromosome and determine its fitness using the objective function. The chromosomes with better target values are paired. We separate three main genetic operations which can be performed on the population. *Crossover*, *mutation* and *reproduction*. The aim of these operations is to create a better population than the current one. The modified population is always evaluated and tested to see if it can meet the stopping condition. If it cannot, it is iteratively modified and evaluated further by genetic operations. The search process does not stop until the stopping condition is satisfied. The

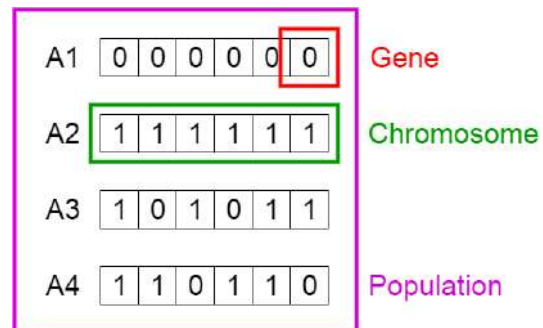


Figure 69: Gene, Chromosome and Population Relationship [25]

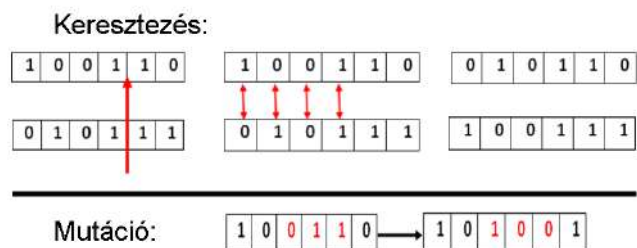


Figure 70: Example of crossover and mutations [25]

combination of a genetic operation cycle and the subsequent evaluation is together called a generation [20]

5.2 Optimization modules for running

For both load-combinations, we optimize using two solvers. The Nelder-Mead solver and the Wallacei X. The former is a fairly efficient and fast solver with few input-parameter options. The data retrieval is a bit harder, but it can provide a fast and fairly accurate solution for the extreme value of a single objective function. The latter Wallacei X, on the other hand, can find the extrema of several objective functions, has many more options, is significantly more intelligent and can perform detailed analysis and data processing. As we suspect, it usually takes more time.

5.2.1 Nelder-Mead module

We want to avoid having to define a penalty term when defining our objective function. We want to solve the problem by using a solver that is capable of optimum search with objective function conditions. The Nelder-mead is essentially based on the working principle of the Galapagos solver in the basic Grasshopper package, but with the additional feature that it can be conditioned directly. By plugging in the largest utilizations of all elements (groups), we ensure that it only considers solutions for which the utilization boundary condition is satisfied. The module can handle one objective function at a time, which will be the structural self-weight in the running.

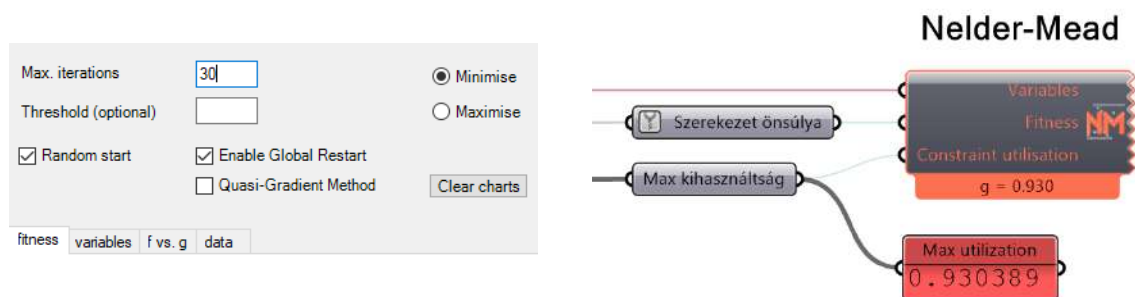


Figure 71: Nelder-Mead genetic solver and the given input data

Since the cross-section optimiser finds a suitable ($u_e < 1.0$) cross-section for each element, in principle, the optimised solution for each resolution will also be a potential geometric solution. However, this is not the case in practice, since for each larger geometric shape (e.g., large span), there is a level of stress and utilization that prevents finding a suitable cross-section from the predefined set of sections. Therefore, it will use the largest one, but this will be a locally destructive design for that load.

Another problem is the possibility of numerical error, as there may be shapes where the newly chosen cross-section is simply wrong. Therefore, an element in the design fails due to the redistribution of stresses caused by the changes in stiffness. Such designs are filtered out by this post-checked utilisation condition.

5.2.2 Wallacei X module

The Wallace X solver is used to find the optimum of multiple objective functions and to select solutions that are good from several points of view. As shown with dark purple in [Figure 72](#), the objective functions used in the run are: the *structural self-weight*, the *number of nodes* and the *net area covered*. We take the reciprocal of the area covered, since the solver can only minimize directly.

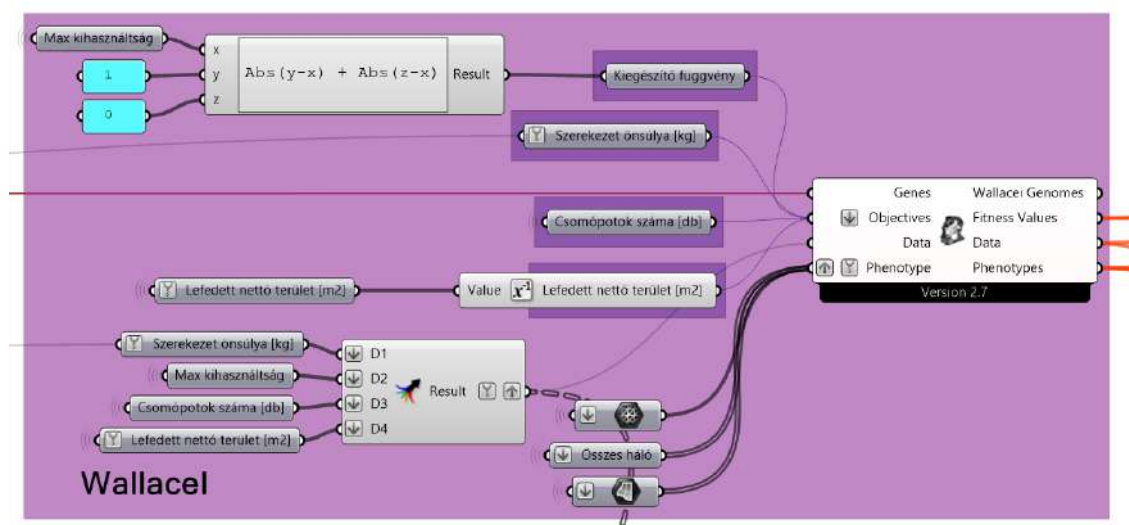


Figure 72: Optimal search configuration

In addition to these, there is a fourth function ("*kiegészítő függvény*"), which is the additional function. In the case of WallaceI X, we cannot give a direct utilization condition, so we must formulate it in a function. However, we do not want to achieve this by modifying the other objective functions with a penalty part, but by a 4th function that can distinguish between good and bad utilization shapes. By writing the following definition, we obtain a function that always returns a minimum value (1) for utilizations below 1 and a different value (greater than 1) for higher utilizations:

$$\text{obj}(x) = |1 - x| + |0 - x|, \quad \text{ahol } x = u_{e,\max} \quad (5.2)$$

$$\text{ha } x \in [0; 1], \quad \text{obj}(x) = 1 \quad (5.3)$$

$$\text{ha } x \in]1; \infty[, \quad \text{obj}(x) > 1 \quad (5.4)$$

If we also minimize this function 4 and only accept solutions that take 1 with regarding this function, all shapes with utilization greater than 1 will be filtered out.

The run will simulate 10-10 solutions from 30 generations, creating a population size of 300. With 1050 possible steel shapes, this means that even if each chromosome were equal to a different shape in the calculation, we would still be looking at less than a third of the possibilities at most. This is a large enough number to give a global solution with high probability, but small enough to justify the use of a genetic algorithm. We take 0.9 for the probability of crossover and $1/n$ for the probability of mutation, where n is the number of genes. The first generation is chosen completely randomly for each run.

In the following section, the results of the optimum finding from snow and wind load are described and analysed. Furthermore, we search for a solution that is not the best from any point of view, but is favourable solution from all points of view (each function), in the multi-objective optimization.

5.3 Structural self-weight minimisation | Snow load-combination

5.3.1 1st run - Nelder-Mead

1st run information:	
Load-combination:	1.0*Prestress + 1.0*Snow
Objective function:	Self-weight
Type:	Minimum search
Solver	Nelder-Mead

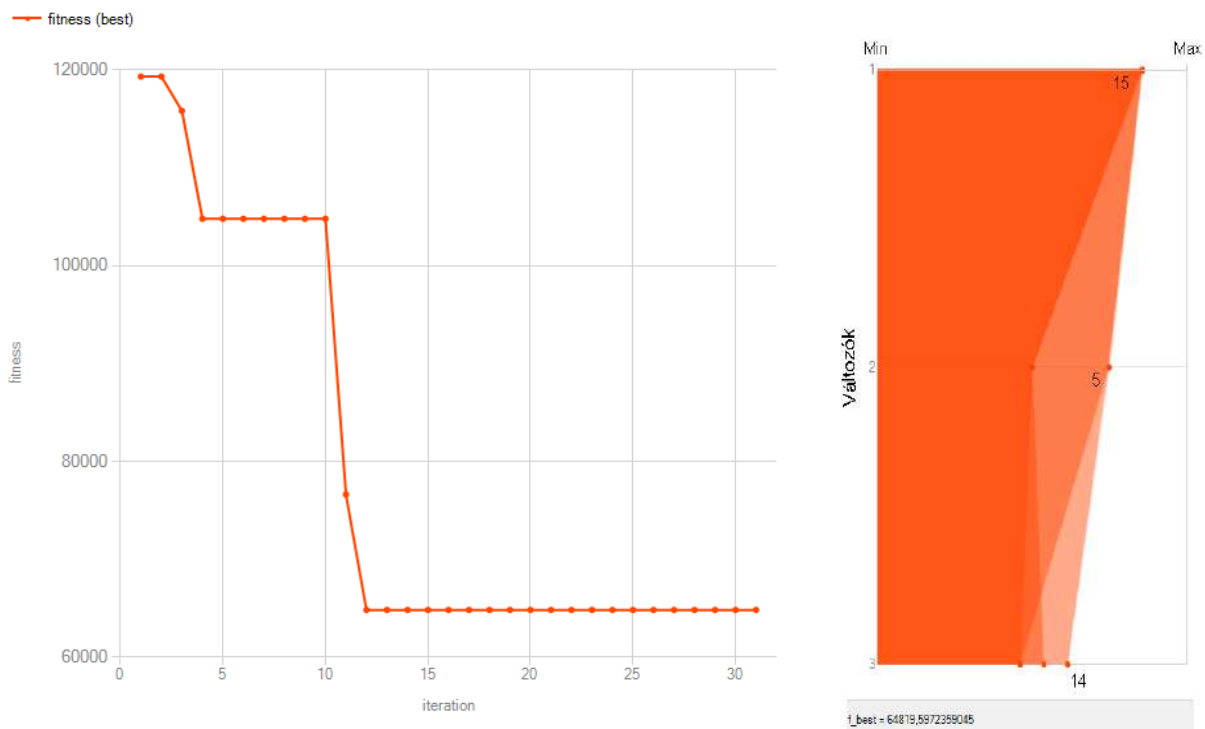


Figure 73: Target value decrease (left) and variables of good solutions per iteration (1: number of beams [pcs], 2: number of arc rings [pcs], 3: height between two supports [m])

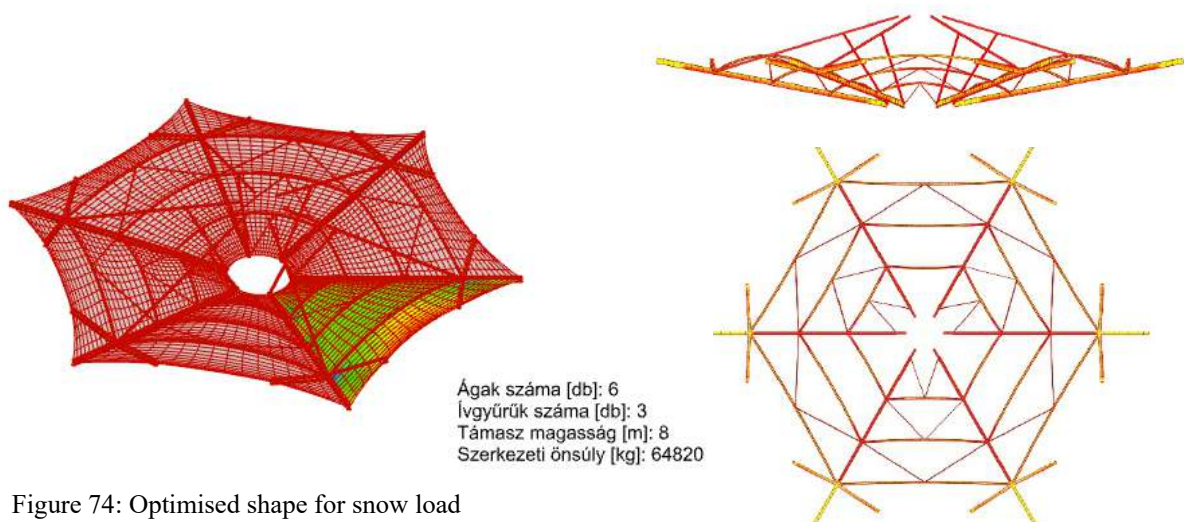


Figure 74: Optimised shape for snow load

In the case of snow loads, the best solution is achieved with 6 main beams, 3 arch rings and a support height difference of 8 metres over the specified range. The fitness-iteration diagraph (Figure 73) clearly shows that the final local solution was reached for the 12th iteration. The run converged rapidly, found a total of 4 shapes which is better than previous one. The total run took about 33 minutes. The right graph in Figure 73 shows the variables that were used at least once during the process.

The target value - utilisation graph (Figure 75) shows how the maximum utilisation for the 5 different local solutions has evolved. It is interesting to see that the smallest structural self-weight has more capacity remaining than a higher self-weight solution of another steel bracing resolution.

Looking at the results, it can be said that the structure has a fairly good utilisation rate, especially for the main beams. The V braces were not considered in the conditions and the support bars only work when the suspension bar is pressed. This will be the case for the loads tested in wind suction.

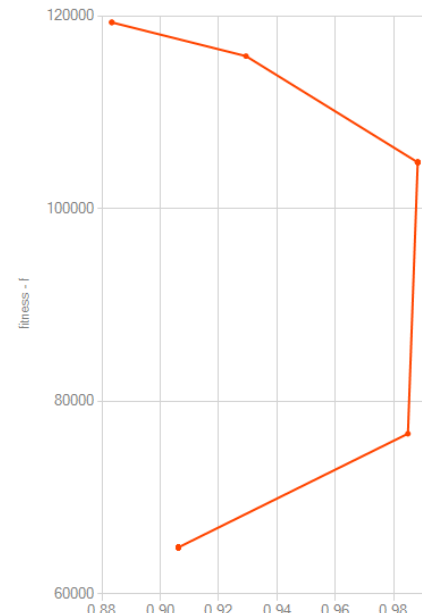


Figure 75: Target - utilisation

Results - Nelder-Mead

Table 11

Main beam [pcs]	6
Arch stiffener [pcs]	3
Upper support position from the lower [m]	8
Self-weight [kg]:	64819.5972
Max. utilization:	0.9086
Number of nodes/connections [pcs]:	54
Covered net area [m2]:	1276.65

5.3.2 2nd run - Wallacei X

2nd Run information:	
Load-combination:	1.0*Prestress + 1.0*Snow
Objective function:	Self-weight, number of nodes, covered net area
Type:	Minimization
Solver	Wallacei X

The second run is done with Wallacei X. The main diagram types for the population are shown in Figure 76. The target value distribution for each generation is shown in diagram 1. The solution's generation (in red) has a relatively large variance. The best solution appears firstly as the 5th individual of generation 11. Diagram 2 shows the total solutions (10) of all generations (30), with the best found in red. During the run, there are several minimum target solutions in

the population. However, this does not mean that they are not from the same chromosome (shape/resolution) in later generations. By checking the written script all the way through, it turns out that the same resolution is obtained for all optimal solutions. This is $6 \times 3 \times 8$, the same what we found in the 1st run.

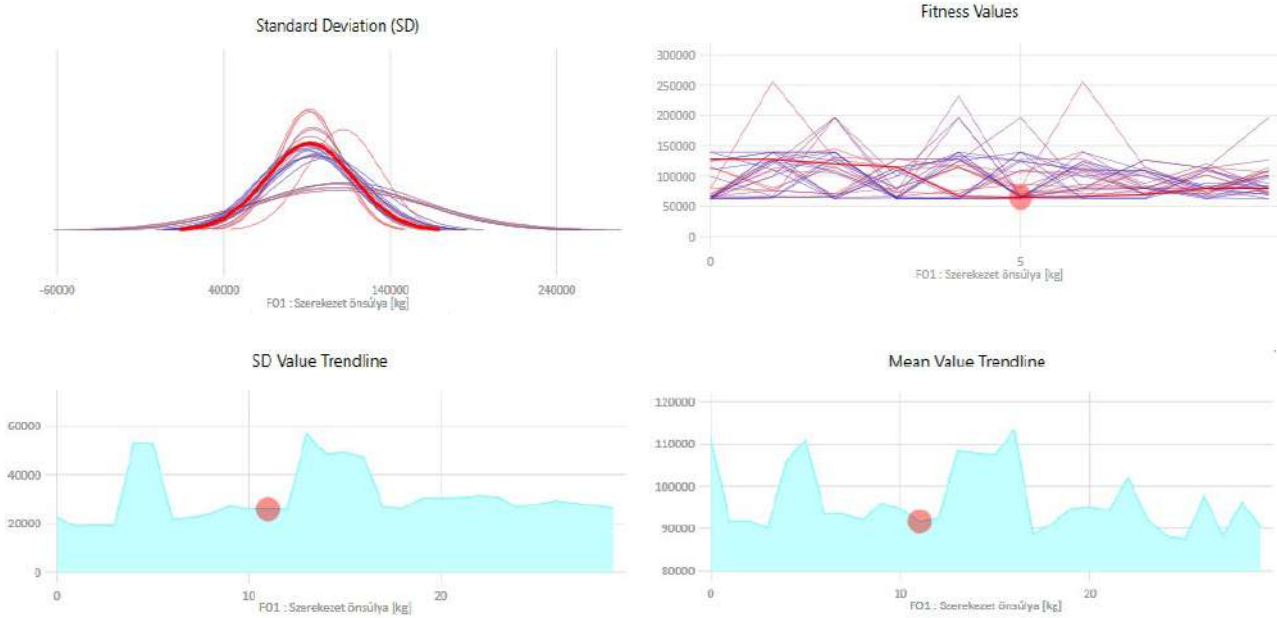


Figure 76: 1: Standard deviation of generational targets, 2: The targets for each solution, 3: Changes in SD over the generations 4: Average target value per generation

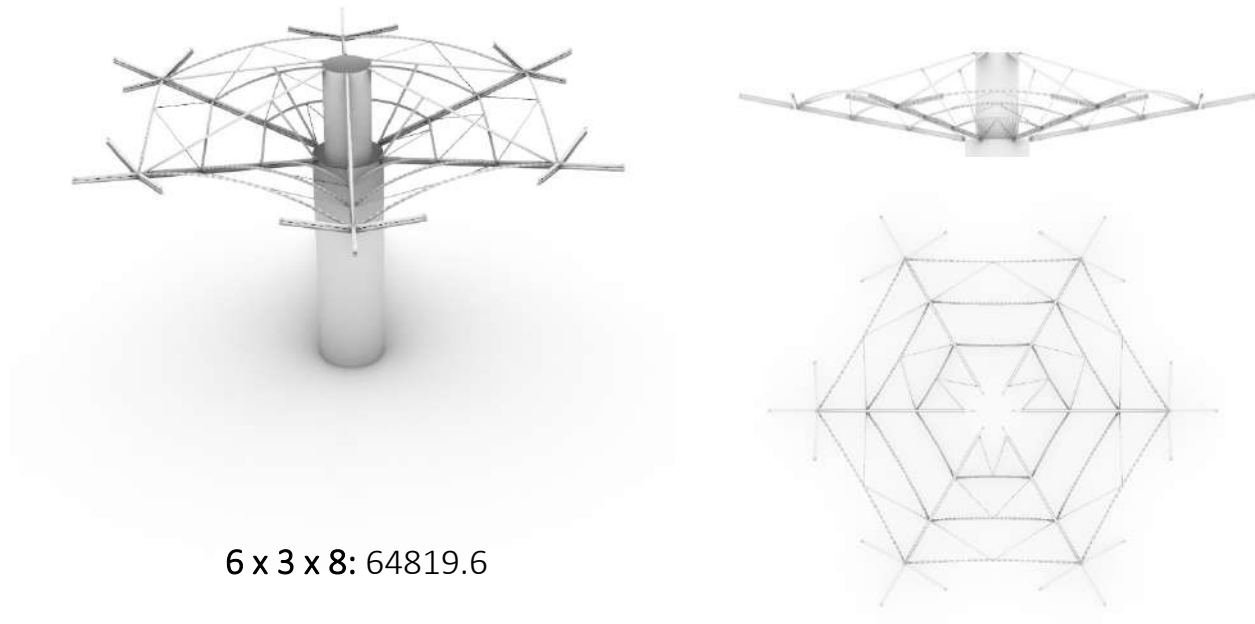


Figure 77: Optimised shape for snow load

The best solution can be examined in the viewpoint of all the other targets together. **Figure 78** shows how our chosen solution "performs" in terms of the other functions. Here the 300 solutions are ranked, the lower the rank of a solution the better it is considered to be.

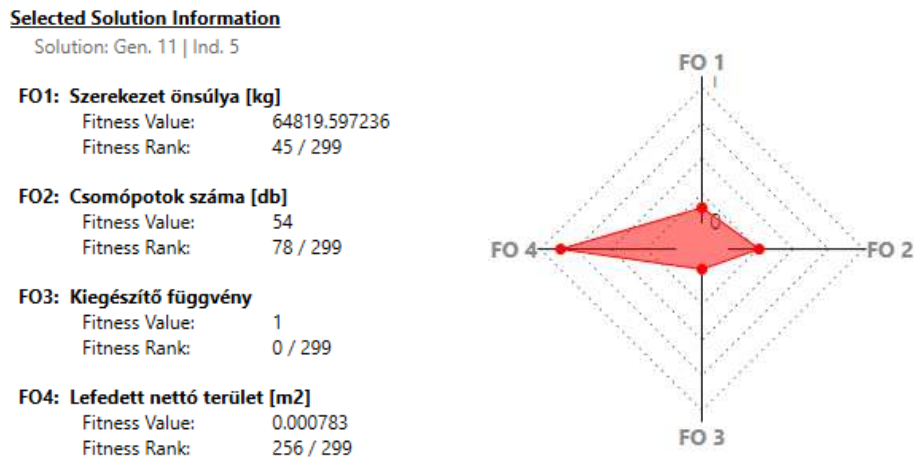


Figure 78: Rank of the solution for all function objectives

It is interesting that our optimal solution is only the 45th best out of 300 based on **FO1 (self-weight)**, but this may be because all the previous individuals although having a lower target value, their utilization is greater than 1. So, 44 individuals end up ahead of the found one, but at **FO3 (additional function)** we can see that it is the first one ranked meeting the utilization condition.

It can be said that also in terms of **FO2 (the node number)**, we obtained a rather favourable 78th best option, which means 54 nodes. **FO4** takes the reciprocal of the area covered, which is now a large value here, so it is relatively far behind in the population in this aspect. This implies that this roof solution covers a relatively small area, therefore it is in the last third of the examined sample (population).

Looking at the results, it can be said that the structure has a fairly good utilisation rate, especially for the main beams. The V braces were not considered in the conditions, and the support bars only work when the suspension bar wants to buckle. This does not occur in case of snow.

Results - Wallacei X

12. Táblázat

Main beam [pcs]	6
Arch stiffener [pcs]	3
Upper support position from the lower [m]	8
Self-weight [kg]:	64819.5972
Max. utilization:	0.9086
Number of nodes/connections [pcs]:	54
Covered net area [m2]:	1276.65

<i>Element name:</i>	<i>Optimized cross-section:</i>	<i>Utilization</i>
Main beam	HEA500	0.9011
Arch stiffener	CHS 219.1X20.0	0.8854
V stiffener	CHS 101.6X8.0	1.0557
Extension	HEA500	0.5291
Suspension rod	CHS 219.1X12.0	0.9086
Support bar	CHS 219.1X12.0	0

Table 13: Cross-sections found and utilization

The second and third most favourable forms are shown in *Figure 79*. Those solutions have been selected which vary in the number of main beams and/or rings, not only in the support height, compared to the optimum.

The 2nd and 3rd best solution (different bracing resolution):

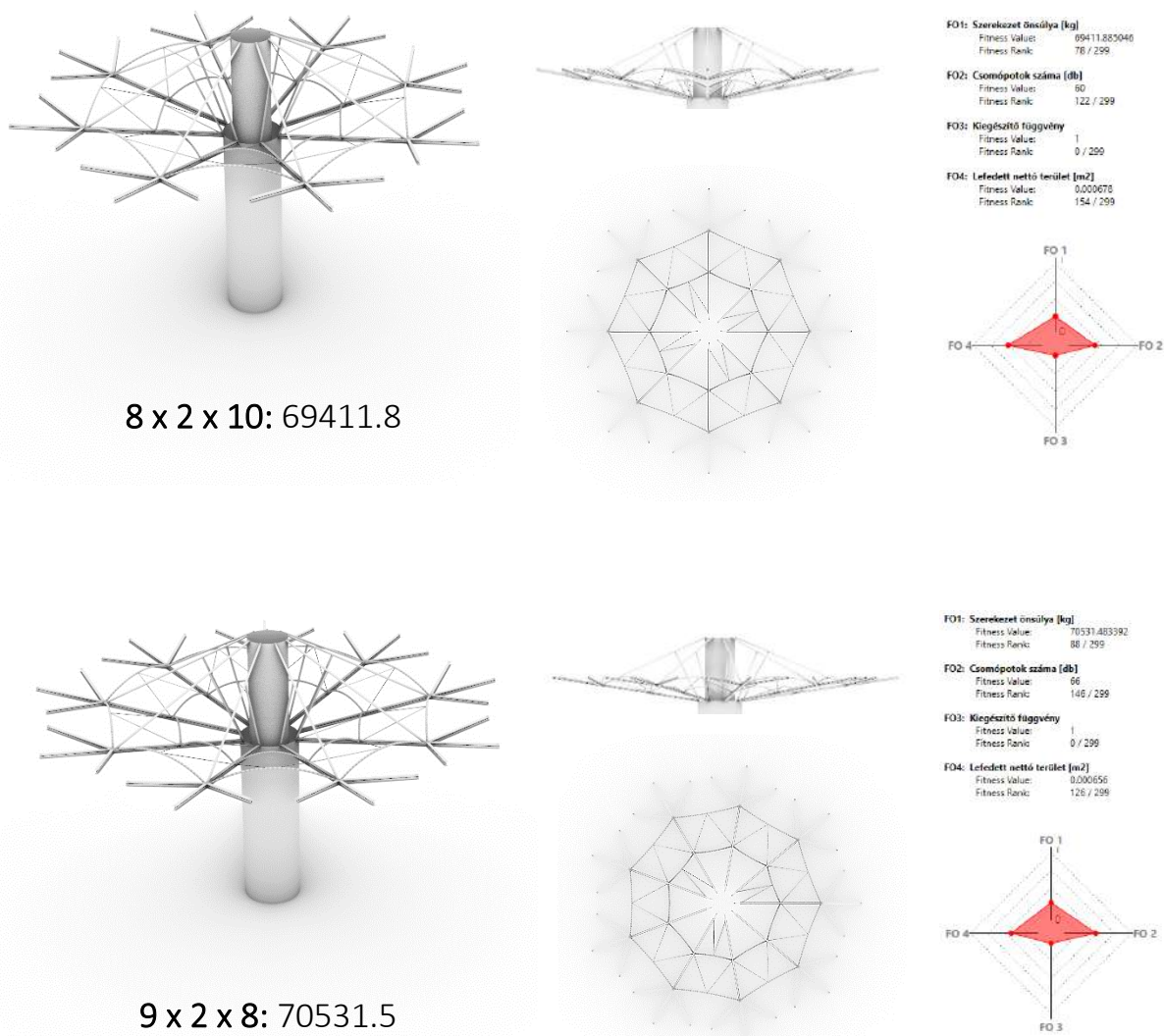


Figure 79: 2nd and 3rd best shape (number 1: number of beams, number 2: number of arch rings, number 3: support height)

5.4 Structural self-weight minimisation | Wind load-combination

5.4.1 1st run -Nelder-Mead

1st run information:	
Load-combination:	1.0*Prestress + 1.0*Wind
Objective function:	Self-weight
Type:	Minimum search
Solver	Nelder-Mead

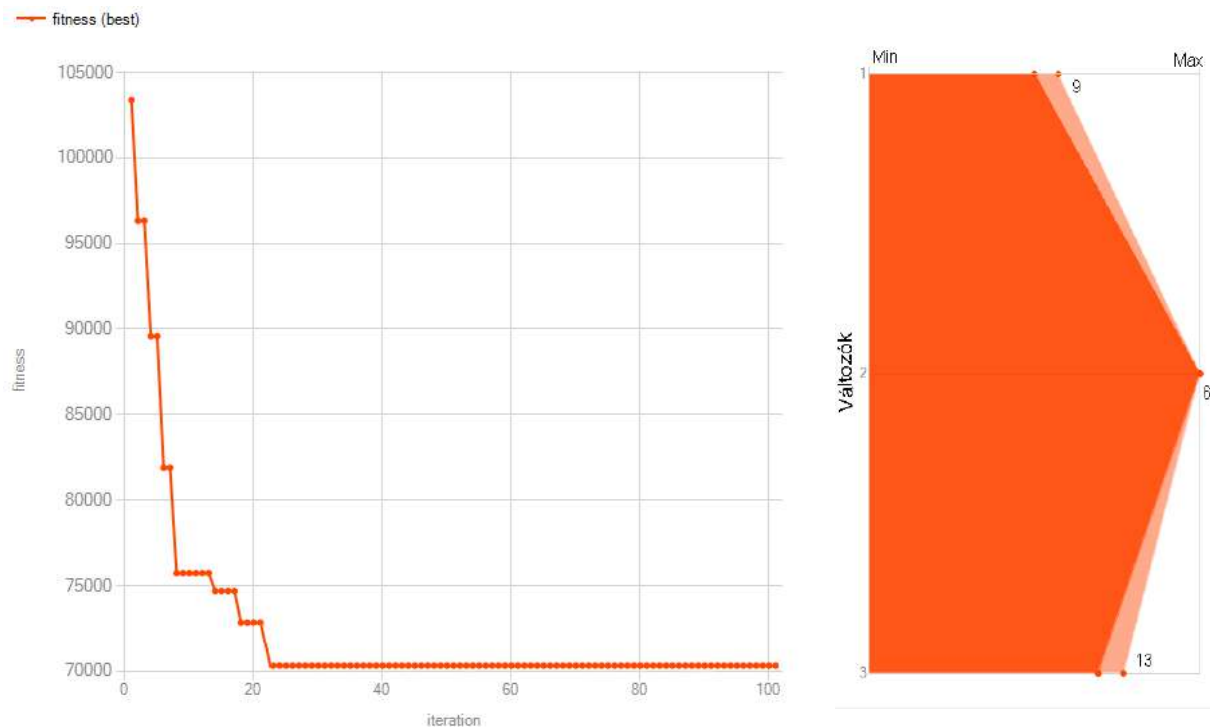


Figure 80: Target value decrease (left) and variables of good solutions per iteration (right) (1: number of beams [pcs], 2: number of arc rings [pcs], 3: height between two supports [m])

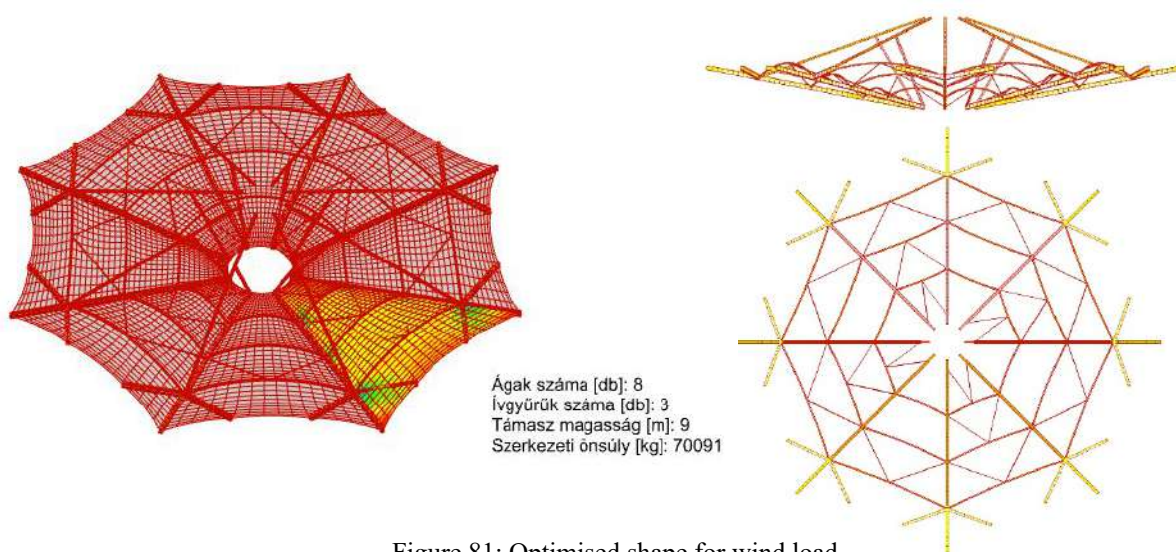


Figure 81: Optimised shape for wind load

In the case of wind loads, the best configuration is achieved with **8 main beams, 3 arch rings** and **support height of 9 metres**. The fitness-iteration graph (Figure 80) clearly shows that the final local solution converged by iteration 22. The analysis found the target more slowly and with more steps, compared to the previous case, finding a total of 7 shapes which were better than the previous one. The total runtime was about 35 minutes. The graph on the right in *Figure 80* shows the variables that were used at least once during the calculation.

The graph of utilisation and target (*Figure 82*) shows how the maximum utilisation for the 7 different local solutions evolved. All the best shapes have a utilization greater than 95%, which means the optimized sections were also found very accurately (*Table 16*)

Looking at the results, it can be said that optimising for the wind load caused a more robust structure than what the snow load did. It required 2 more main beams, 1 m higher support placement and larger CHS sections. This is why this steel bracing resolution also has 5.2 tonnes more of total weight.

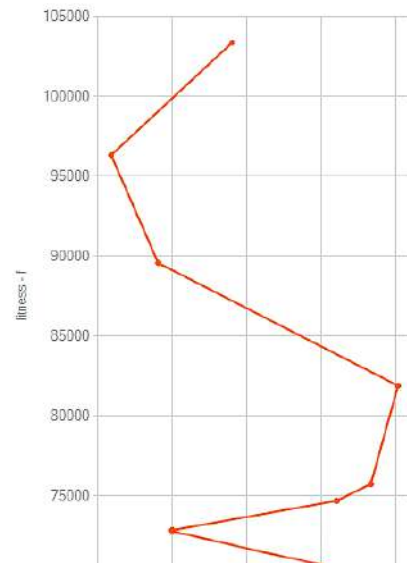


Figure 82: Target – utilisation graph

Results - Nelder-Mead

Table 14

Main beam [pcs]	8
Arch stiffener [pcs]	3
Upper support position from the lower [m]	9
Self-weight [kg]:	70090.66
Max. utilization:	0.98
Number of nodes/connections [pcs]:	72
Covered net area [m2]:	1438,848921

5.4.2 2. run Wallacei X

2nd run information:	
Load-combination:	1.0*Prestress + 1.0*Wind
Objective function:	Self-weight, number of nodes, covered net area
Type:	Minimization
Solver	Wallacei X

For Wallacei X simulation for wind load, we requested 30 generations of size 10 again. The run took about 1 hour 47 minutes. The best target value was obtained as the first solution of generation 20 (index 0). This became a resolution of **8 x 3 x 9**, similar to Nelder-Mead. The first graph in *Figure 83* shows that the variance associated with the structural self-weight

differed relatively little for each generation. The graph plots of the target values suggest that the structural self-weight varied between 70 and 180 tonnes. The most favourable figure appeared several times after generation 20, but as several objective functions were investigated, a significant part of the solutions tended to be minimum of other functions. In general, the simulation showed that there were many shapes with very similar minimum values and that the cross-section optimizer was quite accurate. This is good news, since almost all of the found solutions could have been potential optima, because they fulfilled the utilization condition

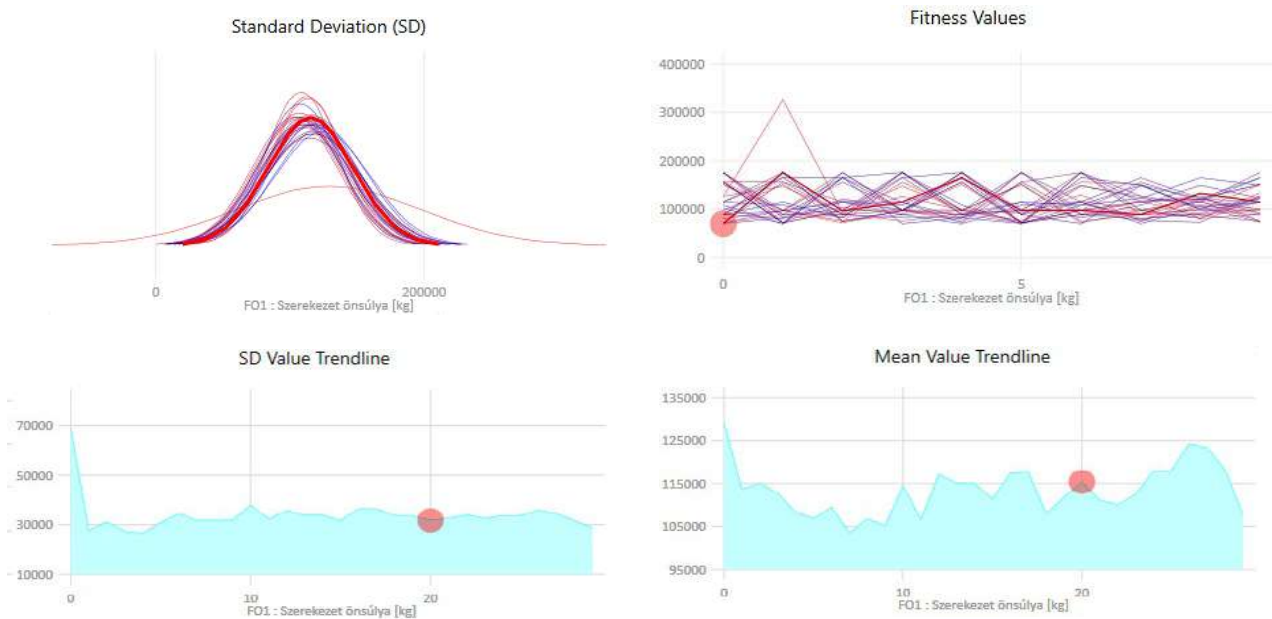


Figure 83: 1: Standard deviation of generational targets, 2: The targets for each solution, 3: Changes in SD over the generations 4: Average target value per generation

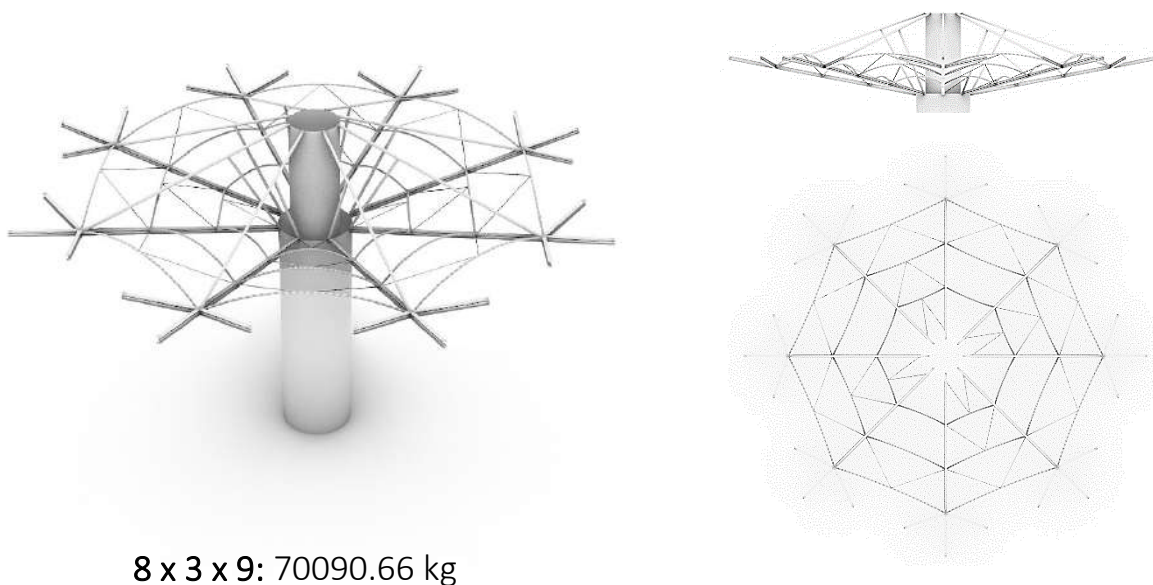


Figure 84: Optimised shape for wind load

The best solution can be considered together with all the other targets. In **Figure 85**, we can see that the result geometry for 70091 kg takes the value 1 for the additive function. Therefore, it satisfies the utilisation condition.

Selected Solution Information

Solution: Gen. 20 | Ind. 0

FO1: Szerekezet önsúlya [kg]	
Fitness Value:	70090.65503
Fitness Rank:	0 / 299
FO2: Csomópotok száma [db]	
Fitness Value:	72
Fitness Rank:	157 / 299
FO3: Kiegészítő függvény	
Fitness Value:	1
Fitness Rank:	0 / 299
FO4: Lefedett nettó terület [m2]	
Fitness Value:	0.000695
Fitness Rank:	160 / 299

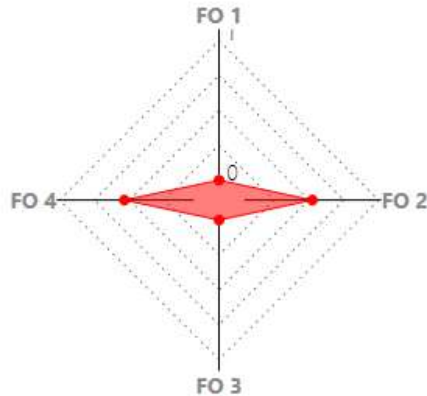


Figure 85: Rank of the solution in every function objectives aspect

The resolution of **8 x 3 x 9** is in the middle of option set based on the **number of nodes (FO2)**. This means 72 connections when designing and building the structure. The situation is similar at the **covered area (FO4)**, where it is 161st best out of 300, with its $1/0.000695 = 1438.85 \text{ m}^2$ of value

Since the same shape was found in both runs, and both simulations include a large population, it is reasonable to assume the existence of the global solution. The utilization of the structural elements is considered to be high, the arch stiffeners, in addition to the main beams, are close to reaching their full-strength capacity. Here, the support bars are also in use, due to wind suction effect. When the section was being found, they were grouped together with the suspension rods, so the utilisation is low in relation to them (*Table 16*)

At the 3rd best solution for different main beam and ring number (*Figure 86*), we can notice that it has a lower resolution compared to the best solution. This configuration could bring 82.6 tonnes with quite huge cross-sections. This is, however, a noticeable difference compared to 71 tonnes, but the number of nodes is a favourable 18 less than in 1st solution.

Results - Wallacei X

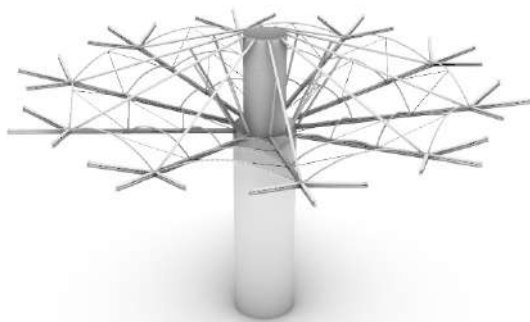
Table 15

Main beam [pcs]	8
Arch stiffener [pcs]	3
Upper support position from the lower [m]	9
Self-weight [kg]:	70090.66
Max. utilization:	0.98
Number of nodes/connections [pcs]:	72
Covered net area [m2]:	1438,848921

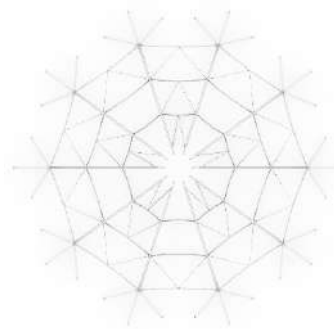
<i>Element name</i>	<i>Opt. section:</i>	<i>Utilization</i>
Main beam	HEA450	0.98
Arch stiffener	CHS 219.1X20.0	0.97
V stiffener	CHS 88.9x4.0	0.98
Extension	HEA450	0.37
Suspension rod	CHS 244.5x25.0	0.85
Support bar	CHS 244.5x25.0	0.22

Table 16: Cross-sections found and utilization with 9x3x8 resolution

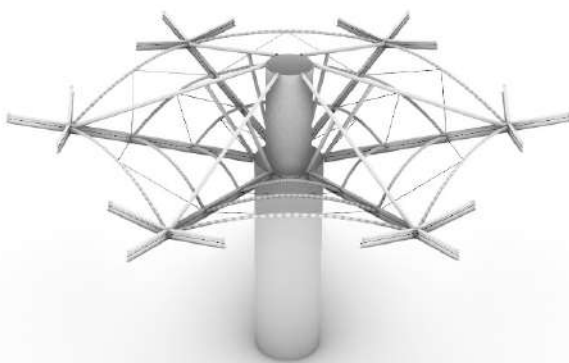
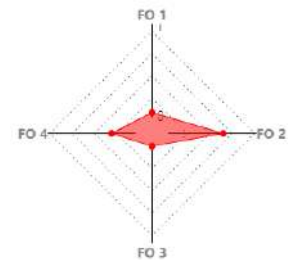
The 2nd and 3rd best solution (different bracing resolution):



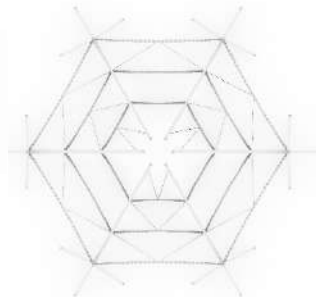
10 x 3 x 9: 73117.2 kg



FO1: Szerkezet önsúlya [kg]	Fitness Value: 73117.200714
	Fitness Rank: 27 / 299
FO2: Csomópontok száma [db]	Fitness Value: 90
	Fitness Rank: 195 / 299
FO3: Kiegészítő függvény	Fitness Value: 1
	Fitness Rank: 0 / 299
FO4: Lefedett nettó terület [m²]	Fitness Value: 0.000655
	Fitness Rank: 92 / 299



6 x 3 x 9: 82674.9 kg



FO1: Szerkezet önsúlya [kg]	Fitness Value: 82674.937329
	Fitness Rank: 52 / 299
FO2: Csomópontok száma [db]	Fitness Value: 54
	Fitness Rank: 76 / 299
FO3: Kiegészítő függvény	Fitness Value: 1
	Fitness Rank: 0 / 299
FO4: Lefedett nettó terület [m²]	Fitness Value: 0.000783
	Fitness Rank: 271 / 299

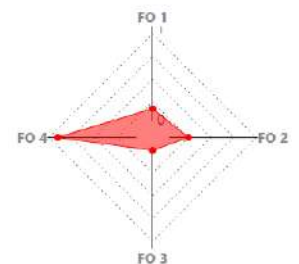


Figure 86: 2nd and 3rd best shape (number 1: number of beams, number 2: number of arch rings, number 3: support height)

5.5 Choosing a favourable and multi-beneficial solution

With the script developed in the thesis, it is also possible to search for solutions that are not optimal in one or another aspect, but perform satisfactorily well in several aspects at the same time. This is now presented for the case of wind load. It is also possible to look for favourable designs for other loads/load combinations.

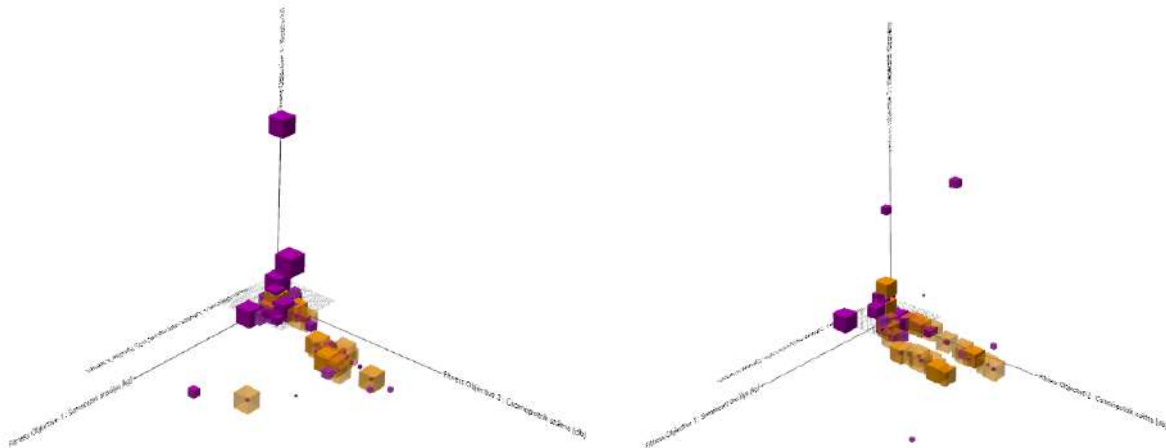


Figure 87: All the solutions of 30 generations for the 3 functions, snow load (left) and wind load (right)

Figure 87 shows the ranking of the generations' solutions by target. The two horizontal axes are the functions FO1 and FO2, and the vertical axis is for FO3. The good solutions will be on the plane stretched by the horizontal axes, and the best solutions will be as close to the origin as possible. Nevertheless, it is not clear how to choose a favourable solution.

For the analysis I choose the 'average target rank' method. Out of the analytics types built into the Wallace Analytics module, this is the one that is applicable to this problem. This method reorders the solutions according to a specific order based on the target values of all 300 individuals, so that the sum of their ranks is minimal.

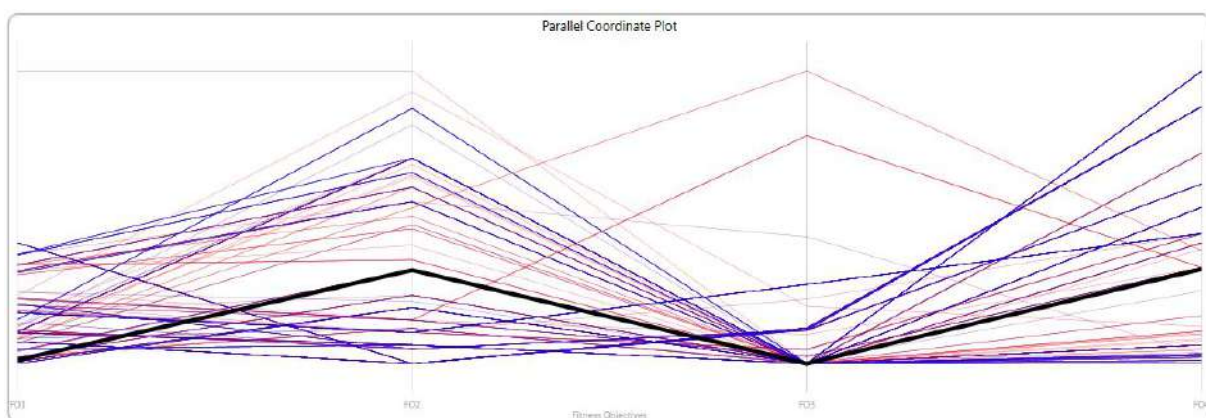


Figure 88: Plotted objectives of each form based in the aspect of all defined functions - FO1: Self-weight, FO2: Number of nodes, FO3: Additional 'condition' function, FO4: Reciprocal of net covered area – wind LC

The best result of the calculation was the 10th solution of the 20th generation (gen. 19 and ind. 9). This is shown in black in *Figure 88*. It was also the second-best solution in terms of total structural self-weight.

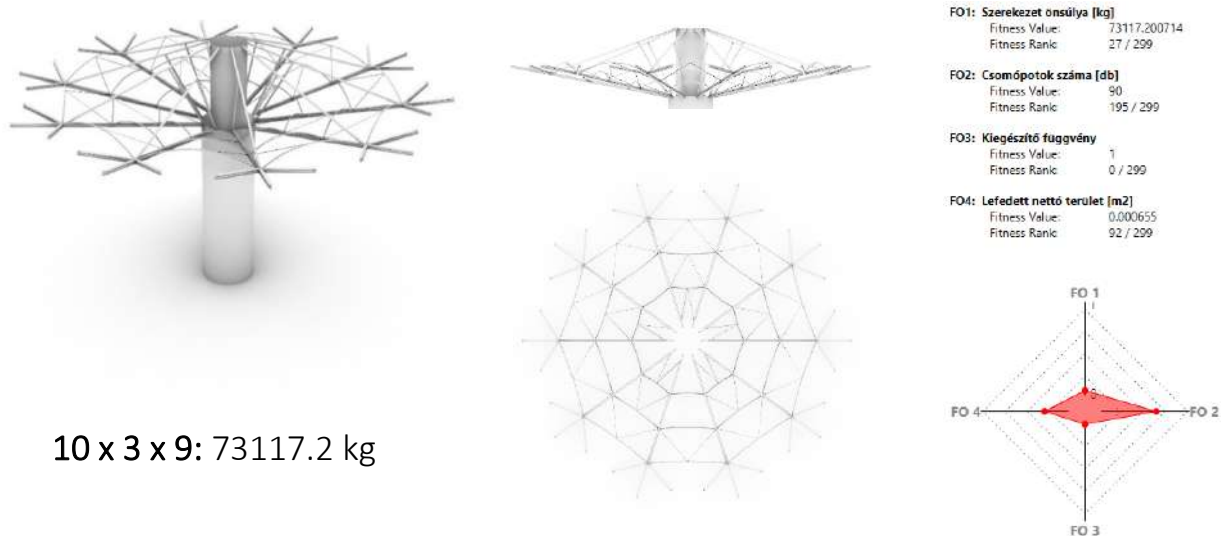


Figure 89: Multi-beneficial solution's performance in each aspect

It is worth pointing out that we have not mathematically weighted the individual targets here (from more important to less), but found the configuration that is the most forward-looking across all criteria. In addition to its structural self-weight, it is also well ranked in terms of net area covered: 1526.7 m², which is 87.75 m² more than the previous one. In terms of connection numbers, it ranks in the mid-range. This is a well-performing design solution, if we consider these three aspects. We mark this form with green in *Figure 90*.

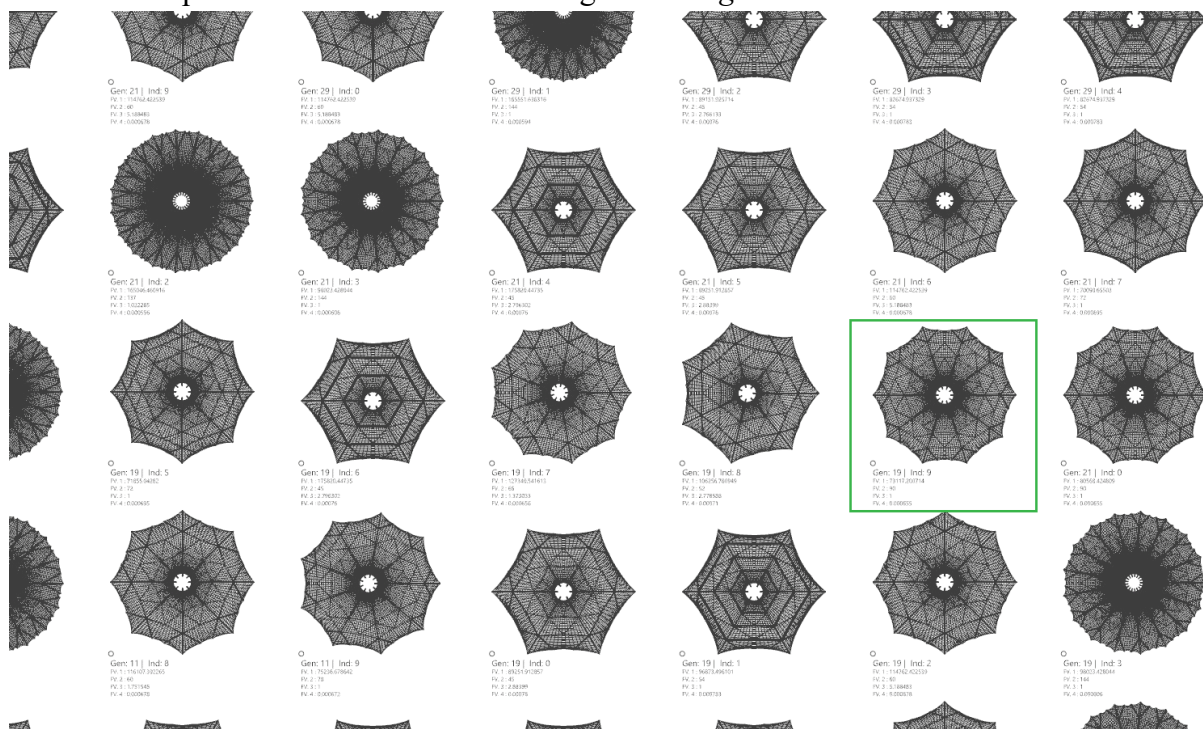


Figure 90: favourable solution selected from the population

6. Summary and conclusion

6.1 Summary

In this thesis I programmed a module for design, form-find and geometric optimization of a specific type of structure. This structure is a barrel vault membrane supported by an umbrella-like steel structure. The process consists of a parametric model that determines the shape of the roofing for different load input values. It also determines its cross sections and optimizes geometry for the given loads.

In this study, we found that for this kind of problem, in this environment, it is most beneficial to use the force-density method and a plugin based on it (in this case BATS). Besides the less mesh resolution dependent results and the fast runtime, we can easily extract the prestressing load from them. The form-finding is performed automatically for both the original structure and the any structures created during optimization.

Secondly, a finite element analysis was then performed on the steel structure. We realized that there is no software yet that can calculate the membrane, the cable and the steel structure in one model, so that all its elements, resolution and geometry can be parametrically changed while the form-finding is also running. Therefore, we went as close to this as possible, using substitute loads for snow and wind loads. The magnitudes of these loads track the variation of the roofing's area and geometry, the magnitude of the deflection used in the rope curve formula depends on the found form in the first segment. The FE model was compared with a reference model which, although non-parametric, simulates the interaction between the membrane and the steel structures. It is also able to calculate the membrane nonlinearly with large displacements. The two models were similar, showed deviations less than 10% in almost all cases.

In the third segment, we programmed the automatic design of the steel structure. The cross-section optimiser goes through all the element types and selects the most appropriate section from a list. The lists consist of regular cross-sections like HEA and RHS.

In the fourth step, the structure was geometrically optimized using 2 different modules operating on two different theoretical bases. The process runs by selecting the most favourable shape out of the options with already optimized cross-sections. The search for the optimum is mainly performed on the self-weight. In addition, the number of nodes and the covered area were considered for every configuration. The most optimal solution for wind and snow load was found among the 1050 design options. We also chose a solution that is the best choice when all three objective functions are considered with the same mathematical weight.

6.2 Advantages and disadvantages

The created algorithm has several major advantages. One is that it is extremely fast. From the moment you specify any input parameters (e.g.: number of main beams, number of arch rings, support height, inclination angle) the calculation time of an analysis is between 15 and 25 seconds depending on the number of elements. The script also documents the membrane displacements, designed sections, and the overall shape data in an Excel file automatically. Another advantage is that the calculation steps and partial results can be followed throughout the workflow. Even if geometric optimisation is performed, it will only give results that meet its preconditions and are the best solution within the given population. In addition, the individual stresses and the behaviour of the structure will be sufficiently accurate.

However, due to the complexity of the task, it is still difficult to perform such an optimization task (especially geometrical) in a cost-effective way and with a strict time interval in design practice. Besides the need to have and harmonise several programs and add-ons, the whole process requires classical and visual programming experience. To choose conditions for each analysis and to have the real optimum requires careful thought. For the full process, the user cannot exclude the nonlinear calculation (partially at least), since the strength of the membrane and the deflections must be tested at least in the extreme cases (maximum and minimum span - in both directions). I also compared the parametric model with a more accurate complex model, the difference between the inner forces increased slightly in case of the lower resolutions, as expected. Considering the factors and uncertainties during the work, it can be said that the maximum stresses deviation of around 10% can be easily achieved for precalculation. However, due to the problems mentioned above, an exact calculation is not yet possible.

6.3 Future potential of the workflow

Virtually all the tasks that were performed in the thesis are a continuously evolving field in design engineering. The huge advantage of solving the whole task in Rhino+Grasshopper environment is its further development potential. On the one hand, parametric analysis of membrane structures with nonlinear plug-ins is a huge gap in the market for software developers. On the other hand, the resulting structure after calculations can be instantly visualise and fabricated using softwares available today within the environment. The Karamba3D finite element plugin can work very well with the most widely used connection design softwares on the market, like Idea Statica. In addition, the module can be implicitly integrated into a BIM model. It can be used to perform excellent visualisations, solar analysis or other operations involving other disciplines. A third direction for further development could

be the development of weighting the optimality criteria. Although some conceptual options are already available or being under development, it is a very promising and challenging area.

Parametric design and optimisation will be an absolute key area of structural design in the near future. The present thesis demonstrates that this is not only available for the likes of frames or trusses, but also for more specialised or unique structures. This of course requires more care and fine-tuning, as well as experience in several fields.

A link to download the full module can be found in the *Appendix*.

References

- [1] Dr. Lámer, G., 2013. *Különleges épületszerkezetek. Esszé a különleges épületek téralkotásának tartószerkezeti kérdéseiről*. Budapest: TERC. Elérhető: https://dtk.tankonyvtar.hu/xmlui/bitstream/handle/123456789/3353/kulonleges_epuletszerkezetek.pdf?sequence=1&isAllowed=y
- [2] Dr. Kovács, N., 2018. *Tartószerkezetek 2. BMEEOHSMT-1*. 5. Előadás - Térbeli rácsok típusai Budapest: BME, Építőmérnöki kar
- [3] L. P. Kollár, L. E. Hlavicka-Laczák, B. Pap, 2020. *Structures II. BMEEOHSMT-1*. Lecture notes: Shells. Budapest: BME, Építőmérnöki kar
- [4] Dr. Kovács, N., 2020. *Tartószerkezetek 2. BMEEOHSMT-1*. 7. előadás – Függesztett tetők és függőtetők. Budapest: BME, Építőmérnöki kar
- [5] A. Buchanan, J. Hillson, N. Webb, 2021. *Digital Analysis of Vaults in English Medieval Architecture* – Routledge kiadó
- [6] Bársony, I. & Szerényi, A. & Szerényi, I., 2019. *Ácsszerkezetek*. Pécs: Szega Books kiadó.
- [7] Herzog, T., 1976. *A Handbook of Inflatable Architecture*. Oxford: Oxford University Press
- [8] Hegyi, D., 2012. Ponyvaszerkezetek. In: Hegyi, D. & Gáspár, Zs. & Fehér, E., 2012. *Különleges tartószerkezetek*. Budapest: TERC. Elérhető: <https://docplayer.hu/19520750-Ponyvaszerkezetek-kulonleges-tartoszerkezetek-hegyi-dezso-jegyzet-kezirat-2012-v1-ponyvaszerkezetek.html>
- [9] Vasúti Járművek és Járműrendszeranalízis Tanszék. 2021. *Szerkezetanalízis. BMEGEGIBGSA*. Szerkezetoptimalás előadásvázlat. Budapest: BME Gépészmérnöki kar <https://docplayer.hu/107221723-Szerkezetoptimalas-szerkezetoptimalas-msc.html>
- [10] Issa, R., 2020. *Essential Algorithms and Data Structures for Computational Design in Grasshopper*. 1st edition. Robert McNeel & Associates. Elérhető: <https://www.rhino3d.com/download/rhino/6.0/essential-algorithms>

- [11] R., A., Danhaive, C., T., Mueller. 2015. Combining parametric modeling and interactive optimization for high-performance and creative structural design. In: IASS, *Symposium, Future visions*. Amsterdam. 2015. MA: Massachusetts Institute of Technology
<http://digitalstructures.mit.edu/files/2015-09/iass2015-524698.pdf>
- [12] Iria Heitel (Engineer) & Feng Fu (Senior Lecturer) (2021) Form Finding and Structural Optimisation of Tensile Cable Dome Using Parametric Modelling Tools, *Structural Engineering International*, 31:2, 271-280, DOI: [10.1080/10168664.2020.1750937](https://doi.org/10.1080/10168664.2020.1750937)
- [13] Dr. Kovács, N., 2020. *Tartószerkezetek 2. BMEEOHSMT-1*. 8. előadás – Ponyvaszerkezetek. Budapest: BME, Építőmérnöki kar
- [14] A., Heslop, 2010. *Basic theories of tensile fabric architecture*. [online] From: <https://www.architen.com/articles/basic-theories-of-tensile-membrane-architecture/>
- [15] *Arizona State Univerity Sky song*. Scottsdale, Arizona. Elérhető: <https://www.ndnsoftware.com/uploads/1/2/4/2/124245976/published/maxresdefault.jpg?1549745193> [Hozzáférés dátuma: 2023.04.02]
- [16] Structureflex.hu, *PTFE Fiberglass*. [kép online]. Elérhető: <https://www.structureflex.com/materials/ptfe-fiberglass/> [Hozzáférés dátuma: 2023.04.02]
- [17] Archdaily.mx/Serge Ferrari, *Pabellón de zona de celebración de Ontario*. [kép online]. Elérhető: <https://www.archdaily.mx/mx/777222/pabellon-de-zona-de-celebracion-de-ontario-hariri-pontarini-architects> [Hozzáférés dátuma: 2023.04.04]
- [18] Daniel Christev, 2017. *Grasshopper - Kangaroo 1 vs. Kangaroo 2*. [video online]. https://www.youtube.com/watch?v=R_Bfmm8y-Ms&ab_channel=DanielChristev
[Hozzáférés dátuma: 2023.04.04]
- [19] Dlubal.com, 2021. *Form-Finding of Mmembrane Structures*. [kép online]. <https://www.dlubal.com/-/media/Images/website/img/020001-030000/024201-024300/024208.jpg?la=en&mlid=7C97E6417030437CB5C7B45B9C3E60D9&hash=D02EFB706ADF62E7635B49566B296B69E7A83908> [Hozzáférés dátuma: 2023.04.06]
- [20] Hegyi, D., 2003. *Ponyvaszerkezetek alakmeghatározási módszerei*. In: *Építés - Építészettudomány*. 31. 10.1556/EpTud.31.2003.3-4.4.
https://www.researchgate.net/publication/250980477_Ponyvaszerkezetek_alakmeghatarozasi_modszerei

- [21] de Souza, Márcio S. V. and Pauletti, Ruy M. O.. "An overview of the natural force density method and its implementation on an efficient parametric computational framework" *Curved and Layered Structures*, vol. 8, no. 1, 2021, pp. 47-60.
<https://doi.org/10.1515/cls-2021-0005>
- [22] Pauletti RMO, Fernandes FL. An outline of the natural force density method and its extension to quadrilateral elements. *Int J Solids Struct.* 2020;185-186:423. DOI: <https://doi.org/10.1016/j.ijsolstr>.
- [23] Hegyi, D., 2006. *Ponyvaszerkezetek és ponyvaanyag nemlineáris vizsgálata numerikus és kísérleti módszerekkel* [egyetemi doktori disszertáció]. Budapest: Csonka Pál Doktori Iskola, Budapesti Műszaki és Gazdaságtudományi Egyetem, Elérhető: <http://hdl.handle.net/10890/573>
- [24] Daniel Piker, szoftverfejlesztő. 2023. Kangaroo alakkereső szoftver működési elvéről való elbeszélése, megkeresésemre [e-mail]
- [25] Erdősné Sélley Cs., Gyurecz Gy., Janik J., Körtélyesi G., 2012. *Mérnöki Optimalizáció*. Budapest: BME Gépészmérnöki Kar, ÓE Bánki Donát Gépész- és Biztonságtechnikai Mérnöki Kar, SZIE Gépészmérnöki Kar
https://dtk.tankonyvtar.hu/xmlui/bitstream/handle/123456789/7825/mernoki_optimalas_HU.pdf?sequence=1&isAllowed=y
- [26] BME Mechatronika, Optika és Gépészeti Informatika Tanszék, *5.fejezet: Optimum kereső módszerek*. [online] Elérhető: https://mogi.bme.hu/TAMOP/szamitogepes_szimulacio/ch05.html#ch-V.1.4 [Hozzáférés dátuma: 2023.04.28]
- [27] S., Migico, K., K., Choong, A., H., Che Malid, C., K., Ng, T., Hamzah, D., Talib, 2020. *Refurbishment of the main grandstand and roof of Sepang International Circuit Malaysia*. In: *Inspiring the Next Generation - Proceedings of the International Conference on Spatial Structures 2020/21*.
<https://openresearch.surrey.ac.uk/esploro/outputs/conferenceProceeding/99634965502346>
- [28] Tilke.de, *Sepang International Circuit Grandstand Tower 2016 Malaysian GP* [online] Elérhető: <https://tilke.de/en/portfolio/sepang-international-circuit/>

Appendix

The full module can be
downloaded from the following
link:



[https://www.dropbox.com/s/irc2gimks2x8zu/Diplomamunka
AndrasDNagy_EsernyosMemb
ranszerkezetParametrikusScript
.gh?dl=0](https://www.dropbox.com/s/irc2gimks2x8zu/Diplomamunka_AndrasDNagy_EsernyosMemb_ranszerkezetParametrikusScript_gh?dl=0)

The module runs under Rhino 7 and
Grasshopper3D. Other accessories used
for the full run:

- BATS_v0.2
<https://www.food4rhino.com/en/app/bats>
- Karamba3D 2.2.0
<https://karamba3d.com/>
- Nelder-Mead 0.5.2
<https://www.food4rhino.com/en/app/nelder-mead-optimisation-eoc>
- Wallacei X v.2.7
<https://www.wallacei.com/>

